

https://dspace.org/

Mathematical modelling of the mixing and flow inside a float glass furnace towards reducing the colour change time

Lotter, Bernardus Johannes Philippus

2018

https://hdl.handle.net/10539/26998

Lotter, Bernardus Johannes Philippus (2018) Mathematical modelling of the mixing and flow inside a float glass furnace towards reducing the colour change time, University of the Witwatersrand, Johannesburg, https://hdl.handle.net/10539/26998

Downloaded from a DSpace repository. https://dspace.org/



Mathematical modelling of the mixing and flow inside a float glass furnace towards reducing the colour change time

BJP LÖTTER

1549509

A dissertation submitted to the Faculty of Engineering and the Built Environment, University of the Witwatersrand, Johannesburg, South Africa, in fulfilment of the requirements for the degree of Masters of Science in Engineering.

Supervisor: Prof. M.O. Daramola

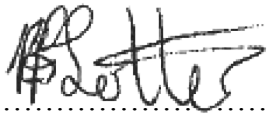
September 2018

Declaration

I declare that this dissertation is my own unaided work. It is being submitted for the degree of Master of Science in Engineering to the University of Witwatersrand, Johannesburg, South Africa. It has not been submitted to any other institution for the purpose of examinations or a degree.

I BJP Lötter (Student number: 1549509) am a student registered for Master of Science in Engineering in the year 2018. I hereby declare the following:

- I am aware that plagiarism (the use of someone else's work without their permission and/or without acknowledging the original source) is wrong.
- I declare that this dissertation is my own unaided work.
- I have followed the required conventions in referencing the thoughts and ideas of others.
- I understand that the University of the Witwatersrand may take disciplinary action against me if there is a belief that this is not my own unaided work or that I have failed to acknowledge the source of the ideas or words in my writing.



…… 3 ……day of……September……/ 2018……

Signature of Candidate Day Month Year

Abstract

The transition between two different glass colours in a float furnace is a costly manufacturing procedure as the glass properties are out of specification during this period. This transition period is determined by the control and understanding of the mixing characteristics for the specific float glass furnace. Initiatives to reduce costs and waste production have led to increased focus on reducing the colour change time. Published research on the mixing characteristics in a glass tank gave reasonable approximations of the response curve. However, the actual response curves of modern float glass furnaces deviate from these systems. Therefore, the aim of this investigation was to create a mathematical mixing model that can approximate the residence time inside the furnace based on the glass flows. This mathematical mixing model was used to reduce the duration of the colour change, with respect to the iron concentration.

The first step was to create a validated CFD model that would provide in depth knowledge and understanding of the flow cells in the furnace. Subsequently a mathematical one or two parameter mixing model was developed for the furnace.

The results from this study indicate that the colour change can be separated into four parts. A one parameter mixing model with five to eight perfect mixers in series can describe the first stage of the colour change, where the inlet iron concentration is set at a certain percentage higher than the final required iron concentration. The number of perfect mixers in series depends on the barrier depth with five mixers used for 0.41 m barrier depth and eight mixers in series for 0.56 m barrier depth. The second stage of the colour change when the barrier is removed causes a change in the furnace mixing characteristics and a sudden increase of iron concentration at the outlet of more than 0.1 mass % Fe_2O_3 within 4 hours. The third stage follows this short period by an increase in the iron outlet concentration that can be modelled by three perfect mixers in series when the barrier is out and the inlet iron concentration is reduced to the required outlet iron concentration. The fourth stage of the colour change is when the barrier is inserted again. This stage can be modelled by a four mixer in series model for the 0.3 m barrier depth.

The colour change time was reduced by 10 hours, with respect to the iron concentration, through adjusting key variables during the colour change. These were the overdope rate,

overdope duration and the time when the barrier is removed. Multiple methods were tested with the mathematic mixing model of which two methods reduced the colour change time by 10 hours. One method was increasing the overdope rate to 180 % from the standard 130 % for a duration of 31 hours and also removing the barrier at 31 hours. Another method was to remove the barrier at 52 hours instead of 33 hours at an over dope rate of 130 % for a duration of 37 hours.

These methods will decrease the colour change time with respect to iron concentration, but may increase the time that the optical distortion is out of specification; as the glass may not homogenise within the required time in the furnace. It is also noteworthy to mention that this model was created for a specific furnace design and bubbling rate and will vary from furnace to furnace; but the perfect mixers in series model could be applied to other furnaces by using the response curve from that furnace.

Acknowledgments

In proverbs 27:17, the bible says “As one piece of iron sharpens another, so friends keep each other sharp”. People improve the skills of other people and I want to acknowledge those people that have been with me through this exciting and testing time of postgraduate studies. And then the Lord Almighty that has always provided the light in difficult times.

I would like to thank my family and fiancé for the support during the studies. They have always been there for me every step giving that much needed push when required.

I want to acknowledge Prof Michael Daramola for his engineering knowledge and insight during the study. Your hard work and dedication to the field of science is an inspiration.

I want to thank PFG for the financial aid and for supplying all the necessary software and analysis for this study. It is an honour to work for a company that focuses on always improving.

The last mention goes to the researchers that have provided the knowledge and science required to complete this study.

Table of Contents

Abstract i

Acknowledgments iii

Nomenclature List x

1 Introduction 1

1.1 Glass and the industrial glass melting process 1

1.2 Research Aim and Objectives 3

1.3 Method and Scope 3

2 Literature Review 4

2.1 Flat glass colour changes 4

2.2 Recent advances of float glass furnace CFD studies 5

2.3 Flow modelling 6

2.3.1 Conservation Equations 6

2.3.2 Numerical solver 8

2.3.3 Discretization 9

2.3.4 Pressure velocity coupling 10

2.3.5 Under-relaxation of variables 12

2.3.6 Transient solution methods 12

2.3.7 Calculation of residuals 13

2.3.8 Judging convergence 15

2.3.9 Bubbler flow and user defined function (UDF) formulation 15

2.4 Residence time distribution of reactors 16

2.4.1 Residence time distribution theory 16

2.4.2 RTD in ideal reactors 17

2.4.3 Predicting conversion for a non-ideal reactor 19

2.5 Glass flow mixing characteristics 20

2.6 Homogenization inside glass tanks and the colour rendering index 23

3 Modelling and Optimization Procedure 24
3.1 Modelling procedure 24
3.1.1 Furnace glass flow modelling 24
3.1.2 Non-ideal reactor mixing model 24
3.1.3 Method of glass sample collection during the colour change 25
4 Glass Flow Modelling 26
4.1 Geometry 26
4.2 Meshing 27
4.3 Steady state solver set-up and optimization 33
4.3.1 Solver and governing equation selection 33
4.3.2 Glass properties 33
4.3.3 Cell zone and boundary conditions. 35
4.3.4 Discretization 37
4.3.5 Under-relaxation factors 38
4.4 Verification and validation 39
4.4.1 Glass flow patterns 39
4.4.2 Boundary conditions and mass and energy conservation 48
4.4.3 Discretization error and validation 51
4.5 Steady state model results and discussions 57
4.6 Transient model set-up and optimization 61
4.7 Results and discussions of the transient model 64
5 Mathematical Mixing Model and Optimisation of the Colour Change Time 68
5.1 Mixing model equation 68
5.2 The root mean square error 68
5.3 Initial mixing model design based on historical studies of the mixing inside a glass furnace 69
5.4 Final mixing model design and optimization 74

5.5 Optimizing the colour change time 78
6 Conclusions and Recommendations 81
7 References 83
Appendices 85
Appendix A: UDF for viscosity 85
Appendix B: UDF for bubblers (ANSYS®, 2005). 86
Appendix C: Top surface heat flux calculations 87
Appendix D: Convergence of glass temperatures 93
D.1 Filling pocket temperature 93
D.2 Bottom hotspot temperature (Bottom 6) 93
D.3 Outlet temperature 93
D.4 Crown 4 temperature 94
Appendix E: Octave (2012) model codes 94
E.1 2017 colour change mixer in series code 94
E.2. 2015 colour change optimized model code 95
E.3. 2016 colour change optimized model code 97
E.4. 2017 colour change optimized model code 99
Appendix F: Appendix references 102
Appendix G: Paper submitted for publication 103

List of Figures

Figure 1-1: Schematic illustration of the different flow cells in a float glass melting furnace (adapted from Feng et al., 2008) 2
Figure 2-1: Colouring ion change during an over dope of the batch 5
Figure 2-2: Flow cell magnitude (values adapted from Feng et al., 2008) 6
Figure 2-3: Procedure for the pressure based solution method (adapted from ANSYS® Fluent release 18, 2017). 9
Figure 2-4: RTD curves for a perfect CSTR and PFR 18
Figure 2-5: RTD curve for a CSTR and PFR in series 19
Figure 2-6: Possible response curves for glass mixing in a furnace (adapted from Bamford, 1977). 21
Figure 2-7: Mixing model developed by Bergman (1999) 22
Figure 3-1: Sampling points in the furnace 25
Figure 4-1: Cross section in length of a glass-melting furnace (adapted from Feng et al., 2008) 26
Figure 4-2: Layout of the furnace with the different sections 29
Figure 4-3: Layout of the furnace 30
Figure 4-4: Hexagonal Mesh of 0.1 m layout for the furnace up to refiner 31
Figure 4-5: Hexagonal Mesh of 0.1 m layout for the refiner up to the canal 32
Figure 4-6: Residuals for optimised under-relaxation factors. 39
Figure 4-7: Schematic viewed from the side of the furnace showing the x-velocity component for the whole furnace. 41
Figure 4-8: Schematic viewed from the side of the furnace showing the x-velocity component from the bubblers to the barrier. 42
Figure 4-9: Schematic viewed from the side of the furnace showing the x-velocity component in the working end and canal. 43
Figure 4-10: x-velocity component viewed from the top, with a section trough the top surface of the glass volume. 44
Figure 4-11: x-velocity component viewed from the top, with a section made 0.3 m from the bottom of the glass volume. 45
Figure 4-12: z-velocity component at the doghouse, with a section made at the doghouse through the glass volume height. 46
Figure 4-13: Velocity magnitude of glass at the bubblers, with a section made at the bubblers through the glass volume height 47

Figure 4-14: Furnace bottom temperature distribution. 52
Figure 4-15: Furnace top temperature distribution. 53
Figure 4-16: 30 mm mesh at the barrier. 53
Figure 4-17: 60 mm mesh at the barrier. 54
Figure 4-18: Refined mesh at the barrier. 54
Figure 4-19: Refined mesh at the inlet and doghouse. 55
Figure 4-20: Refined mesh at the canal and working end. 55
Figure 4-21: Schematic viewed from the side of the furnace showing the x-velocity component from the bubblers to the barrier for the 30 mm mesh. 56
Figure 4-22: Schematic viewed from the side of the furnace showing the x-velocity component from the bubblers to the barrier for the refined mesh. 56
Figure 4-23: Flow magnitude of different cells. (adapted from Pilkington , 2008). 57
Figure 4-24: Flow magnitude of different cells and recirculation flows (this study). 58
Figure 4-25: Temperature distribution on the symmetry axis of the furnace. 59
Figure 4-26: Glass streamlines with particles injected from section 0 to inlet. 60
Figure 4-27: Iron during colour change 65
Figure 4-28: Iron concentration expressed as % Fe_2O_3 in the furnace during the colour change. 66
Figure 4-29: Iron concentration expressed as % Fe_2O_3 in the furnace during the colour change. The barrier was removed at 37 h and the inlet iron concentration changed to 0.61 % Fe_2O_3 from 1.287 % Fe_2O_3.The barrier was inserted at 0.3 m deep after 80 h. 67
Figure 5-1: 2015 colour change outlet iron mass percentage comparison between mixing model and actual data. 72
Figure 5-2: 2016 colour change outlet iron mass percentage comparison between mixing model and actual data. 72
Figure 5-3: 2017 colour change outlet iron mass percentage comparison between mixing model and actual data. 73
Figure 5-4: Optimized model prediction for the 2015 colour change outlet iron mass percentage and comparison with the actual data. 75
Figure 5-5: Optimized model prediction for the 2016 colour change outlet iron mass percentage and comparison with the actual data. 76
Figure 5-6: Optimized model prediction for the 2017 colour change outlet iron mass percentage and comparison with the actual data. 77

Figure 5-7: Optimized model prediction for the 2017 colour change doghouse iron mass percentage and comparison with the actual data. 78
Figure 5-8: Model predicted outlet iron concentration change for different times when the barrier is removed. 79
Figure 5-9: Model predicted outlet iron concentration change for different overdope (OD) rates. 80

List of Tables

Table 4-1: List of named selections for the flow model 28
Table 4-2: Glass properties 34
Table 4-3: Side and bottom wall heat flux. 36
Table 4-4: Top surface heat flux. 37
Table 4-5: Top surface heat flux 48
Table 4-6: Bottom and side wall heat flux 49
Table 4-7: Furnace energy balance 50
Table 4-8: Residuals for different meshes. 52
Table 4-9: Tint glass properties. 63
Table 4-10: OD glass properties. 63
Table 5-1: Colour change variables 69
Table 5-2: RMS errors for perfect mixers in series 71
Table 5-3: RMS error for period before barrier is removed. 71

Nomenclature List

Symbols used

$\mathbf{A}$	Surface area vector	m^2
a	Linearized coefficients	
B	External body forces	N/m^3
b	Source terms	
C_f	The bubbling frequency	bubble/m
C_l	Colorant level defined as the concentration of the colourant in the product as a fraction of the input	
C_p	Heat capacity	J/(kg·K)
$C(t)$	Concentration function	
c	A factor found to be 2/9 by Wijshoff et al. (2010) at fining temperatures	
D	Mass diffusivity	m^2/s
d_f	Pressure velocity coupling variable	
E	Energy term in the energy conservation equation	J/kg
$E(t)$	Residence-time distribution function	
F	The effluent volumetric flow rate	m^3/s
f	Net force per unit volume	N/m^3
g	Gravitational acceleration, which is 9.81 m/s^2	m/s^2
H	The height from the bubbler tip to the glass level	m
h	Sensible enthalpy	J/kg
$I(t)$	Cumulative distribution function	
J	Diffusion flux	kg/m^3
J_f	Face flux	
k_{eff}	Effective conductivity	W/(m·K)
k	Thermal conductivity	W/(m·K)
L	Characteristic length	m
M	Furnace deadweight capacity	kg
N	Tracer Material	
n	Number of samples	

P	Pressure matrix	Pa
p	Pressure	Pa
Q	Furnace throughput	kg/h
Re	Reynolds number	
RMS	Root mean square error	
R	Residual	
r_b	Radius	m
S_h	Energy Source term	J/m^3
S_m	Mass source term	kg/(m^3·s)
S_φ	Source of φ per unit volume	φ/m^3
T	Temperature	K
t_r	Furnace residence time	h
t	Time	s
u_k	Velocity component	m/s
V	Volume	m^3
$\mathbf{v}$	Velocity vector	m/s
v	Velocity	m/s
W	Throughput	kg/h
W_{tot}	Total furnace capacity	kg
x	Fe_2O_3 mass percentage	
x^i	Model predicted Fe_2O_3 output mass percentage	
$\hat{x}^i$	Actual measured Fe_2O_3 output mass percentage	
y	Mole fraction	

Greek symbols

Γ_φ	Diffusion coefficient	
α	Under-relaxation factor	
μ	Viscosity	Pa·s
ρ	Density	kg/m^3
$\bar{\bar{\tau}}$	Stress tensor	
τ	Average residence time	s
φ	Scalar variable	

1 Introduction

1.1 Glass and the industrial glass melting process

Glass manufacturing has been in existence since 3500 BC but it was only in the 19th century, at the end of the industrial revolution that mass production of glass became significant (Wijshoff et al., 2010). Since then there were two important developments. The full mechanization of bottle manufacture around 1920, and the introduction of the float process invented in 1952 for flat glass (Wijshoff et al., 2010). With developments made especially in longer furnace lifetimes, improved thermal efficiency, new production techniques and product innovation.

The float glass process for manufacturing flat glass was introduced by the Pilkington Brothers in 1959 (Wijshoff et al., 2010). This process is used mainly for automotive, architectural and display glass panes (Wijshoff et al., 2010). Every application requires glass with different properties. All these properties are dependent on the chemical composition and oxidation state of the glass. In the float process, flat glass is manufactured from continuously pouring molten glass onto a bath of liquid tin. The glass floats on top of the tin giving the glass a smooth flat surface (Wijshoff et al., 2010). The molten glass is manufactured by melting raw materials consisting mainly of silica sand, soda ash and limestone with other components added to improve the glass properties for a specific application (Wijshoff et al., 2010). An important property for commercial flat glass is the colour of the glass that is interdependent on the specific light transmission and energy absorption band. Numerous glass colours are made with the main colours for architectural and automotive applications consisting of clear glass (0,12 % $Fe_2O_{3)}$, tint glass (0,62 % $Fe_2O_{3)}$ and dark tint glass (0,72 % Fe_2O_3).

Feeding of the raw materials is done by pushing the batch of materials onto the glass melt. The batch will spread across the surface of the glass and form a batch blanket on top of the glass as shown in Figure 1-1 (Feng, Li, Qin & Liu, 2008). This batch blanket gets heat energy from the top and bottom by the radiation from the firing area and the warm glass from the melt cell, respectively. The chemicals in the batch start to react with each other and dissolve after reaching certain temperatures and form a melt. This molten glass then flows through the different sections of the furnace before it exits in the canal.

The length of the colour change is determined by how long the Colour Rendering Index (CRI) and the optical properties are out of specification, during which glass is dumped to waste. Due to the high residence times of glass in the furnace a clear to tint colour change of 5 days is expected and a tint to dark tint colour change takes about 3 days. Tens of thousands of Rands is lost per hour, based on a glass-to-stock cost, even if the glass that is out of specification is recycled back to the furnace. It is required to predict the residence time inside the melter and the influences of the key variables involved in the colour change to reduce the colour change time.

Studies by Cooper (1959) showed that the mixing inside a furnace could be approximated by multi-complete mixing cells with a plug flow cell. However, actual data from furnaces shows that the best case is to make allowance for dead time with a complete mixing model (Bamford, 1977). More recently, Bergman (1999) found that plug flow with perfect mixers in series and parallel was found to be the most accurate mixing model. These findings are still used in literature today as described in Wijshoff et al. (2010) but do not accurately depict the effect of changing key process variables for example the barrier height. The modern enhancements in computational fluid dynamics modelling of the flows in glass furnaces could also provide additional insight into the mixing of glass inside a float glass furnace. This can be instrumental in reducing the colour change time.

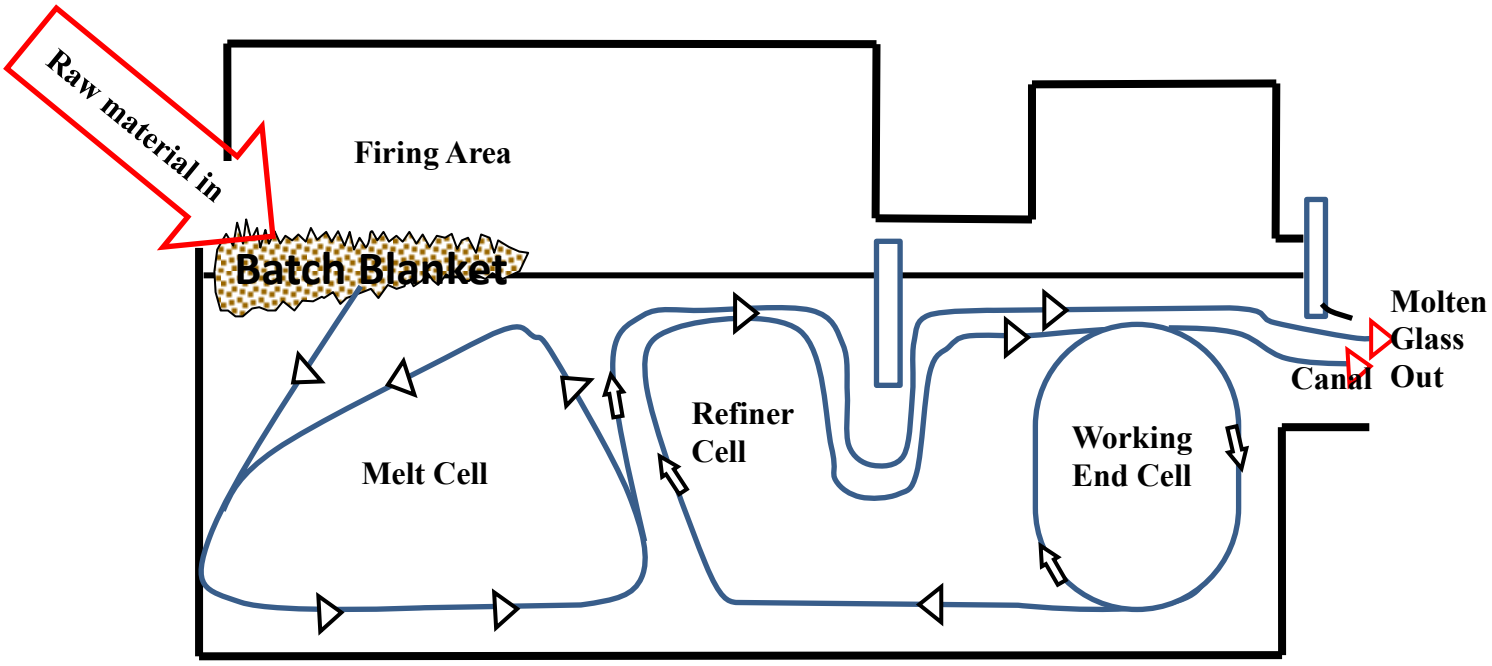


Figure 1-1: Schematic illustration of the different flow cells in a float glass melting furnace (adapted from Feng et al., 2008)

1.2 Research Aim and Objectives

This is a study aimed at reducing the colour change time during the production of glass. The study was done to provide answers to the following questions:

1. What is the influence of different furnace variables on the iron dilution and rate of mixing within a float glass furnace?
2. How can the mixing inside the furnace be optimized to reduce the colour change time?

To provide answers to the above-mentioned questions, the objectives of the study were:

1. Develop a validated mathematical mixing model that could determine the iron concentration at crucial stages inside a float glass furnace during the colour change.
2. Perform simulation studies on the validated model towards optimising the mixing in order to reduce the colour change time.

1.3 Method and Scope

This study was divided into two different phases. Phase one was to understand the link between the flow inside the furnace and the mixing of the glass. This included modelling the flow of the glass in the computational fluid dynamics software (CFD), ANSYS® Fluent (release 18, 2017), and then using the data obtained from the CFD model as a basis of creating the mathematical mixing model to predict the colour change time. Actual colour change data was then collected from the plant to validate the model. The standard error between the actual and theoretical data was used to determine the accuracy of the model. All data available only included the inlet and outlet composition of the glass during the colour change. Additional samples of glass at different times and different positions inside the furnace were required. This was to determine the chemical composition distribution with time during the colour change at different stages inside the furnace. There were limited opportunities to take these samples because of limited colour changes from clear to tint.

The second phase of the study involved further simulation and optimisation studies towards different combinations of key variables during the colour change to reduce colour change times.

2 Literature Review

2.1 Flat glass colour changes

Changing colour in a glass furnace involves many procedures that are combined to optimise the time. These procedures include over-compensating for the composition of the colouring material; removing or inserting the barrier; changing the bubbling; changing the electric boost and changing the energy input (Wijshoff et al., 2010).

The most significant procedure is over-compensating for the composition of the colouring material. It would take up to three to four times the residence time by changing the input batch composition to the specified product composition. Therefore, the technique used is to over compensate or over dope (OD) the colouring material composition. Wijshoff et al. (2010) states that care should be taken to not over-compensate the required concentration by a large amount or to use the over-compensated composition for too long. This procedure reduces the changeover time by a factor of 3 to 5. Figure 2-1 shows that when the OD is continued for too long or the initial colouring material concentration is too large that the final product composition will over shoot before stabilizing.

Other procedures include (Wijshoff et al., 2010):

(i) Change of the redox state of the batch for different colours.
(ii) Adjustment of bubblers to enhance mixing and avoid dead water zones.
(iii) Maximising throughput.
(iv) Drainage of old glass if a drainage system is available.
(v) Schedule products with lower quality for immediately before and after the colour change.

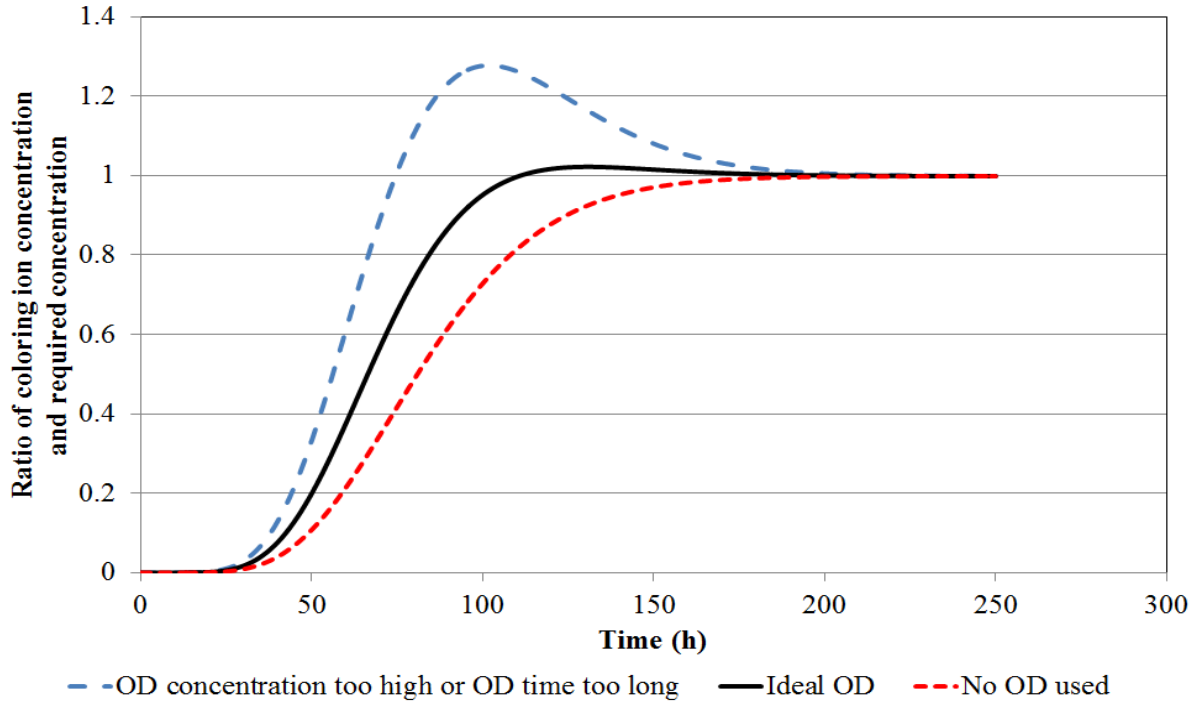


Figure 2-1: Colouring ion change during an over dope of the batch

2.2 Recent advances of float glass furnace CFD studies

Computational fluid dynamics or CFD has been used extensively in finding solutions to operational problems in the glass industry since the significant advances in CFD for float glass furnaces during the period 1996 to 2000 according to Choudhary (2002). Feng et al. (2008) did a study on combining CFD and glass homogeneity inspection of the float glass melting process. Feng et al. (2008) used the Ansys software to simulate and compare the fluid flow in the melter to experimental results and found it to be consistent. The flow quantities of the glass fluid in the furnace for furnace producing glass at a load of 500 tons per day is as shown in Figure 2-2 (Feng et al., 2008). Xu, Liu, Xing & Li (2016) used a similar CFD model and assumptions as Feng et al. (2008) to study the effect that glass iron content has on the glass flow. Xu et al. (2016) obtained similar results with velocities of the magnitude of 10^{-3} m/s.

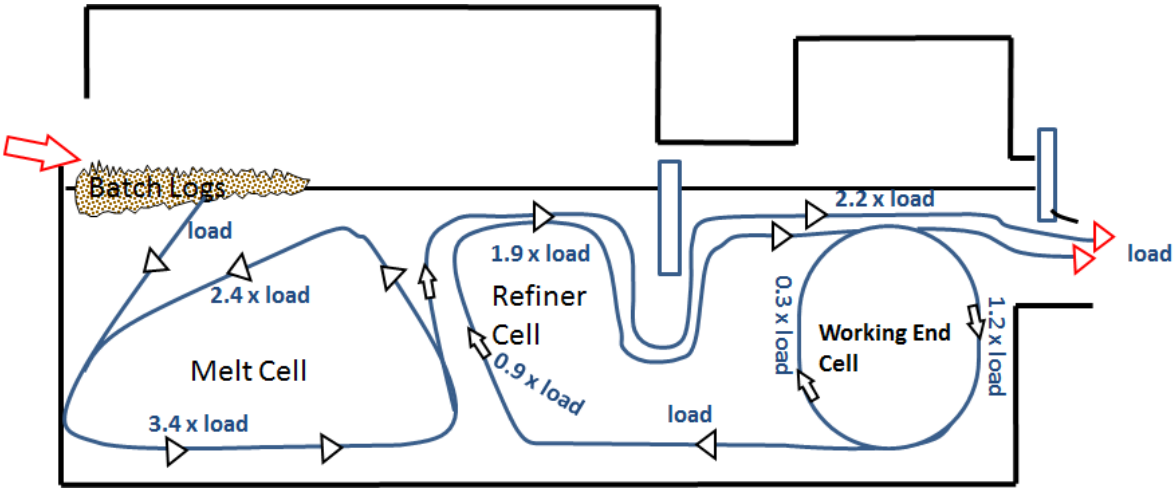


Figure 2-2: Flow cell magnitude (values adapted from Feng et al., 2008)

Fasilow (2007) did a study on reducing the colour change time on float furnaces with the help of CFD and concluded that it is possible to find operational conditions to reduce the crushing time by simulations. Fasilow (2007) also found that the ream index is the limiting factor in reducing the colour change time. By using the ream index approach developed through CFD results coupled with other non CFD tools the colour changes of a number of furnaces where reduced by a collective 385 hours in a year. Fasilow (2007) did however, state that the optimum settings for colour changes depend on the furnace design and operation and that every furnace needs to be optimized individually using CFD.

2.3 Flow modelling

The flow modelling was done in the CFD software ANSYS® Fluent (release 18, 2017). This software provides a wide range of laminar and turbulent, incompressible and compressible and steady or transient flow problems. Mathematical models for transport phenomena is combined with complex geometries and examples of applications include glass flow models, heat transfer in turbomachinery and automotive engine components, combustion models etc. This commercial modelling package is very useful in solving complex problems related to transport phenomena in chemical engineering.

2.3.1 Conservation Equations

ANSYS® Fluent (release 18, 2017) solves the conservation equations for mass and momentum. For flow with compressibility and heat transfer, the energy conservation equation is solved. For species mixing or reactions, the conservation equation is solved. The

differential form of the mass conservation equation or continuity equation can be written as (Welty et al., 2008):

$$\frac{\partial \rho}{\partial t} + \nabla \cdot \rho \mathbf{v} = 0 \tag{2.1}$$

Where ρ is the density in kg/m^3 and **v** is the velocity vector.

Fluent added an additional source term S_m, to Equation (2.1), for mass added to the phase due to a secondary phase.

$$\frac{\partial \rho}{\partial t} + \nabla \cdot \rho \mathbf{v} = S_m \tag{2.2}$$

The conservation of momentum equation solved in ANSYS® Fluent (release 18, 2017) is written as in Equation (2.3).

$$\frac{\partial}{\partial t}(\rho \mathbf{v}) + \nabla \cdot (\rho \mathbf{v}\mathbf{v}) = -\nabla P + \nabla \cdot (\bar{\bar{\tau}}) + \rho g + B \tag{2.3}$$

With the stress tensor $\bar{\bar{\tau}}$ given by:

$$\bar{\bar{\tau}} = \mu \left[(\nabla \mathbf{v} + \nabla \mathbf{v}^{\boldsymbol{T}}) - \frac{2}{3} \nabla \cdot \mathbf{v} I \right] \tag{2.4}$$

B are the external body forces and also contains the user-defined source terms. *P* is the pressure matrix and g is the gravitational acceleration, which is 9.81 m/s^2.

The form of the energy conservation equation solved by ANSYS® Fluent (release 18, 2017) is:

$$\frac{\partial}{\partial t}(\rho E) + \nabla \cdot [\mathbf{v}(\rho E + P)] = \nabla \cdot \left[k_{eff} \nabla T + \sum_j h_j J_j - (\bar{\bar{\tau}} \cdot \mathbf{v}) \right] + S_h \tag{2.5}$$

With:

$$E = h - \frac{P}{\rho} + \frac{v^2}{2} \tag{2.6}$$

And the sensible enthalpy for incompressible flow was taken as:

$$h = \sum_j y_j h_j + \frac{P}{\rho} \tag{2.7}$$

In Equation (2.7), y_j is the mole fraction and the enthalpy in equation (2.7) can be expressed as:

$$h_j = \int_{T_{ref}}^{T} C_{p,j} dT \tag{2.8}$$

With k_{eff} the effective conductivity in W/(m·K); T, the temperature in K; J_j, the diffusion flux; P, the pressure in the system in Pa; the heat capacity $C_{p,j}$ in J/(kg·K) and S_h, the source term.

2.3.2 Numerical solver

ANSYS® Fluent (release 18, 2017) allows the user to decide between the pressure-based solver and the density-based solver. For both methods the velocity field is obtained from the momentum equations. In the density approach, the continuity equation is used to obtain the density field while the pressure field is determined from the equation of state. On the other hand, the pressure-based solver extracts the pressure field by solving a pressure correction equation, which is obtained by manipulating continuity, and momentum equations. Both methods solve the governing integral equations by using a control-volume-based technique that consist of:

- Dividing the domain into discrete control volumes using a grid.
- Integrating the governing equations on the individual control volumes to construct algebraic equations for the discrete dependent variables such as velocities, pressure, temperature and conserved scalars.
- Linearization of the discretized equations and solution of the resultant linear equation system to give new values of the dependant variables.

These two numerical methods use a similar discretization process called the finite volume method, but the approach used to linearize and solve the discretized equations is different.

ANSYS® Fluent (release 18, 2017) provides two forms of pressure-based solution methods; the segregated and the coupled algorithms. The procedure for these two solution methods is shown in Figure 2-3.

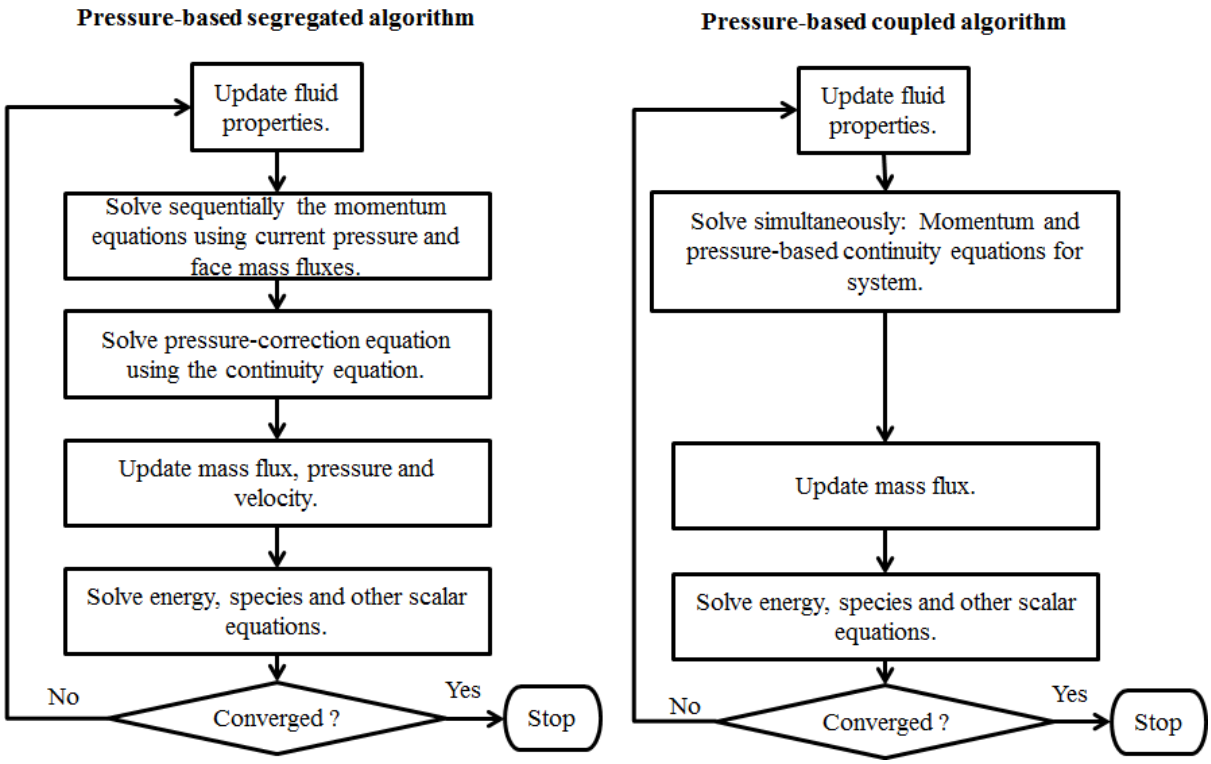


Figure 2-3: Procedure for the pressure based solution method (adapted from ANSYS® Fluent release 18, 2017).

2.3.3 Discretization

The linearized discretized scalar transport equation in ANSYS® Fluent (release 18, 2017) is written as:

$$a_p \varphi = \sum_{nb} a_{nb} \varphi_{nb} + b \tag{2.9}$$

Where the subscript *nb* refers to neighbouring cells. a_p and a_{nb} are the linearized coefficients for the scalar variable, φ. Schäfer (2006) explains the method for discretization of the conservation equations through the finite-volume method to get Equation (2.9).

The coefficients, a_p and a_{nb}, are determined from the different discretization techniques used for determining φ at the cell centres called spatial discretization; and for the discretization of the different diffusive fluxes.

The discretization for transient calculations is identical to the spatial discretization of the steady state case (ANSYS® Fluent release 18, 2017). The time derivative, shown in Equation (2.10), is discretized using backward differences (ANSYS® Fluent release 18, 2017):

$$\frac{\partial \varphi}{\partial t} = \mathrm{f}(\varphi) \tag{2.10}$$

The first order accurate temporal discretization is given by (ANSYS® Fluent release 18, 2017):

$$\frac{\varphi^{n+1} - \varphi^{n}}{\Delta t} = \mathrm{f}(\varphi) \tag{2.11}$$

With *n*+1, the value at the next time level t; and *n*, the value at the current level.

2.3.4 Pressure velocity coupling

Schäfer (2006) states that one of the biggest problems when solving the discrete mass and momentum system is the simultaneous fulfilment. Reason being that the pressure does not appear in the continuity equation and makes the system very large and unsolvable due to the degree of freedom being high. ANSYS® Fluent (release 18, 2017) makes provision for solving the system of equations with the coupled algorithm where the pressure can be solved simultaneously. The discretized form of the momentum equation for component u_k is defined as (ANSYS® Fluent release 18, 2017):

$$\sum_j a_{ij}^{u_k u_k} u_{kj} + \sum_j a_{ij}^{u_k p} p_j = b_i^{u_k} \tag{2.12}$$

With $a_{ij}^{u_k u_k}$ and $a_{ij}^{u_k p}$, the linearized coefficients; u_{kj}, the velocity; p_j, the pressure; and $b_i^{u_k}$, the source terms. The balance of fluxes is replaced using the flux expression resulting in the discretized form that can be solved simultaneously (ANSYS® Fluent release 18, 2017):

$$\sum_k \sum_j a_{ij}^{pu_k} u_{kj} + \sum_j a_{ij}^{pp} p_j = b_i^p \tag{2.13}$$

The segregated algorithm uses an approach described by Schäfer (2006). A guessed pressure field p^* is used in the momentum equation resulting in a face flux J_f^* computed from (ANSYS® Fluent release 18, 2017):

$$J_f^* = \widehat{J_f^*} + d_f(p_{co}^* - p_{c1}^*) \tag{2.14}$$

The face flux J_f^* does not satisfy the continuity equation. A correction J_f' is added so that the corrected flux J_f satisfies the continuity equation (ANSYS® Fluent release 18, 2017):

$$J_f = J_f^* + J_f' \tag{2.15}$$

The SIMPLE algorithm used by ANSYS® Fluent (release 18, 2017) postulates that J_f' be written as (ANSYS® Fluent release 18, 2017):

$$J_f' = d_f(p_{co}' - p_{c1}') \tag{2.16}$$

Where p' is the cell pressure correction.

In the SIMPLE algorithm, the flux correction is substituted into the discrete continuity equation to obtain a discrete equation for pressure correction (ANSYS® Fluent release 18, 2017):

$$a_p p' = \sum_{nb} a_{nb} p'_{nb} + b \tag{2.17}$$

Where *b*, the source term, is the net flow rate into the cell (ANSYS® Fluent release 18, 2017):

$$b = \sum_{f}^{Nfaces} J_f^* A_f \tag{2.18}$$

The pressure correction equation is solved in ANSYS® Fluent (release 18, 2017) by the algebraic multigrid method. Once the solution is obtained, the cell pressure and face flux are corrected by:

$$p = p^* + \alpha_p p' \tag{2.19}$$

$$J_f = J_f^* + d_f(p'_{co} - p'_{c1}) \tag{2.20}$$

With α_p, the under-relaxation factor for pressure.

2.3.5 Under-relaxation of variables

Due to the nonlinearity of equations being solved, it is necessary to control the amount by which the variable φ changes. In a simple form the new value of the variable within a cell depends on the old value. The computed change in the variable with the under-relaxation factor, α, is calculated as follows (ANSYS® Fluent release 18, 2017):

$$\varphi = \varphi_{old} + \alpha \Delta\varphi \tag{2.21}$$

2.3.6 Transient solution methods

For time-dependent flows, the discretized form of the generic transport equation is of the following form ANSYS® Fluent (release 18, 2017):

$$\int_V \frac{\partial p\varphi}{\partial t} \mathrm{d}V + \oint \rho\varphi \mathbf{v} \cdot \mathrm{d}\mathbf{A} = \oint \Gamma_\varphi \nabla\varphi \cdot \mathrm{d}\mathbf{A} + \int_V S_\varphi \mathrm{d}V \tag{2.22}$$

Where;

$\frac{\partial p\varphi}{\partial t}$ = conservative form of the transient derivative of transported variable φ

ρ = density

v = velocity vector

A = surface area vector

Γ_φ = diffusion coefficient

$\nabla\varphi$ = gradient of φ $\left[=\left(\frac{d\varphi}{dx}\right)\hat{\imath}+\left(\frac{d\varphi}{dy}\right)\hat{\jmath}\right]$ in 2d

S_φ = source of φ per unit volume

The pressure based solver in ANSYS® Fluent (release 18, 2017) uses an implicit discretization of the transport equation. As a standard, all terms are evaluated from the field for time level n+1(ANSYS® Fluent release 18, 2017):

$$\int_V \frac{\partial p\varphi}{\partial t}\mathrm{d}V + \oint \rho^{n+1}\varphi^{n+1}\mathbf{v}^{n+1}\cdot\mathrm{d}\mathbf{A} = \oint {\Gamma_\varphi}^{n+1}\nabla\varphi^{n+1}\cdot\mathrm{d}\mathbf{A} + \int_V {S_\varphi}^{n+1}\mathrm{d}V \tag{2.23}$$

In the pressure-based solver, the overall time-discretization error is determined by both the choice of temporal discretization and the manner in which the solutions are advanced to the next time step. There are two approaches to the time-advancement scheme depending on the control of the splitting error. These two methods are the iterative time-advancement scheme and the non-iterative time-advancement scheme. The non-iterative time-advancement scheme is not recommended for highly viscous flow or flow with a strong dependence of fluid density on species concentration and can therefore not be used for glass (ANSYS® Fluent release 18, 2017). In this study, the iterative time-advancement scheme is appropriate and was used. In the iterative time-advancement scheme, all the equations are solved iteratively as per the segregated method, for every time step, until the convergence criteria is met. With this iterative time-advancement scheme, non-linearity of the individual and inter equation couplings are fully accounted for, eliminating the splitting error.

2.3.7 Calculation of residuals

The residuals are used in ANSYS® Fluent (release 18, 2017) to give a record and history of the convergence of the solver. The residual can be as low as six orders of magnitude for single precision solvers and as low as twelve orders of magnitude for double precision solvers. Keeping in mind the discretized Equation (2.9) ANSYS® Fluent (release 18, 2017):

$$a_P\varphi_P = \sum_{nb} a_{nb}\varphi_{nb} + b \tag{2.24}$$

Where a_P is the centre coefficient; and a_{nb}, the coefficient for all the neighbouring cells; and b, the contribution from a source. The residual, R^{φ}, is calculated in ANSYS® Fluent (release 18, 2017) by the imbalance summed over all the cells and is referred to as the unscaled residual. It can be written as (ANSYS® Fluent release 18, 2017):

$$R^{\varphi} = \sum_{cells\ P} \left| \sum_{nb} a_{nb}\varphi_{nb} + b - a_P\varphi_P \right| \tag{2.25}$$

Scaling has to be applied in order to evaluate the residual. There are two types of scaling in ANSYS® Fluent (release 18, 2017) referred to as global scaling and local scaling. The globally scaled residual is defined as (ANSYS® Fluent release 18, 2017):

$$R^{\varphi} = \frac{\sum_{cells\ P} |\sum_{nb} a_{nb}\varphi_{nb} + b - a_P\varphi_P|}{\sum_{cells\ P} |a_P\varphi_P|} \tag{2.26}$$

The locally scaled residual is defined as (ANSYS® Fluent release 18, 2017):

$$R^{\varphi} = \frac{\sqrt{\sum_{cells}^{n} \left(\frac{1}{n}\right) \left(\frac{\sum_{nb} a_{nb}\varphi_{nb} + b - a_P\varphi_P}{a_P}\right)^2}}{(\varphi_{max} - \varphi_{min})_{domain}} \tag{2.27}$$

The unscaled residual used for the continuity and other relevant equations is defined (ANSYS® Fluent release 18, 2017):

$$R^{C} = \sum_{cells\ P} |rate\ of\ mass\ creation\ in\ cell\ P| \tag{2.28}$$

The local scaling for all equations are the same. The global scaling for the continuity equation is different and is defined as (ANSYS® Fluent release 18, 2017):

$$\frac{R^{C}_{iteration\ N}}{R^{C}_{iteration\ 5}} \tag{2.29}$$

ANSYS® Fluent (release 18, 2017) does allow for normalizing the residual after a certain amount of iterations to determine by how much the residual has decreased during the calculations.

2.3.8 Judging convergence

ANSYS® Fluent (release 18, 2017) states that there is no universal metrics for judging convergence. For most applications the default convergence criteria in ANSYS® Fluent (release 18, 2017) requires that the globally scaled residuals decrease to 10^{-3} for all equations except for energy and radiation equations for which the criterion is 10^{-6}. Locally scaled residuals decrease to 10^{-5} for all equations.

2.3.9 Bubbler flow and user defined function (UDF) formulation

Work has been done by ANSYS® (2005) in formulating a UDF that can be used to describe the bubbler section in the melter. The rise velocity of a bubble can be calculated from Equation (2.30) that is derived from Stokes' Law (Rhodes, 2008):

$$v_s = \frac{c\rho g {r_b}^2}{\mu} \tag{2.30}$$

With:

v_s = ascension velocity (m/s)

ρ = melt density (kg/m^3)

g = acceleration of gravity (9.8 m/s^2)

r_b = bubble radius (m)

μ = melt viscosity (Pa·s)

c = a factor found to be 2/9 by Wijshoff et al. (2010) at fining temperatures

The net force per unit volume due to the bubbles in the glass tank is given in ANSYS® (2005) as:

$$f = \frac{C_f H}{V} 4\mu\pi r_b v_s \tag{2.31}$$

With:

f = net force per unit volume (N/m^3)

C_f = the bubbling frequency (bubble/m)

H = the height from the bubbler tip to the glass level (m)

V = the bubbler volume (m^3)

2.4 Residence time distribution of reactors

2.4.1 Residence time distribution theory

The time that chemical elements or particles spend inside a reactor is the reactor's residence time. Ideal plug flow and batch reactors are the only two classes of reactors where the atoms that were fed into the reactor will all have the same residence time (Fogler, 2006). In a continuous stirred tank reactor (CSTR) the atoms that are added are perfectly mixed with all the other atoms in the reactor and because of this, some atoms will leave the reactor almost immediately and other atoms will remain in the reactor for a very long time, giving a distribution of residence times. The resident time distribution (RTD) of a reactor is a characteristic of the mixing in the reactor (Fogler, 2006).

The RTD is determined with a pulse input experiment where an inert chemical is injected into the reactor with the same physical properties as the reaction mixture. The outlet concentration is measured as a function of time giving the C curve. The concentration of the tracer material leaving the reactor between time t and $t + \Delta t$ if Δt is sufficiently small is the same. The amount of tracer material ΔN leaving the reactor between time t and $t + \Delta t$ can be defined as (Fogler, 2006):

$$\Delta N = FC(t)\Delta t \tag{2.32}$$

With F the effluent volumetric flow rate. Dividing Equation (2.32) trough with the total amount that entered the reactor N_0, one obtains:

$$\frac{\Delta N}{N_0} = \frac{FC(t)}{N_0}\Delta t \tag{2.33}$$

For a pulse input (Fogler, 2006):

$$E(t) = \frac{FC(t)}{N_0} \tag{2.34}$$

So that Equation (2.33) becomes (Fogler, 2006):

$$\frac{\Delta N}{N_0} = E(t)\Delta t \tag{2.35}$$

The quantity $E(t)$ is called the residence-time distribution function (Fogler, 2006). It is a function that describes the amount of time different fluid elements have spent in the reactor. N_0 can be calculated by summing all the amounts of material that has left the reactor between time zero and infinity (Fogler, 2006).

$$\mathrm{d}N = FC(t)\mathrm{d}t \tag{2.36}$$

Integrating Equation (2.36) gives (Fogler, 2006):

$$N_0 = \int_0^\infty FC(t)\mathrm{d}t \tag{2.37}$$

With the volumetric flowrate F constant, $E(t)$ can be defined as (Fogler, 2006):

$$E(t) = \frac{C(t)}{\int_0^\infty C(t)\mathrm{d}t} \tag{2.38}$$

The fraction of the outlet that has stayed inside the reactor a period of time shorter than t, is equal to the sum over all times less than t of $E(t)\,\Delta t$, or expressed continuously (Fogler, 2006):

$$\int_0^\infty FC(t)\mathrm{d}t = \begin{bmatrix}\text{Fraction of effluent}\\ \text{that has been in reactor}\\ \text{for less than time } t\end{bmatrix} = I(t) \tag{2.39}$$

Danckwerts defined Equation (2.39) as a cumulative distribution function and called it $I(t)$ (Fogler, 2006).

2.4.2 RTD in ideal reactors

The cumulative distribution function for a CSTR is derived to be (Fogler, 2006):

$$I(t) = 1 - e^{-\frac{t}{\tau}} \tag{2.40}$$

With (Fogler, 2006).

$$\tau = \frac{V}{F} \tag{2.41}$$

The cumulative distribution function for a PFR is:

$$I(t) = \begin{cases} 0 & t < \tau \\ 1 & t \geq \tau \end{cases} \tag{2.42}$$

Figure 2-4 shows the cumulative RTD curves for a perfect CSTR and a perfect PFR. The cumulative distribution function of a CSTR and PFR in series can be expressed by Equation (2.43) (Fogler, 2006) with the response curve as shown in Figure 2-5. The same RTD is obtained no matter what the sequence of PFR/CSTR is (Fogler, 2006) for reactors without reactions.

$$I(t) = \begin{cases} 0 & t < \tau_{pfr} \\ 1 - e^{-\frac{t-\tau_{pfr}}{\tau_{cstr}}} & t \geq \tau_{pfr} \end{cases} \tag{2.43}$$

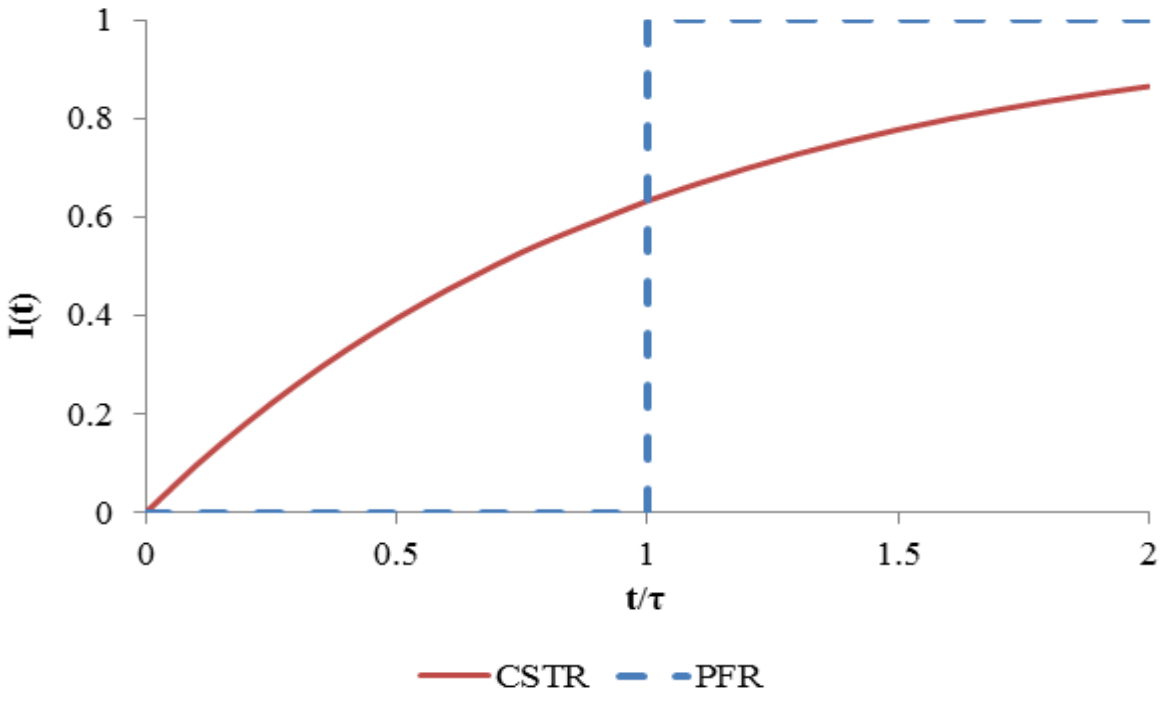


Figure 2-4: RTD curves for a perfect CSTR and PFR

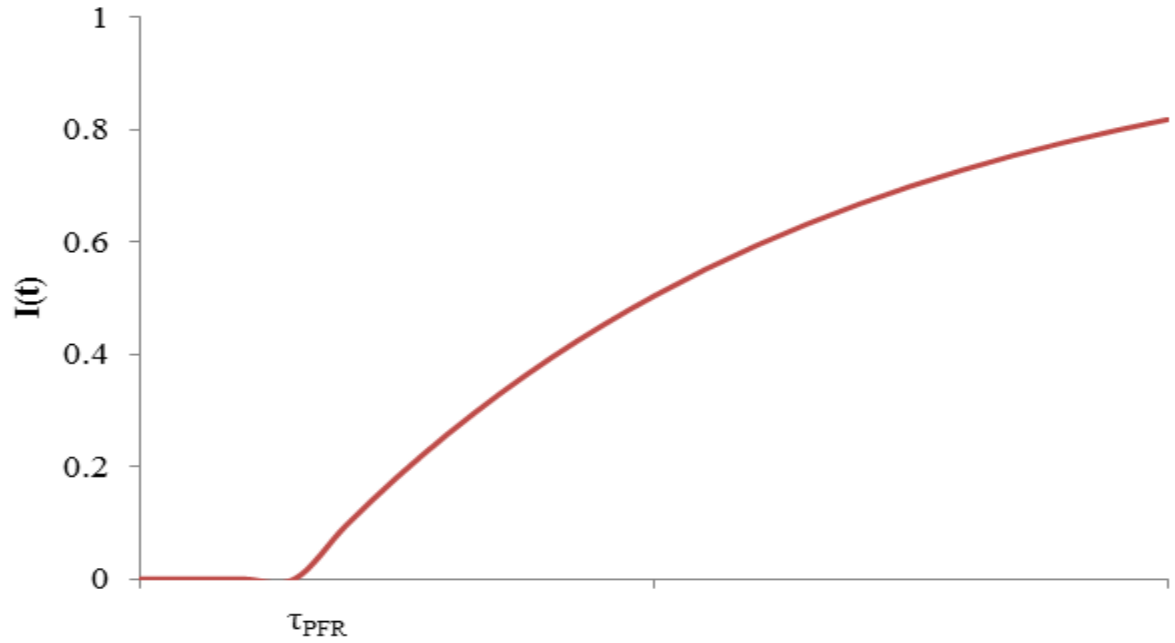


Figure 2-5: RTD curve for a CSTR and PFR in series

2.4.3 Predicting conversion for a non-ideal reactor

Fogler (2006) gives some general guidelines when developing models for non-ideal reactors. They must be mathematically tractable and be solved without an inordinate expenditure of human or computer time. The models must realistically describe the characteristics of the non-ideal reactor. The phenomena must be reasonably described physically, chemically and mathematically. The model must not have more than two parameters.

The procedure from Fogler (2006) for choosing a model to predict the conversion of a non-ideal reactor is:

(i) Look at the reactor

   a. Where are the inlet and outlet streams to and from the reactors?
   b. Look at the mixing system for example are there multiple mixing zones in the reactor?
   c. Look at the configuration of the different mixing zones, recirculation, dead zones etc.

(ii) Look at the tracer data.

   a. Plot the $E(t)$ and $F(t)$ curves.
   b. Analyse the shapes of the curves to the shapes of ideal reactors, deadzones, bypassing etc.

c. Calculate the mean residence time and variance and determine how it compares to the mean residence time.

(iii) Choose a model.

(iv) Use the tracer data to determine the model parameters.

(v) Calculate the conversion for the model system selected.

The different models that can be used is a one-parameter model for tubular reactors that consists of the tank in series model and the dispersion model. For the tank in series model the number of tanks is the parameter and the dispersion coefficient for the dispersion model. A two-parameter model can also be used were bypassing, dead volume or different number of tanks in parallel or series are used to describe the mixing in the non-ideal reactor.

2.5 Glass flow mixing characteristics

Extensive glass flow mixing characteristics have been determined for furnaces before 1977 and before modern flow modelling software. These furnaces consisted of a single tank with a throat compared to modern furnaces that consist of the melter, refiner waist and working end. The float furnace will also have either a flat or stepped bottom and a waist barrier.

The research that was conducted proved that the furnace mixing is a composite of all three response forms; plug flow, complete mixing or deadwater flow (Bamford, 1977). Some variables need to be defined before explaining these different flows.

- The colourant level (C_l) defined as the concentration of the colourant in the product as a fraction of the input.
- The residence time of the melter defined as:

$$t_r = \frac{M}{W} \tag{2.44}$$

With

M = furnace deadweight capacity (kg)

t_r = residence time (h)

W = throughput (kg/h)

For plug flow, there is no mixing and the colorant concentration will only change after the residence time of the furnace is reached as shown in Figure 2-6 (Bamford, 1977). Complete mixing works on the premise that there is instantaneous mixing and accordingly a uniform distribution of the glass in the furnace. Subsequently the concentration of the glass output will be the same as the glass in the furnace; with a response curve as shown in Figure 2-6 (Bamford, 1977) and described by Equation (2.45) (Bamford, 1977):

$$C_l = 1 - e^{\left(-\frac{t}{t_r}\right)} \tag{2.45}$$

With *t* the time in hours.

Deadwater flow is such that the majority of the flow is in a restricted channel effectively in a reduced furnace capacity. A percentage of the glass will be trapped in the "deadwater" with a larger residence time. The response curve is shown in Figure 2-6 (Bamford, 1977).

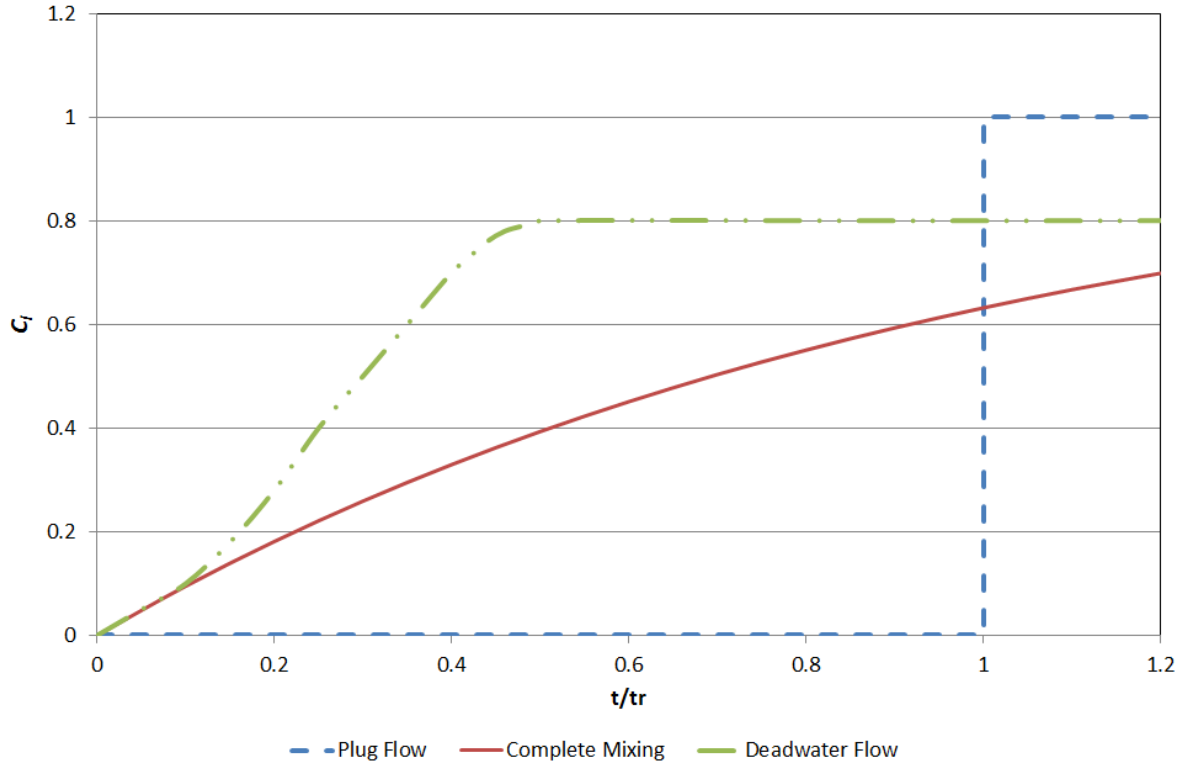


Figure 2-6: Possible response curves for glass mixing in a furnace (adapted from Bamford, 1977).

Cooper (1959) argued that any response curve is the result of multi complete mixing cells with a plug flow cell. More recently, Bergman (1999) created a mixing model from using a tracer input response on a new furnace. Four different mixing model combinations were tested namely plug flow with one perfect mixer, plug flow with two perfect mixers in series, plug flow with three perfect mixers in series and plug flow followed by two perfect mixers in parallel and 1 perfect mixer in series. The plug flow with perfect mixers in series and parallel was found to be the most accurate mixing model and is shown in Figure 2-7 (Bergman, 1999). The factor k is a fraction of the total flow through perfect mixer 1. Perfect mixer 2 is the stagnation cell and has a large effective volume. The volume of the perfect mixer cannot be bigger than the furnace volume and is therefore, compensated for by the recirculation flow. Bergman (1999) did recommend using a step change tracer rather than a pulse tracer to establish a response model.

There is a shortcoming in how the glass flow both from transfer flow and secondary flow, as mentioned by Cooper (1959), influences the mixing in a modern day float glass furnace; especially in cases where the secondary flows due to the thermal convection currents are changed when conditions in the melter is changed. Some of these conditions include the barrier, stirring speed, energy supplied to the glass by combustion or electrical heating and bubbling.

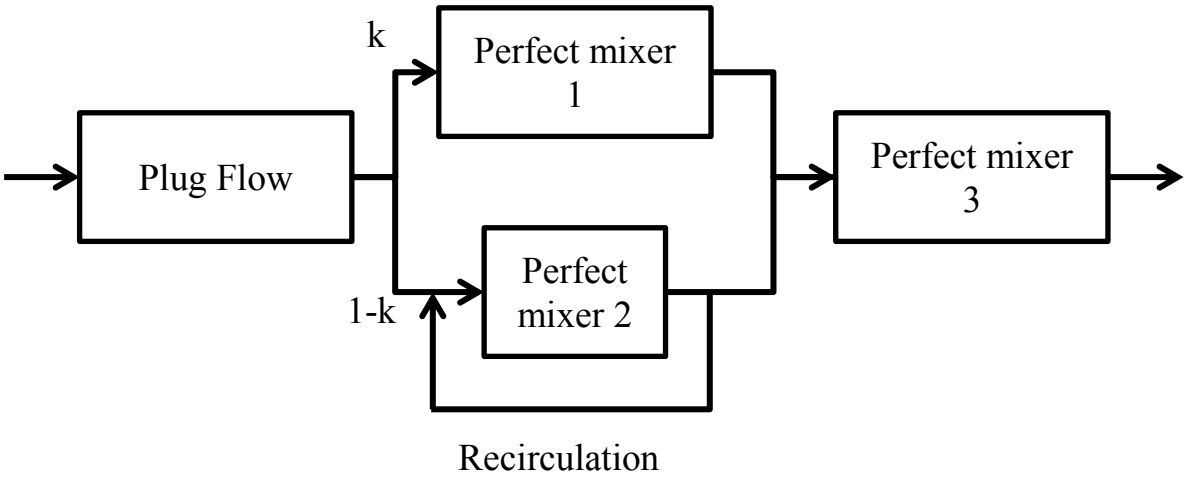


Figure 2-7: Mixing model developed by Bergman (1999)

2.6 Homogenization inside glass tanks and the colour rendering index

Chemical inhomogeneity in the glass gives different local refractive index. The human eye can see these differences in refraction of light. In float glass, optical distortion can be caused by either cords or differences in refractive index (Wijshoff et al., 2010). This inhomogeneity in the glass is measured by viewing the glass in refraction of light and assigning a colour rendering index or CRI number to it. With a CRI value of zero equal to no inhomogeneity. During colour changes a glass with different properties is added to the existing glass in the furnace. This creates chemical inhomogeneity and the glass will be out of specification until the chemical inhomogeneity is diffused. Homogenization of the melt is based on two principles micro-and-macro-mixing. Micro-mixing is the diffusion driven homogenization of the melt and is very slow. In practice micro-mixing cannot homogeneous the glass within the residence time for furnaces. Macro mixing is the physical blending of the melt where the stirring, convective flows, bubbling and other related processes will deform large inhomogeneity cords into longer, thinner cords due to shear forces (Wijshoff et al., 2010).

3 Modelling and Optimization Procedure

This study was divided into two different phases. Phase one was to understand the link between the flow inside the furnace and the mixing of the glass. This included a CFD model of the glass in the furnace and then using the data obtained from the flow model as a basis of creating the mathematical mixing model to predict the colour change time. Actual colour change data was then collected from the plant to validate the model.

The second phase of the study involved further simulation and optimisation studies towards different combinations of key variables during the colour change to achieve reduced colour change times.

3.1 Modelling procedure

3.1.1 Furnace glass flow modelling

The flow cells in the furnace were obtained from the CFD software ANSYS® Fluent. The development of the model consists of three main parts: drawing the geometry, setting up the mesh for the CFD solver and setting up the CFD solver. The geometry was drawn from the furnace design drawings, and exact position of the bubblers were verified from field observations. The furnace fits a hexagonal mesh that gives stable solving. The solver requires material properties, boundary conditions and the necessary governing equations with its relevant assumptions. The material properties were obtained in-house and the boundary condition fluxes and temperature profiles calculated with data obtained from the plant. A steady state model was done first to determine if the model is accurate before moving to a transient model. A starting point for the solver settings was obtained from ANSYS® Fluent training. The solver settings were then adjusted until the solution diverged. The solution was validated through comparison of plant and experimental data; and verified by adjusting the mesh size and using theoretical knowledge of glass flow inside a furnace.

3.1.2 Non-ideal reactor mixing model

The glass flow model obtained was used to create a one or two parameter mixing model for the furnace, which is a non-ideal reactor. This was done in Octave (2012). The results from this model was compared to actual data from the plant. The actual data from the plant included data already collected from previous colour changes as well as data that were collected for purpose of this study. This was to determine the chemical composition

distribution with time during the colour change at different stages inside the furnace. There were limited opportunities to take these samples because of limited colour changes from clear to tint. The root mean square error between the actual and theoretical data was be used to determine the accuracy of the model.

3.1.3 Method of glass sample collection during the colour change

The apparatus required for glass sample collection from the melter includes a stainless steel roller, stainless steel mold (10 cm in diameter and 3 mm thick), a stainless steel plate to pour the glass on and a steel ladle to scoop the glass from the furnace.

The samples were collected at different times from the start of the colour change and at different positions inside the furnace. The positions for collection are shown in Figure 3-1. Sample point 1 is at the feeder that represents the melter flow cell, sample point 2 was taken at the cold end and represents the outlet glass. Glass from sample point 1 was taken from the top surface of the molten glass and gave some degree of error as the sample may not represent the bulk of the glass. Samples for position 2 was taken every 2 hours from the start of the first composition change. Samples for position 1 was taken every 6 hours starting from 4 hours after the first composition change. The sample at position 1 could only be taken every 6 hours because of the high risk in this area. Samples for position 2 was from the end of the process where the glass is already annealed and could be taken more frequently.

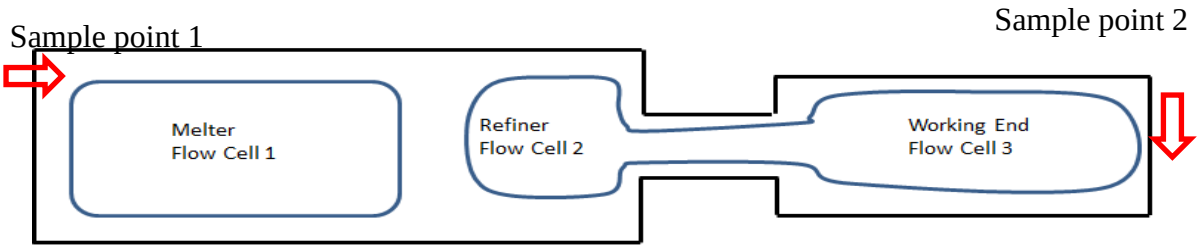


Figure 3-1: Sampling points in the furnace

The samples for position 1 were taken by inserting the ladle into the furnace. A small glob of glass was then scooped into the mould that was placed on top of the stainless-steel plate. The roller was then used to roll the glass flat for the laboratory to easily analyse the glass. Samples for position 2 were taken as a sample plate from the end of the line. All samples were analysed at the PFG laboratory, using standard procedures that comply with the standards for float glass sample analysis.

4 Glass Flow Modelling

4.1 Geometry

The model requires a geometry of the furnace to be drawn in the CFD software. A general furnace layout with the inlet and outlet is shown in Figure 4-1.

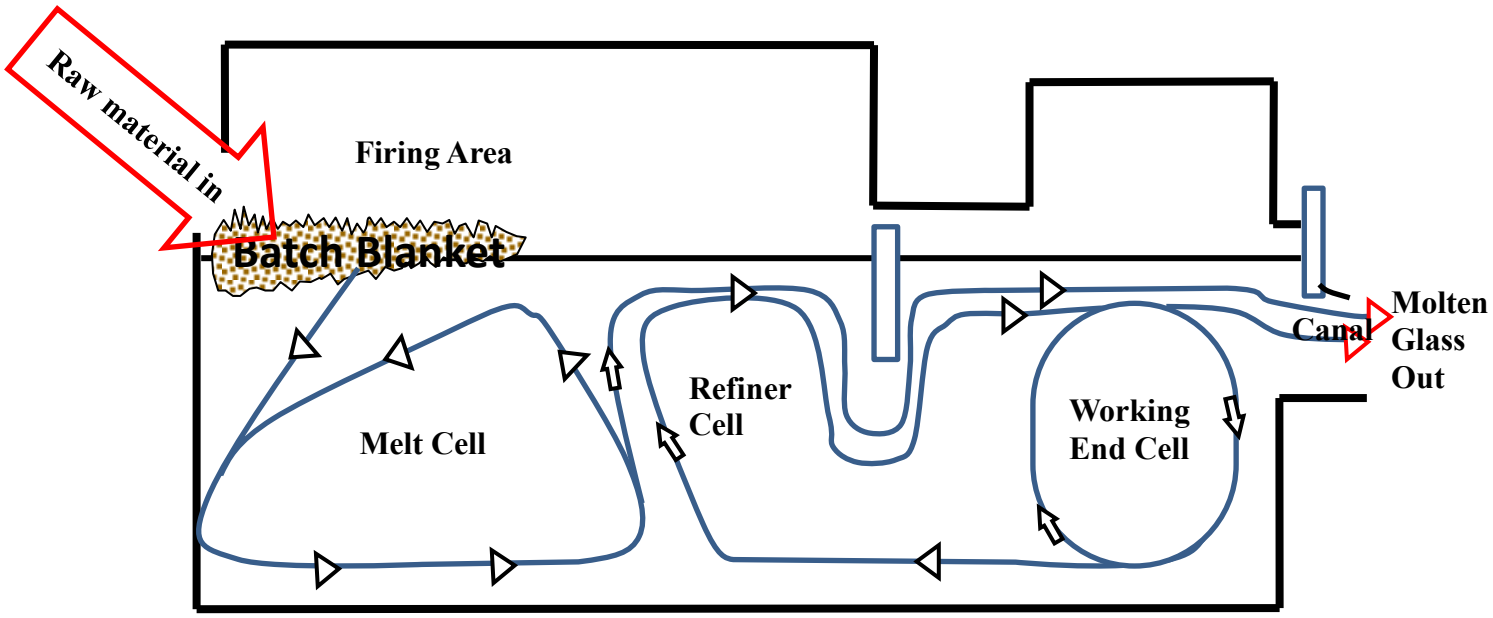


Figure 4-1: Cross section in length of a glass-melting furnace (adapted from Feng et al., 2008)

The strategy of solving the model has to be identified before creating the geometry as all the boundaries are already identified in the CFD software. The strategy used to model the glass flow in the furnace is described below.

The batch can be modelled in the CFD software but gives uncertainties when included in the model due to the complexity of the batch melting and the interaction between the batch and the glass. It was decided to exclude the batch blanket from the model. The inlet was placed in port 2, shown in Figure 4-2. This is where the batch blanket is completely melted in the furnace that was modelled. Only the top part of the inlet section was used as the inlet. The heat loss or gain from the glass to the batch blanket was then calculated and used as the heat flux boundary condition from section 0 up to the inlet for the layout provided in Figure 4-2.

The firing area was excluded and the heat loss or gain into the glass from the fired area was calculated from theory and used as a heat flux boundary condition.

The furnace was divided into 17 different sections namely section 0, doghouse, port 1, port 2 upstream, inlet, port 2 dowsntream, port 3, port 4, port 5, refiner, waist, working end, canal, bubbler 2, bubbler 3, bubbler 4 and bubbler 5. It was decided to do a symmetry model of the furnace, shown in Figure 4-3, to reduce the amount of cells by half and therefore, reducing the computing time. The bubblers were drawn as a separate volume from 0.3 m into the melter to the top of the glass volume, with the area of the bubbler pipe cut out of the glass volume. The barrier was drawn as a section cut through the waist with walls at the barrier and the glass volume joint that will be used as a heat flux boundary describing the heat loss from the glass to the barrier. The height of the barrier was defined as a variable set so that it could be moved up and down. The transition from clear to tint was investigated in this study and therefore three barrier depths studied at 0.508 m , 0.3048 m and 0 m with the glass depth at 1.169 m. All sections were chosen to be fluid and was grouped under 1 part named the glass volume.

Named selections were created in the CFD software. These named selections describe the boundaries of the glass volume. Every section except the bubblers and barrier has a side, bottom, top and symmetry wall. The bubblers have a top and glass contact wall with only bubbler 5 having an additional symmetry wall as the symmetry of the furnace, is through bubbler 5. The barrier has a glass contact wall. The list of named selections is provided in Table 4-1.

4.2 Meshing

The Furnace consists mainly of rectangular dimensions except for the bubblers and canal. The automatic mesh option with a maximum face size of 0.1 m, in the CFD software gives a hexagonal mesh with 384 235 cells and a minimum Orthogonal quality of 0.21 which is above the minimum allowed for a good mesh of 0.01 in the CFD software. The standard mesh options were chosen. This mesh was refined later and explained in more detail in section 4.4. The mesh for the furnace is shown in Figure 4-4 and Figure 4-5.

Table 4-1: List of named selections for the flow model

Named Selection	Location in glass volume
Inlet	Top of inlet
Outlet	exit of canal
Furnace top	Top Section 0 to refiner excluding inlet
Working end top	Top waist to canal
Furnace sidewall	Side of section 0 to refiner
Waist sidewall	Side of waist
Working end sidewall	Side of working end and canal
Furnace bottom	Bottom section 0 to refiner
Waist bottom	Bottom waist
Working end bottom	Bottom working end
Canal bottom	Bottom canal
Barrier wall	Area of barrier and glass contact
Bubbler 2 wall	Bubbler and glass contact
Bubbler 3 wall	Bubbler and glass contact
Bubbler 4 wall	Bubbler and glass contact
Bubbler 5 wall	Bubbler and glass contact
Symmetry wall	Section through centre line of furnace

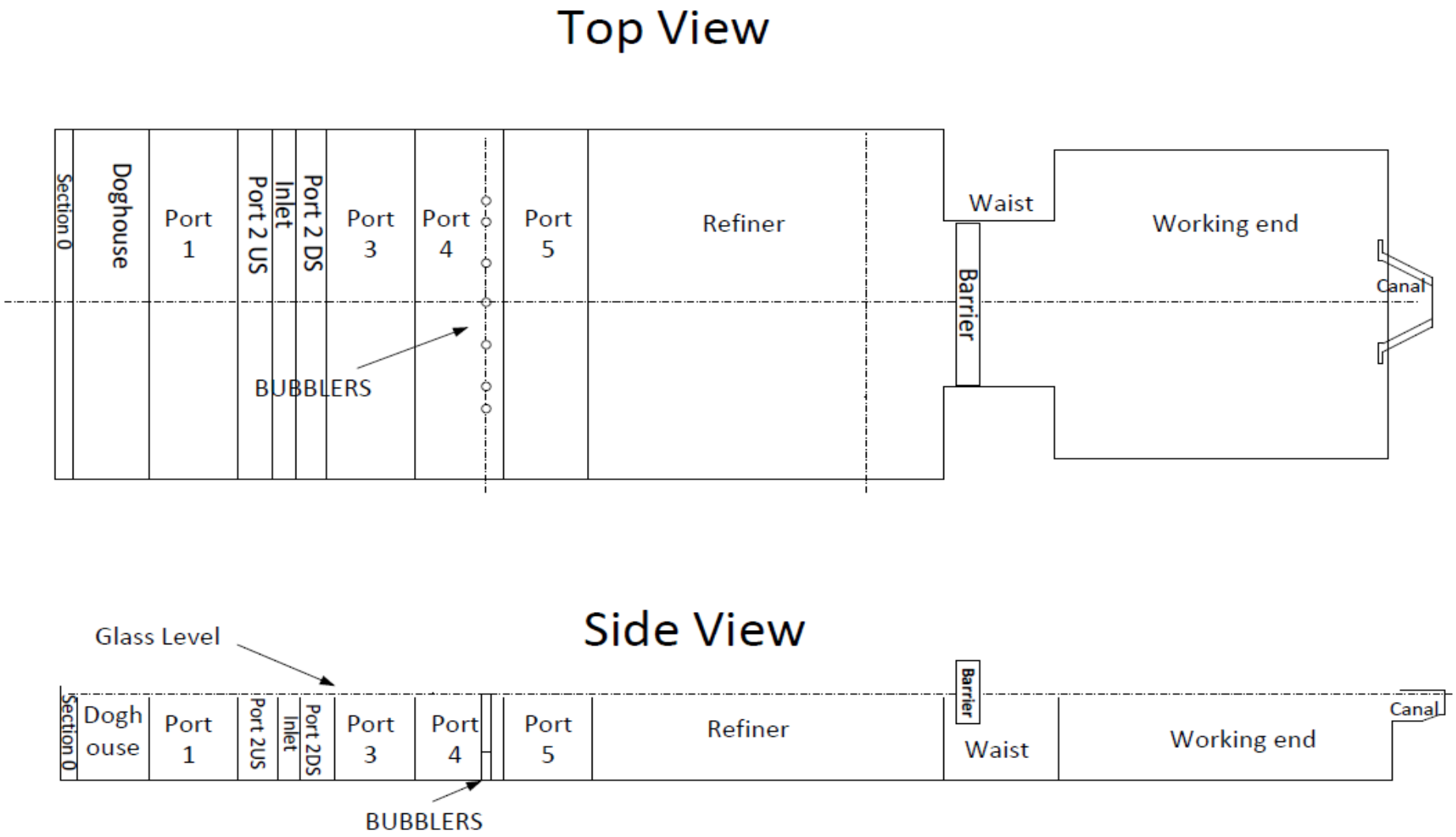


Figure 4-2: Layout of the furnace with the different sections

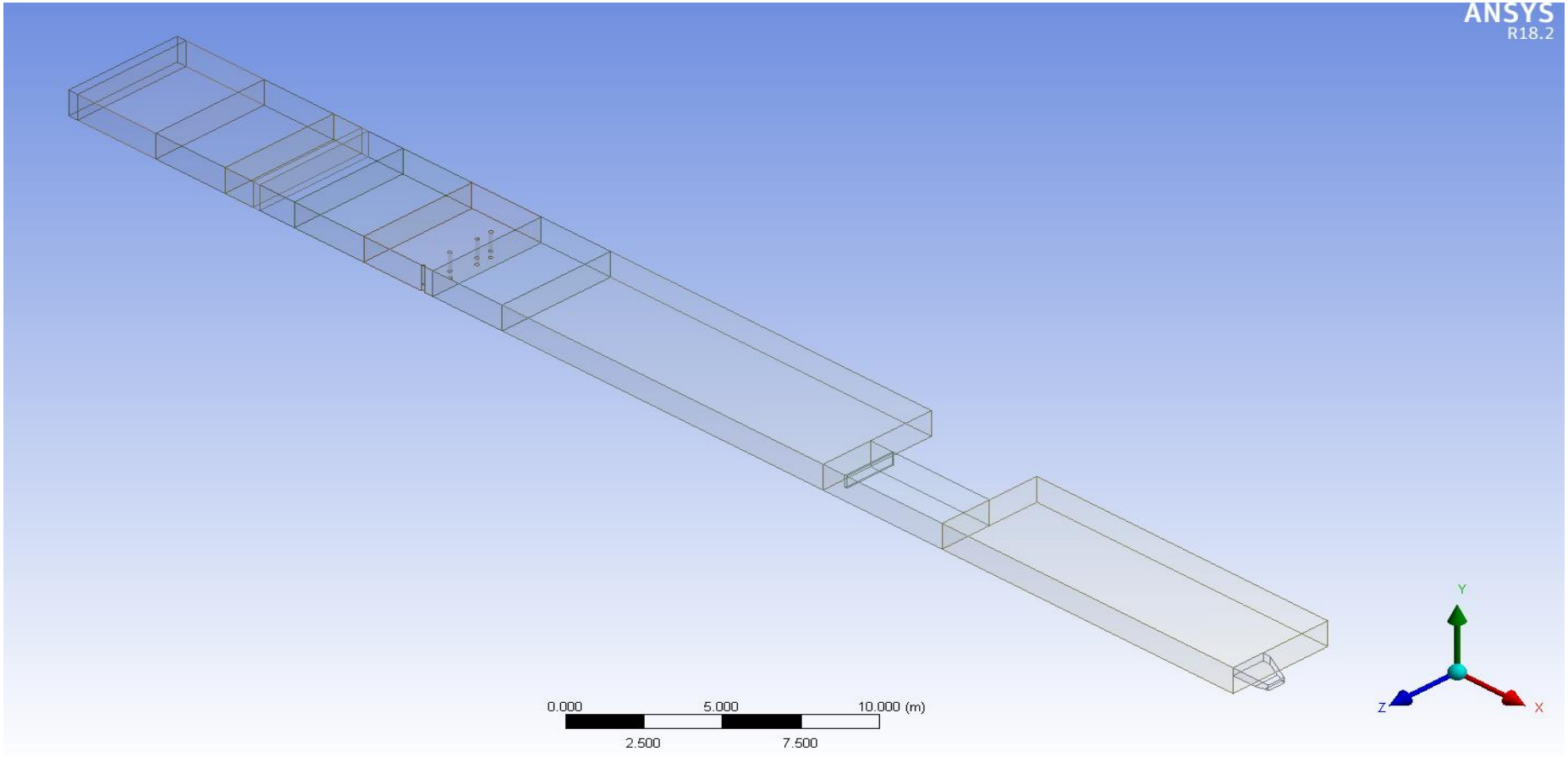


Figure 4-3: Layout of the furnace

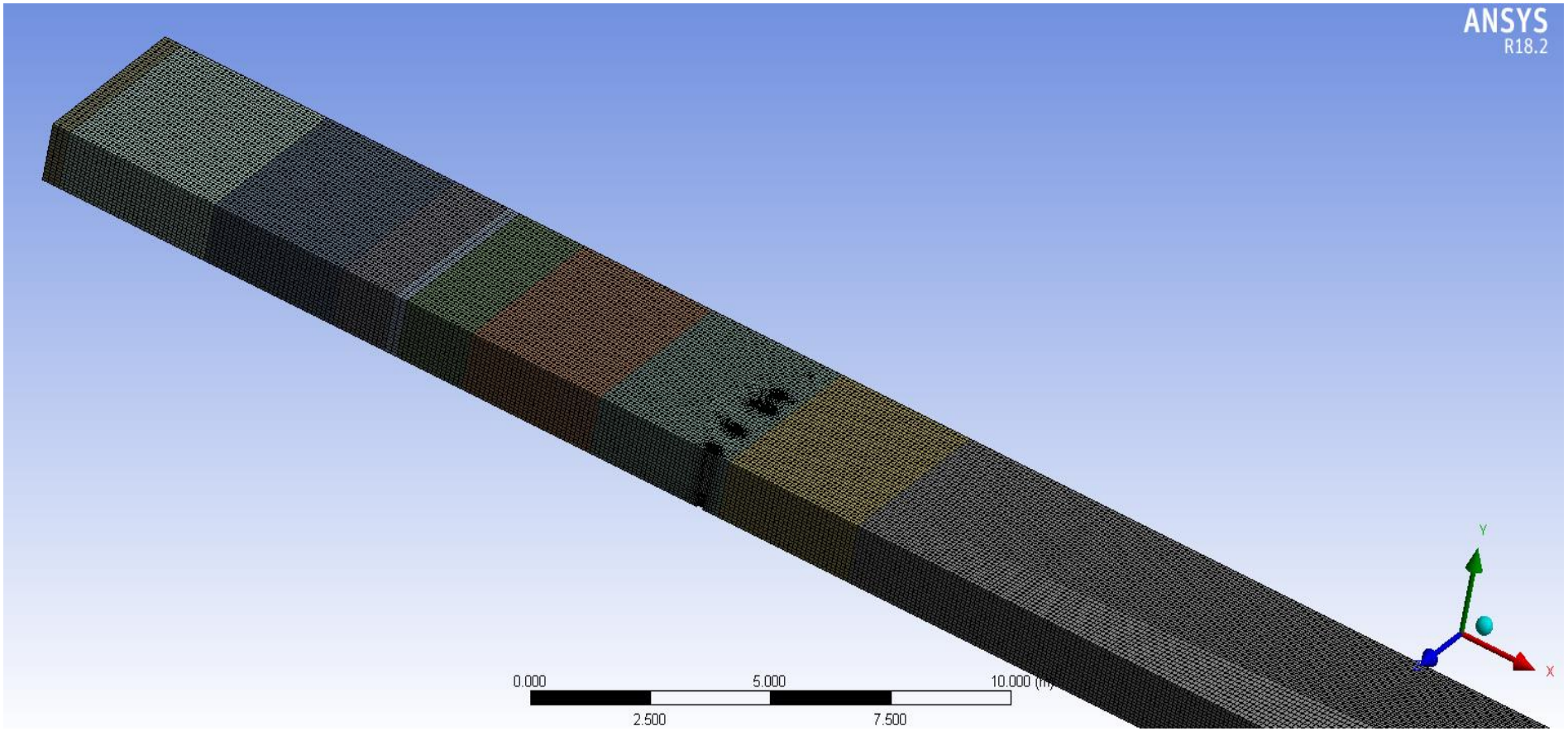


Figure 4-4: Hexagonal Mesh of 0.1 m layout for the furnace up to refiner

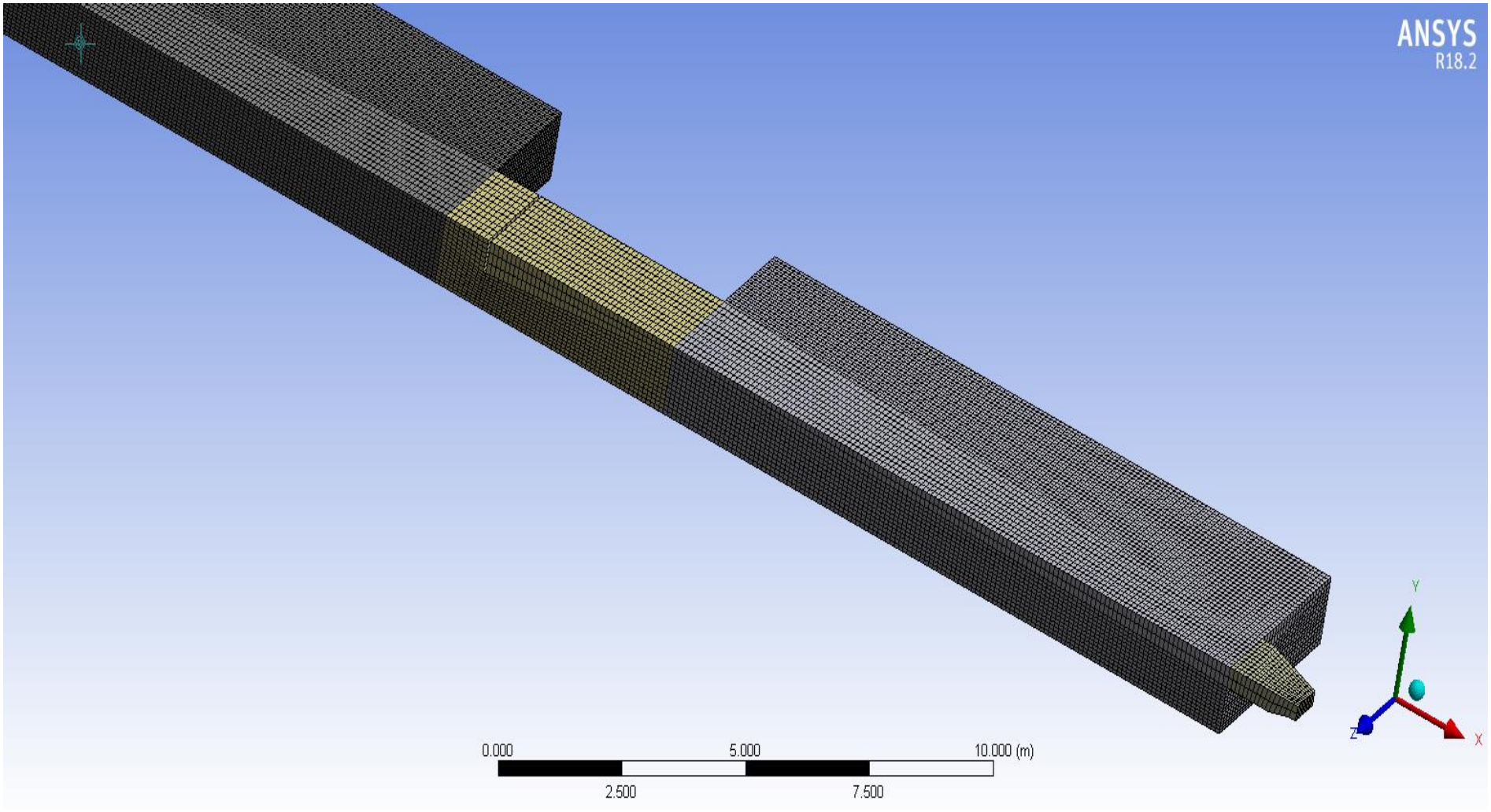


Figure 4-5: Hexagonal Mesh of 0.1 m layout for the refiner up to the canal

4.3 Steady state solver set-up and optimization

4.3.1 Solver and governing equation selection

When opening the CFD software select double precision solver because of the number of significant figures required due to the glass model that has a high aspect ratio and the glass properties and flow that vary on the decimal place.

The pressure-based solver was chosen with absolute velocity formulation. The pressure-based solver was historically developed for low velocity incompressible flows which is applicable to glass flow in a furnace. The SIMPLE method is used due to the large amount of equations to be solved. The solution will converge slower but every calculation step will be faster.

The mass, momentum and energy equations were selected. The Reynolds number was calculated from Equation 4.1 (Cengel, 2006).

$$Re = \frac{\rho v_{avg} L}{\mu} \tag{4.1}$$

With ρ, the density in kg/m^3; v_{avg}, the average velocity in m/s; L, the characteristic length in m; and μ, the dynamic viscosity in kg/(m·s). The average velocity of glass in the furnace was around 0.01 m/s, the average density was 2400 kg/m^3, the characteristic length 55.195 m and the average viscosity was 100 kg/(m·s). With the values substituted into Equation (4.1) a Reynolds number of 13 was obtained, making the flow of glass laminar and therefore, the viscous model was chosen as laminar. Gravity was selected with the acceleration of gravity 9.8 m/s^2 in the negative y-direction shown in Figure 4-3.

4.3.2 Glass properties

Glass properties were obtained in-house. The temperature dependant equation for density is:

$$\rho = 2674.69465 - 0.19445T \tag{4.2}$$

With ρ, the density in kg/m^3 ; and T, the temperature in K.

The temperature dependant equation for specific heat is:

$$C_p = 1051.94108 + 0.32985T - 7.41422 \times 10^{-5}T^2 \quad (4.3)$$

With C_p, the heat capacity in J/(kg·K); and T, the temperature in K.

The temperature dependant equation for effective thermal conductivity is:

$$k = -1.77379 + 0.00753T - (6.42503 \times 10^{-6}T^2) + (1.40151 \times 10^{-8}T^3) \quad (4.4)$$

With k, the thermal conductivity in W/(m·K); and T, the temperature in K.

The temperature dependant equation for viscosity is:

$$\mu = 10^{-2.845+\frac{4644.0189}{T-507.333567}} \quad (4.5)$$

With μ, the viscosity in kg/(m·s); and T the temperature in K.

Three temperature ranges were defined and used in this study, 0-1073 K, 1073-2000 K and 2000-2100 K. A constant value for all the glass properties was used for the range of 0-1073 K and 2000-2100 K, as the properties are only defined between 1073 and 2000 K. Furthermore, the maximum temperature glass reaches in a furnace is around 1900 K and glass becomes almost stagnant at temperatures below 1000 K in the furnace. The constant values for the different properties are shown in Table 4-2. The density, specific heat and thermal conductivity were defined as piecewise polynomial in the range 1073-2000 K. The viscosity was calculated from a user-defined function or UDF with Equation 4.5. The UDF is shown in Appendix A.

Table 4-2: Glass properties

Temperature Range	Density	Heat capacity	Thermal conductivity	Viscosity
K	**kg/m3**	**J/(kg·K)**	**W/(m·K)**	**kg/(m·s)**
0-1073	2466	1321	16.23	704
2000-2100	2272	1417	111	1.32

4.3.3 Cell zone and boundary conditions.

The cell zone conditions for all the sections were chosen as glass fluid. The bubblers had an additional source term defined by a UDF. The source term was used as a y-momentum source term (opposite to direction of gravity). The background to the UDF is explained in section 2.3.9 and the UDF given in Appendix B.

The inlet boundary condition was chosen as a mass flow inlet at a temperature of 1590 K with a mass flux normal to the boundary of 1.29 kg/(m^2s). This mass flux is calculated from the load of the furnace, which was 2290 tons per week, over an area of 2.928 m^2. The outlet was defined as an outflow with a flow rate weighting of one. All the other boundaries are wall boundaries.

The glass top surface boundary is the most complex and inaccurate boundary to estimate in terms of energy in or out of the boundary. The most accurate option would be to model the combustion space and the batch blanket, but this would require a large amount of time and computing power. To simplify the model the combustion space was not modelled. Instead one of two possible conditions was used, the temperature profile boundary condition with a UDF or the heat flux boundary condition. The temperature profile boundary condition is the more accurate of the two options and was tested, but the solver did not converge with this boundary condition. Therefore, the top surface of the glass was defined as stationary walls with zero specified shear as the glass has little or no shear due to the interface with the combustion space. The shear force between the glass and batch blanket was not taken into account as the inlet velocity of the glass is taken as the negative y-direction and will create a force on the return flow. The thermal boundary condition was defined as a heat flux, based on a combustion yield in the range of 0.5 to 0.8, and included the energy required to melt the batch in the necessary sections. The calculation for the top surface heat flux is shown in Appendix C. The fluxes for the top surface boundaries are shown in Table 4-4.

The boundaries for the sidewalls and bottoms were defined as stationary walls with the no slip condition due to the interface of the glass with the refractory wall. The thermal boundary condition was specified as heat flux. The heat fluxes for the sidewall and bottom boundaries are shown in Table 4-3.

Table 4-3: Side and bottom wall heat flux.

Section	Heat Flux Theoretical kW/m^2
Canal bottom	0.0
Bottom doghouse	-2.0
Bottom Port 1	-2.0
Bottom Port 2	-2.0
Bottom Port 3	-2.0
Bottom Port 4	-2.0
Bottom Port 5	-2.0
Furnace bottom Refiner	-2.0
Bottom Section 0	-2.0
Furnace side wall doghouse	-5.0
Furnace side Port 1	-5.0
Furnace side Port 2	-5.0
Furnace side Port 3	-5.0
Furnace side Port 4	-5.0
Furnace side Port 5	-5.0
Furnace side refiner	-3.0
Side Section 0	-9.0
Waist bottom	-0.6
Waist side	-5.0
WE bottom	-0.6
Canal side	-0.4
Working End side	-2.6

Table 4-4: Top surface heat flux.

Section	Heat Flux Theoretical kW/m^2
Top Section0	-58
Doghouse top	-179
Top Port 1	-52
Top Port 2 upstream	69
Top Port 2 downstream	81
Top Port 3	144
Top Port 4	154
Top Port 5	113
Top Refiner	1
Canal Top	0
Waist Top	-5
Working End Top	-3

The boundaries for the interface between the bubbler pipe and the glass was defined as stationary walls with the no slip condition due to the interface of the glass with the refractory wall. The thermal boundary condition was specified as zero heat flux because the local cooling effect it has modifies the CFD model in such a way that it becomes unstable.

The boundary for the interface between the barrier and the glass was defined as stationary walls with the no slip condition due to the interface of the glass with the barrier wall. The thermal boundary condition was specified as a heat flux of –230 000 W/m^2.

The operating pressure was defined as 101325 Pa. The Boussinesq operating temperature was defined as 1600 K and the operating density as 2500 kg/m^3. Temperature limits were defined as 300 and 2100 K.

4.3.4 Discretization

The method used for the discretization was “PRESTO!” for pressure, first order upwind for both momentum and energy and least squares cell based for the gradient. The choice of discretization was obtained from ANSYS® (2005).

4.3.5 Under-relaxation factors

The proposed under relaxation factors for glass given by ANSYS® (2005) is 0.3 for pressure, 0.5 for body forces, 0.2 for momentum and 0.9 for the energy equation. ANSYS® (2005) suggests solving the model for a few 100 steps and then increasing the under-relaxation factor for pressure to 0.5, body force to 0.7 and momentum to 0.3 while changing the under-relaxation factor for energy slowly to 0.99.

Schäfer (2006) states that typical values for the pressure under-relaxation factor is between 0.2 and 0.4; and that all the under-relaxation factors are interdependent. It is a trial and error method to determine which under-relaxation factors are optimal for the model that is being solved. The optimal under-relaxation factor was found to be 0.3 for pressure, 1 for density, 0.7 for body forces, 0.05 for momentum and 0.98 for energy. Start with the under-relaxation factor for momentum above 0.2 and the energy on 0.9 before working to 0.05 and 0.98 respectively. Figure 4-6 shows the residuals with the optimised under-relaxation factors. The solution converges well within 2000 iterations. The energy residuals drop to below 10^{-6} and the rest of the residuals drop below 10^{-3} except for the y-velocity, because of the large velocity gradients in the y-direction. See Appendix D for the plot of four important temperatures namely filling pocket temperature, bottom hotspot temperature, outlet temperature and crown temperature. These temperatures converge to a specific temperature showing that the model is converging.

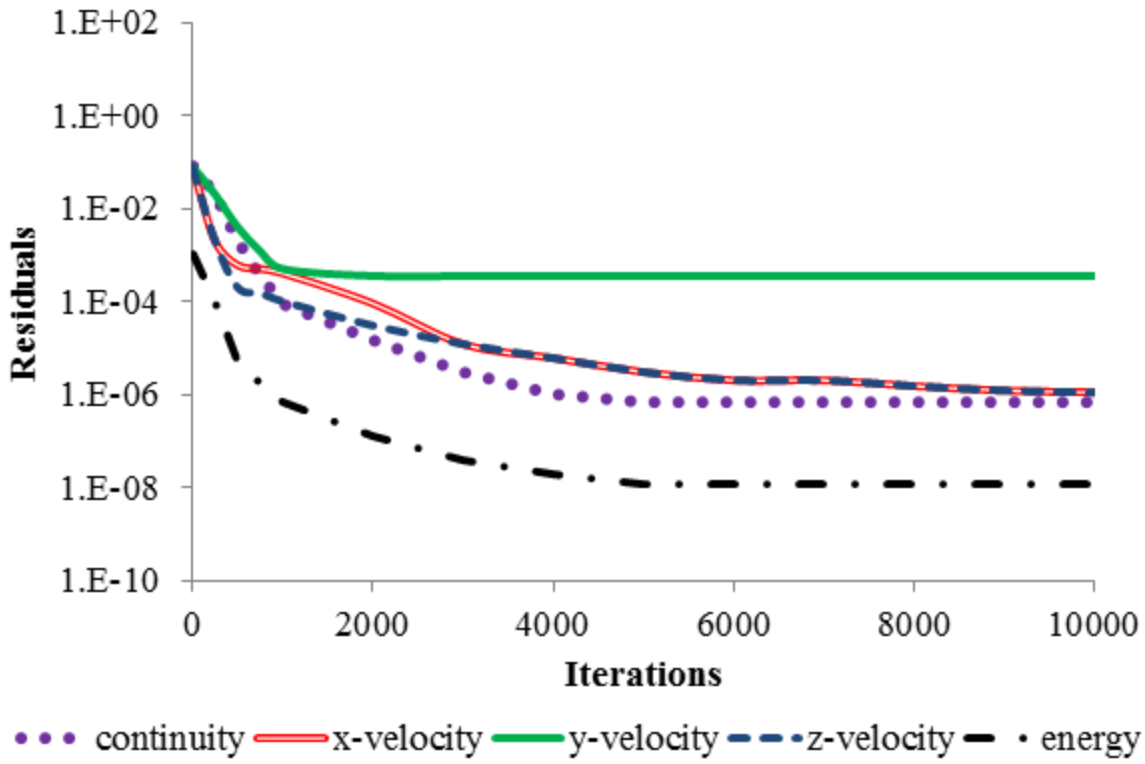


Figure 4-6: Residuals for optimised under-relaxation factors.

4.4 Verification and validation

Verification was divided into four sections namely flow patterns of glass, boundary conditions, mass and energy conservation and discretization error. Validation was done by checking the model temperatures with actual temperatures from the furnace.

4.4.1 Glass flow patterns

The glass flow pattern that is expected was shown in Figure 4-1. Figure 4-7 shows the horizontal or x-velocity component in the furnace. The white coloured section is velocities close to zero and indicates a transition region or boundary between forward flow and back flow. The uprise position is also indicated by this boundary layer. The glass flows back to the doghouse at the top and forward at the bottom, which is correct. There is a small uprise at the bubblers. Initially the bubbler flow was taken as 0.4 m/s or 20 bubbles/min but was reduced as this fixed the uprise at the bubblers, which is not the case in the actual furnace based on the temperatures. The velocity at the bubblers was reduced to 0.002 m/s or 1 bubble/min which gave more accurate description of the flows and temperatures in the furnace. The reason for this is that there is a shear force between the glass and the bubbles which will cause the glass to flow at a much lower velocity than the bubble rise velocity. With the UDF it is assumed

that the glass velocity is the same as the bubble rise velocity. Therefore, it was necessary to reduce the velocity in the UDF to get a more accurate representation.

Figure 4-8 shows the flow of the glass from the bubblers up to the barrier. As expected the uprise starts in the refiner at the bottom and ends at the bubblers on the top. Figure 4-9 shows the recirculation of glass in the working end with glass flowing from and to the refiner.

The glass flow when viewed from the top on the top surface is shown in Figure 4-10. The uprise position at the top is at the bubblers and the glass flows to the doghouse and to the barrier on the top with the glass flowing to the canal in the working end, which is as expected. Figure 4-11 shows the glass flows viewed from the top with a section made 0.3 m from the bottom of the furnace. It shows that the position of the uprise at the bottom is in the refiner and that the glass flows from the doghouse and refiner to the uprise position at the bottom. The glass also flows back from the canal to the refiner in the working end at the bottom. All of this is as expected. Figure 4-12 shows the glass flow at the doghouse or filling pockets and the flow is as expected with the uprise in the centre and down flow on the side. The flow at the bubblers in Figure 4-13 indicates that the glass flows up at the bubblers at a velocity of around 0.002 m/s. All the glass flows are as expected when compared to theoretical knowledge.

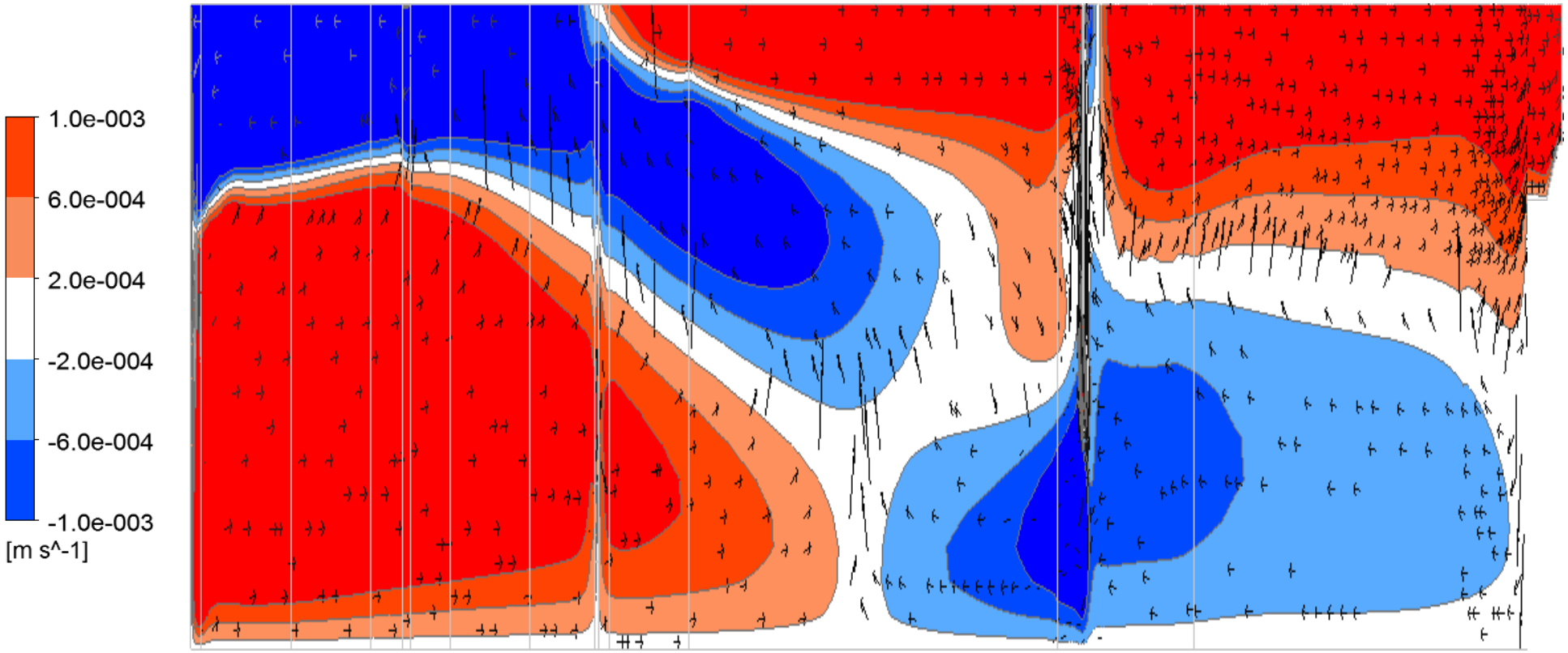


Figure 4-7: Schematic viewed from the side of the furnace showing the x-velocity component for the whole furnace.

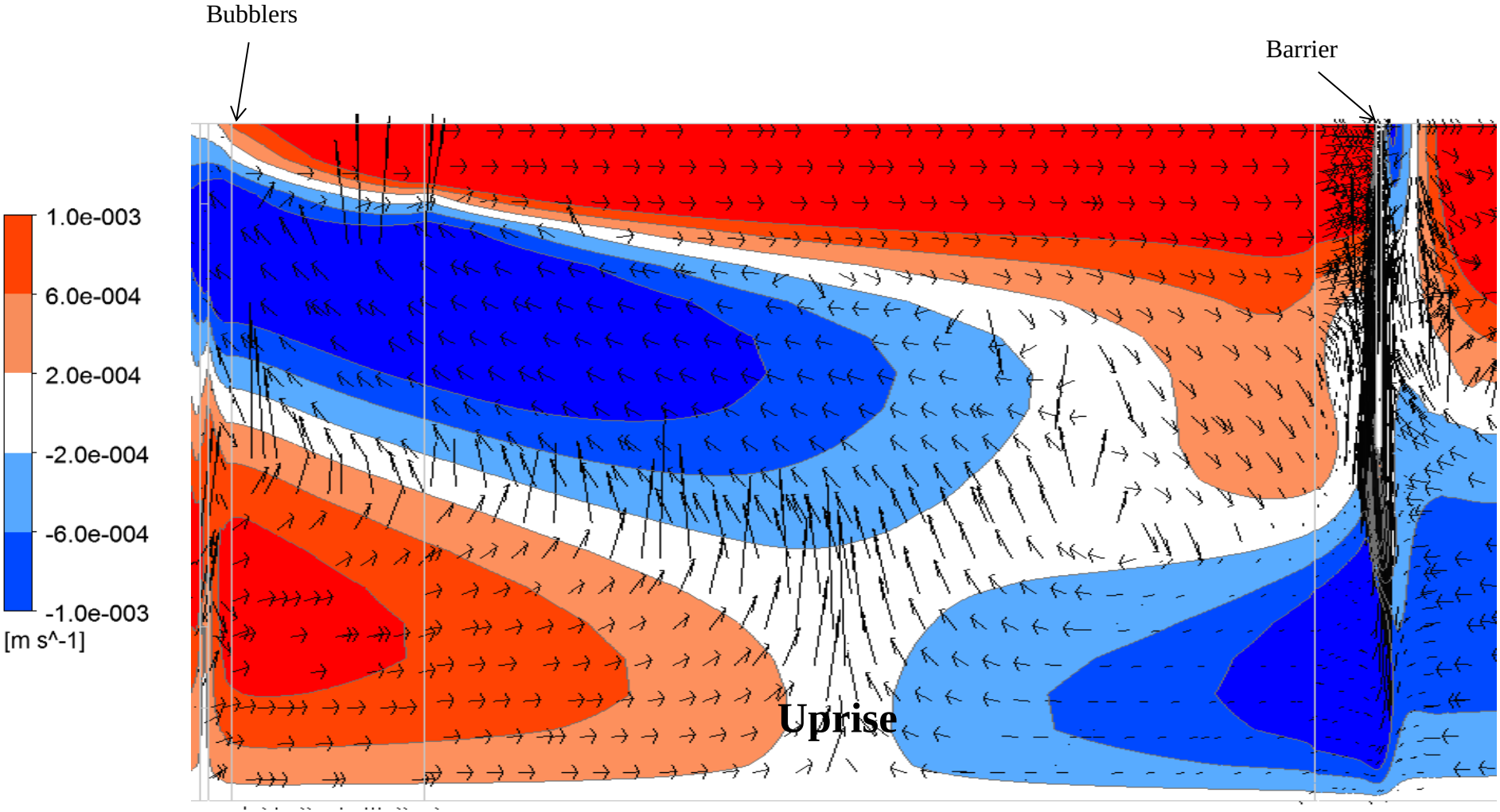


Figure 4-8: Schematic viewed from the side of the furnace showing the x-velocity component from the bubblers to the barrier.

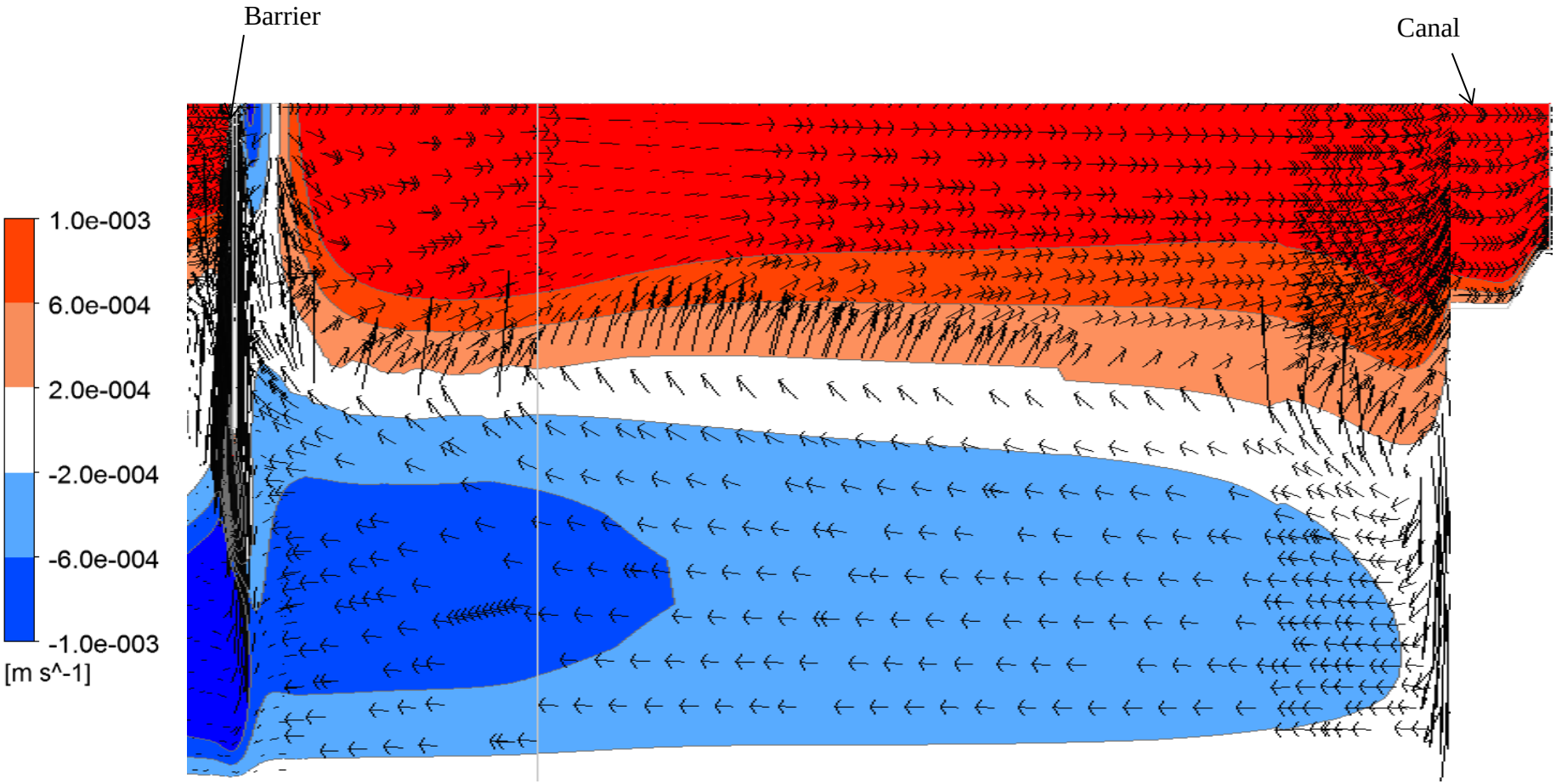


Figure 4-9: Schematic viewed from the side of the furnace showing the x-velocity component in the working end and canal.

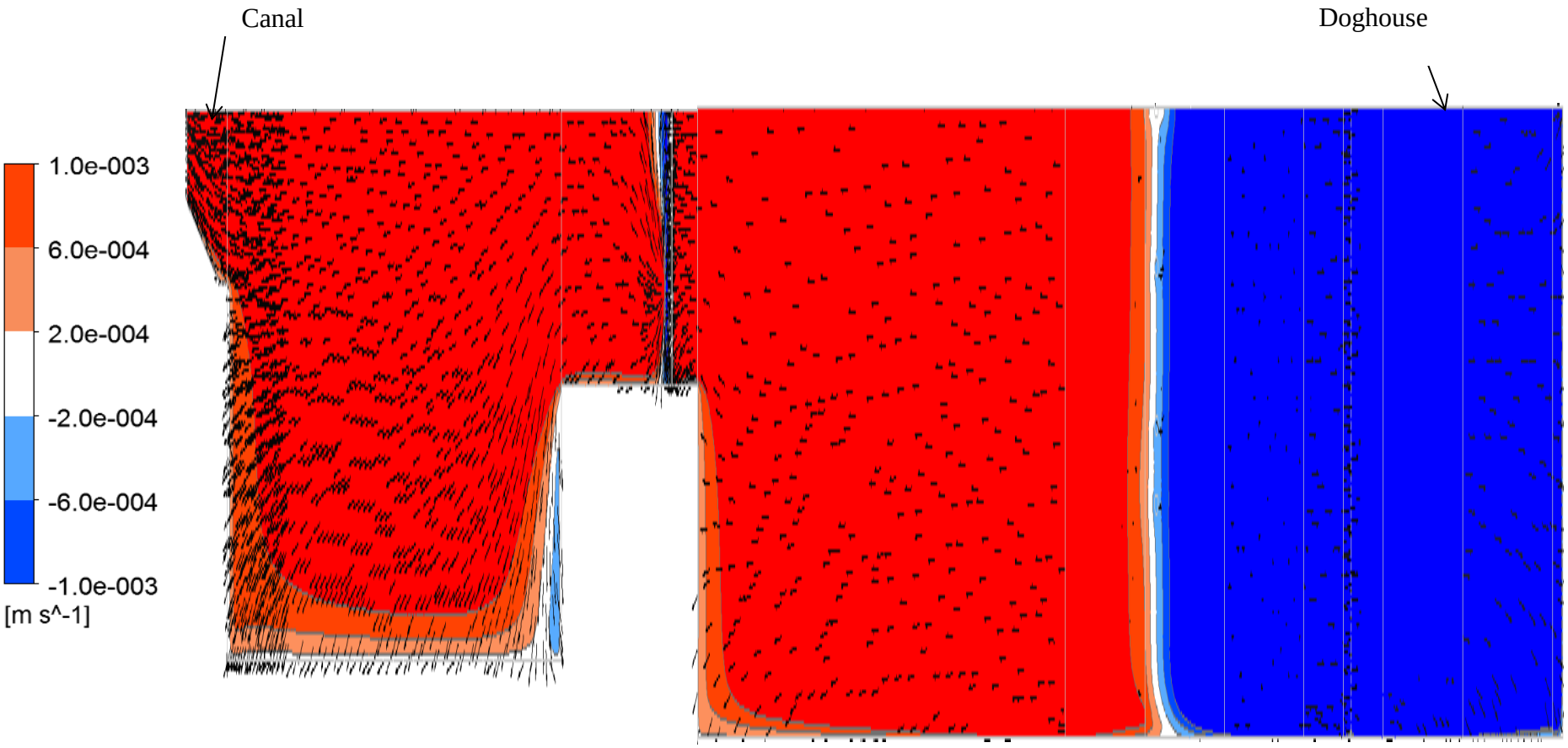


Figure 4-10: x-velocity component viewed from the top, with a section trough the top surface of the glass volume.

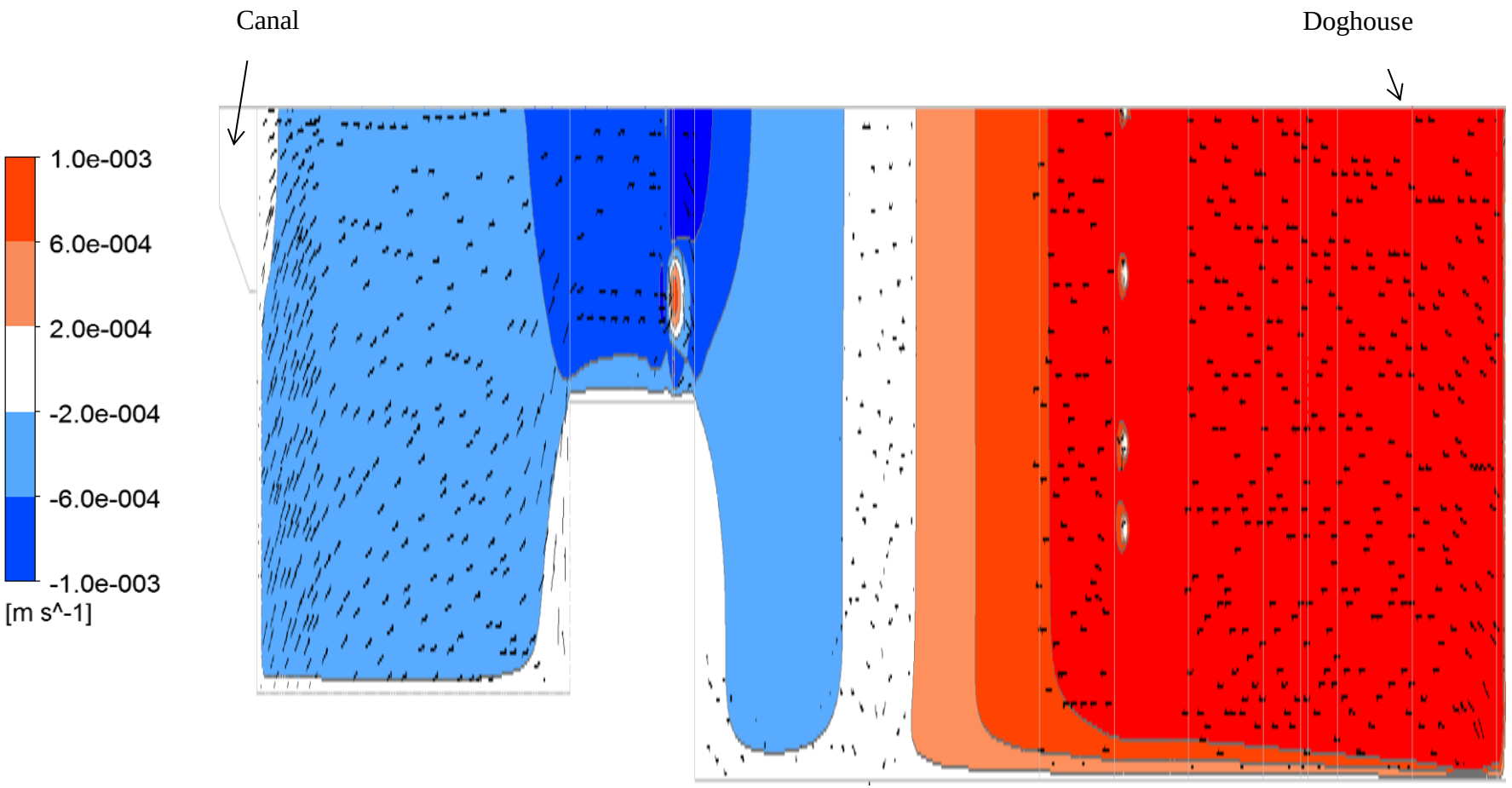


Figure 4-11: x-velocity component viewed from the top, with a section made 0.3 m from the bottom of the glass volume.

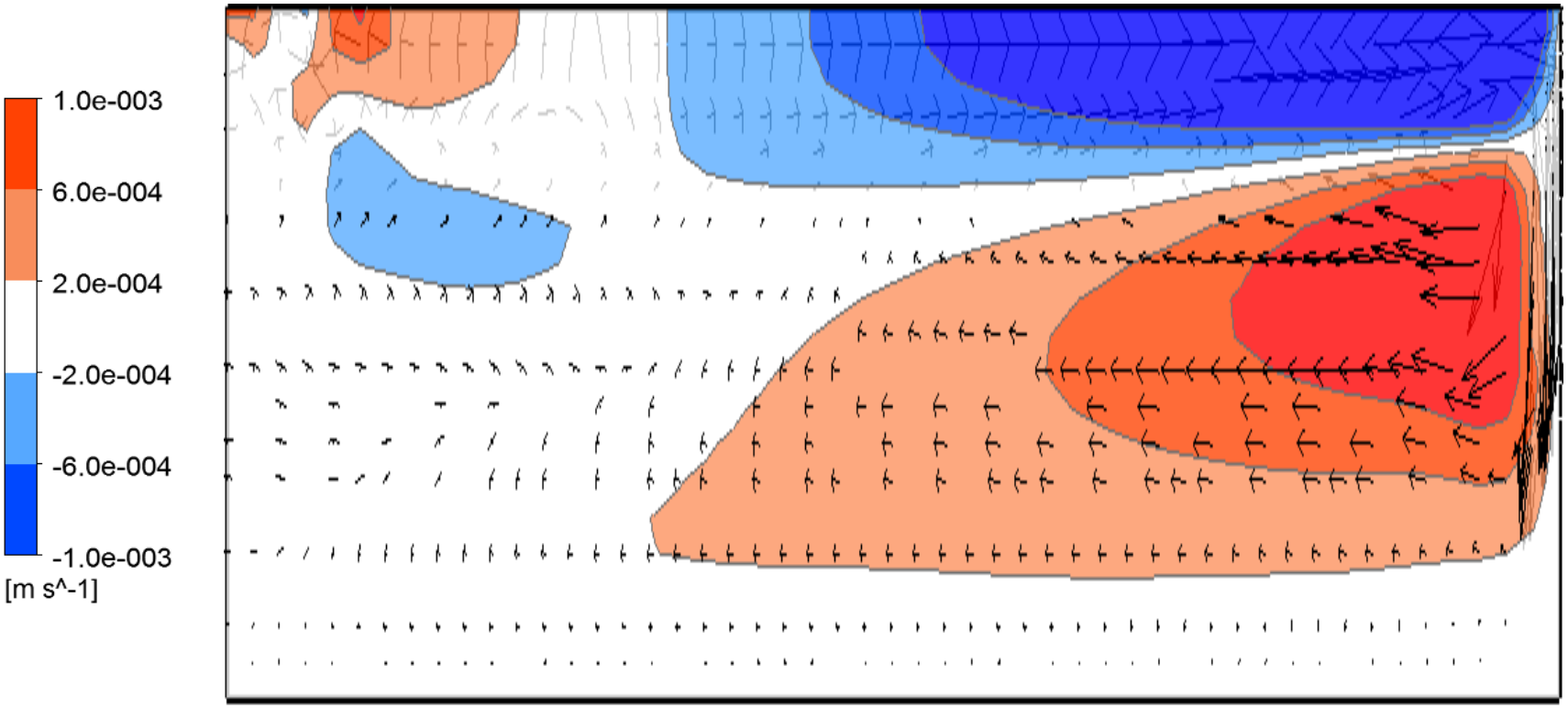


Figure 4-12: z-velocity component at the doghouse, with a section made at the doghouse through the glass volume height.

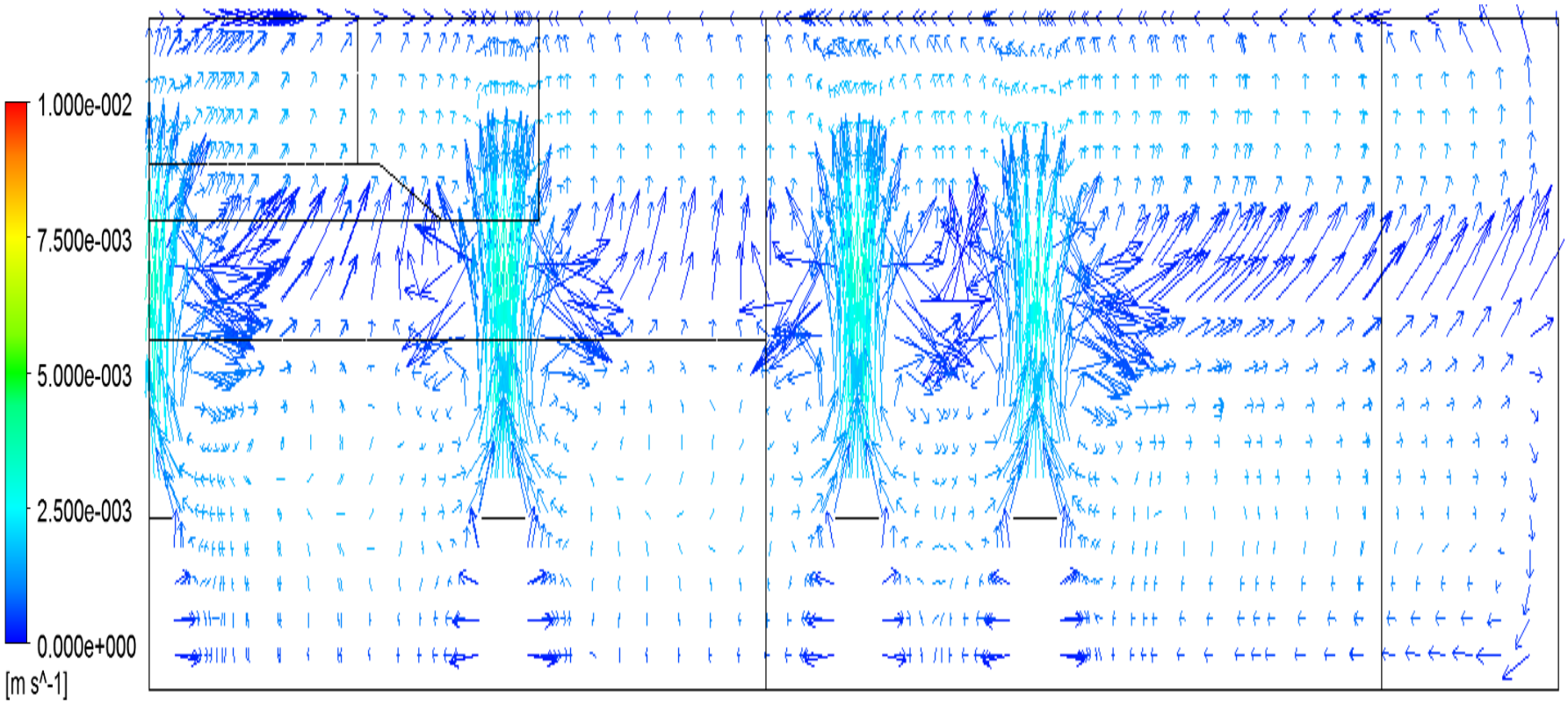


Figure 4-13: Velocity magnitude of glass at the bubblers, with a section made at the bubblers through the glass volume height

4.4.2 Boundary conditions and mass and energy conservation

The mass in and mass out = 1.88856 kg/s or 1 137 tons per week. It would be 2274 tons per week if the full model was used instead of the symmetry model. The CFD model and theoretical boundary conditions is shown in Table 4-5 and Table 4-6, respectively. The top surface heat flux was adjusted from theoretical values to get more accurate model temperatures. The large differences between the CFD model and theoretical heat flux are at the section with the batch blanket and the working end. The difference for the working end is because of over estimation of superstructure heat loss. The difference for the batch blanket section is mainly because the energy to melt the batch is more than what theory predicts. This is because every batch has its own unique heat of reaction and heat capacity that has to be determined experimentally. The heat of reaction and heat capacity used in this study was obtained from theoretical calculations based on other batches as shown in Appendix C.

The difference between energy in and energy out for the whole furnace comes to 38 W which is 0.0004 % of the total energy in or out. All the heat loss and gain from the glass model is shown in Table 4-7.

Table 4-5: Top surface heat flux

Section	Heat Flux Model kW/m2	Heat Flux Theoretical kW/m2	Percentage Difference
Top Section0	-120	-58	107%
Doghouse top	-215	-179	20%
Top Port 1	-140	-52	169%
Top Port 2 upstream	30	69	57%
Top Port 2 downstream	80	81	1%
Top Port 3	168	144	17%
Top Port 4	168	154	9%
Top Port 5	124	113	9%
Top Refiner	1	1	9%
Canal top	0	0	0%
Waist top	-5	-5	1%
Working End top	-5	-3	73%

Table 4-6: Bottom and side wall heat flux

Section	Heat Flux Model kW/m2	Heat Flux Theoretical kW/m2	Percentage Difference
Canal bottom	0.0	0.0	0%
Bottom doghouse	-2.0	-2.0	0%
Bottom Port 1	-2.0	-2.0	0%
Bottom Port 2	-2.0	-2.0	0%
Bottom Port 3	-2.0	-2.0	0%
Bottom Port 4	-2.0	-2.0	0%
Bottom Port 5	-2.0	-2.0	0%
Furnace bottom Refiner	-2.0	-2.0	0%
Bottom Section 0	-2.0	-2.0	0%
Furnace side wall doghouse	-5.0	-5.0	0%
Furnace side Port 1	-5.0	-5.0	0%
Furnace side Port 2	-5.0	-5.0	0%
Furnace side Port 3	-5.0	-5.0	0%
Furnace side Port 4	-5.0	-5.0	0%
Furnace side Port 5	-5.0	-5.0	0%
Furnace side refiner	-3.0	-3.0	0%
Side Section 0	-9.0	-9.0	0%
Waist bottom	-0.6	-0.6	0%
Waist side	-5.0	-5.0	0%
WE bottom	-0.6	-0.6	0%
Canal side	-0.4	-0.4	0%
Working End side	-2.6	-2.6	0%

Table 4-7: Furnace energy balance

Area	Heat from Model (+ gain, - loss)
	W
Canal bottom	0
Bottom doghouse	-34 355
Bottom port 1	-30 451
Bottom port 2	-30 452
Bottom port 3	-30 451
Bottom port 4	-30 330
Bottom port 5	-30 451
Furnace bottom refiner	-140 983
Bottom Section 0	-3 904
Furnace side wall doghouse	-20 574
Furnace side Port 1	-18 236
Furnace side Port 2	-18 237
Furnace side Port 3	-18 236
Furnace side Port 4	-18 236
Furnace side Port 5	-18 236
Furnace side refiner	-60 285
Side Section 0	-55 551
Doghouse top	-3 693 184
Top Port 1	-2 131 584
Top Port 2 upstream	184 464
Top Port 2 downstream	609 024
Top Port 3	2 557 900
Top Port 4	2 557 418
Top Port 5	1 887 974
Top Refiner	70 492
Top Section 0	-234 240
Inlet	2 616 710
Outlet	-2 767 972
Waist bottom	-6 866
Waist side	-31 161
WE bottom	-33 523
Canal side	-343
Working End side	-111 559
Canal top	-348
Waist top	-56 578
Working End top	-279 358
Barrier	-578 260
Total Balance	38

4.4.3 Discretization error and validation

The discretization error was tested by using three different meshes. A 60 mm mesh size, a 30 mm mesh size and a refined mesh using the CFD software mesh refining. Examples of the 30 mm, 60 mm and refined mesh are shown in Figure 4-16, Figure 4-17 and Figure 4-18, respectively. The refined mesh was refined for velocity gradients bigger than 0.0009 m/s. It was then refined from the canal up to the barrier as this is smaller areas where a large amount of flow passes through. Especially the barrier needs a refined mesh as the flow forward into the working end and back into the refiner is very important; and there is a very small area for all this flow to occur. The refined mesh for the barrier is shown in Figure 4-18. The refined mesh for the inlet and doghouse is shown in Figure 4-19. The velocity gradient refinement made the mesh smaller at the inlet and doghouse as well as on the sidewalls as the velocity gradient is high here. The canal and working end refined mesh is shown in Figure 4-20. The orthogonal quality for the 30 and 60 mm mesh was 0.21 and 0.15, respectively, for the refined mesh. All three meshes were above the minimum allowed orthogonal quality of 0.01. The residuals for all the different meshes in the study, using the same boundary conditions are shown in Table 4-8. The refined mesh residuals are the lowest and is very close to the 60 and 30 mm mesh. The 60 mm mesh has 384 235 cells, the 30 mm mesh 3 073 880 cells and the refined mesh 1 198 454 cells. This means that the model with the 30 mm mesh will take much longer time to solve when compared to the model with the 60 mm mesh. The refined mesh also has many cells but is a balance between the most accurate solver and faster solution time.

The furnace bottom temperature from the three meshes compared to the actual temperature from the plant is shown in Figure 4-14; and the top temperatures shown in Figure 4-15. The error in temperatures when the model was compared to the actual temperatures from the plant is very small for the refined mesh. There is a difference between the model temperatures and the actual temperatures that may be because of incorrect thermocouple readings or incorrect material and boundary conditions. One big difference is the top temperatures at 8 to 20 m from the doghouse. The boundary conditions were adjusted to achieve lower crown temperatures; but the model bottom temperatures then decrease far below actual. The reason for this may be that the thermal conductivity for the glass is lower than the calculated thermal conductivity, which would lead to the top surface being warmer than the body of the glass inside the furnace. The model temperature errors are at most 60 °C for the top (excluding the working end upstream temperature that is 80 °C) and 50 °C for the bottom. These errors are

acceptable for this study as the general flow pattern corresponds to theoretical glass flows, which is the topic of concern in this study.

The flow patterns for the three different meshes are similar as shown in Figure 4-21 and Figure 4-22 for the 30 mm mesh and the refined mesh, respectively.

Table 4-8: Residuals for different meshes.

Mesh type	Continuity	x-velocity	y-velocity	z-velocity	Energy
60 mm	1.40E-06	1.13E-05	2.20E-04	1.03E-05	6.12E-08
30 mm	2.17E-05	2.16E-04	5.38E-05	4.72E-05	1.55E-07
Refined mesh	1.53E-06	1.81E-06	2.39E-05	2.08E-06	2.54E-08

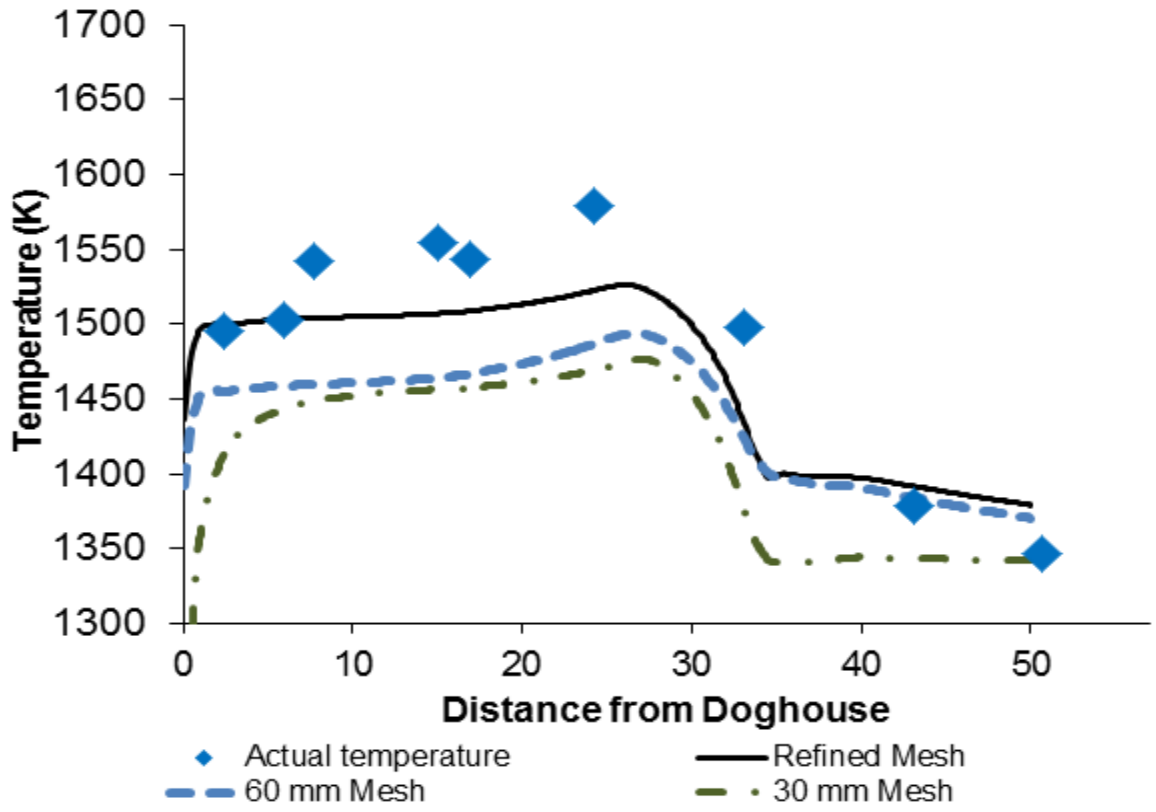


Figure 4-14: Furnace bottom temperature distribution.

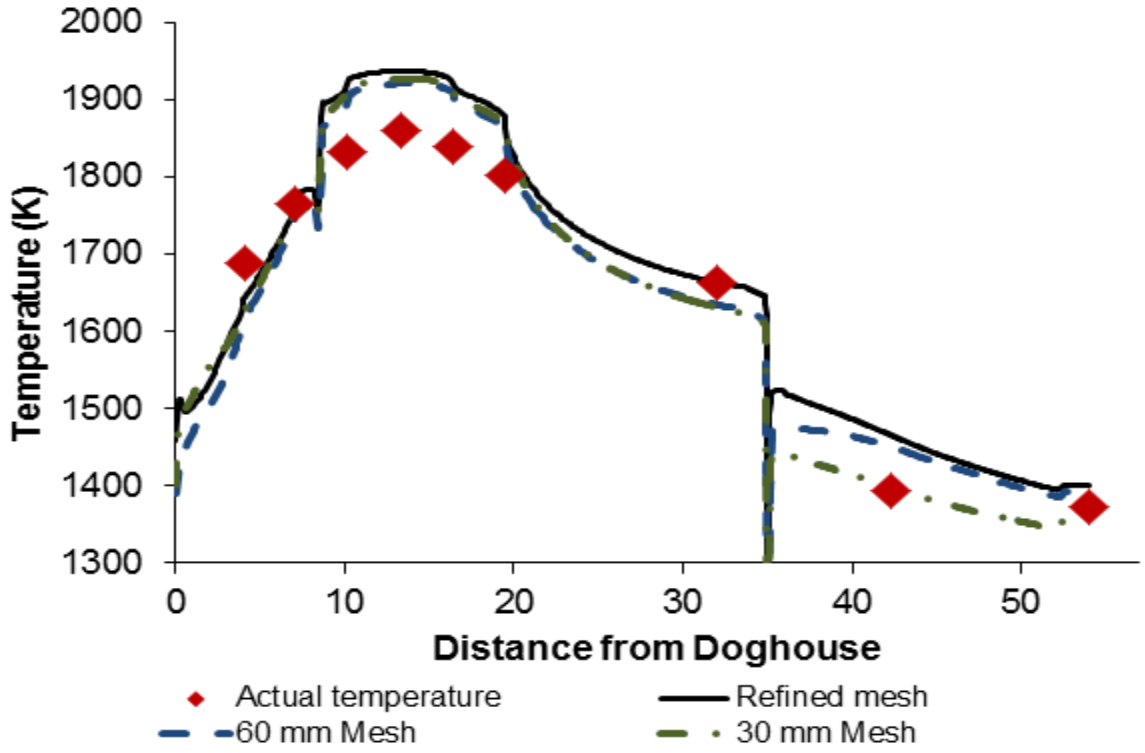


Figure 4-15: Furnace top temperature distribution.

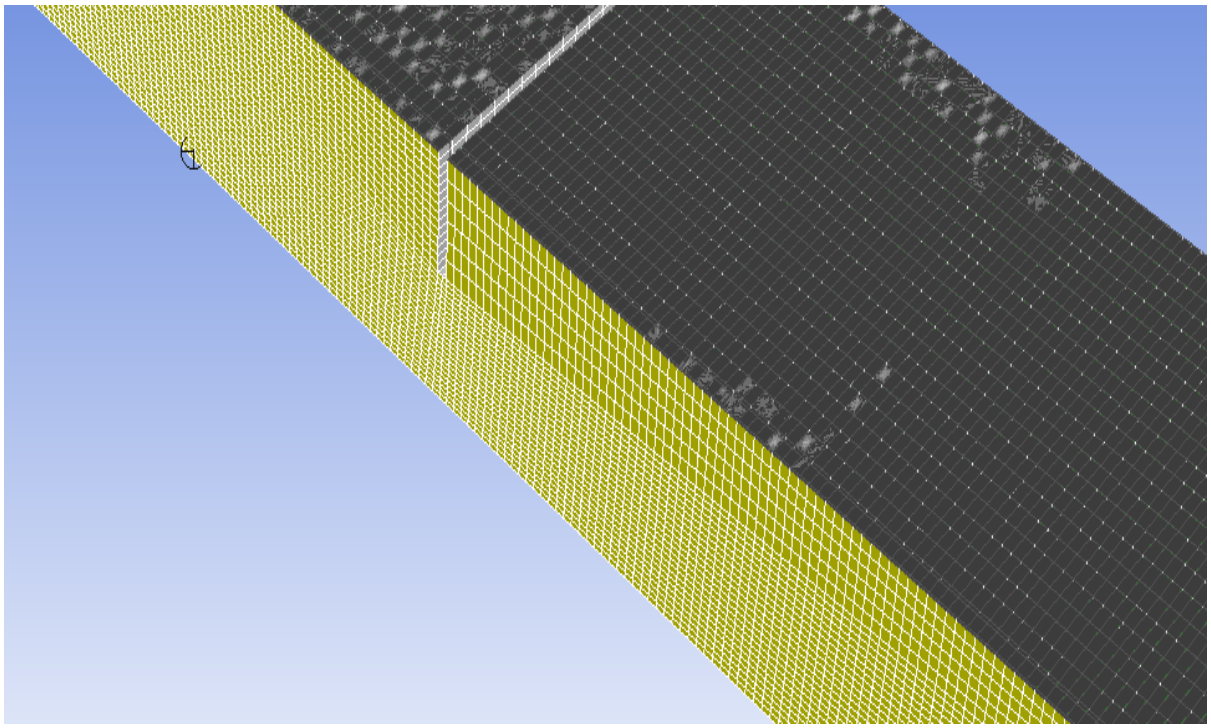


Figure 4-16: 30 mm mesh at the barrier.

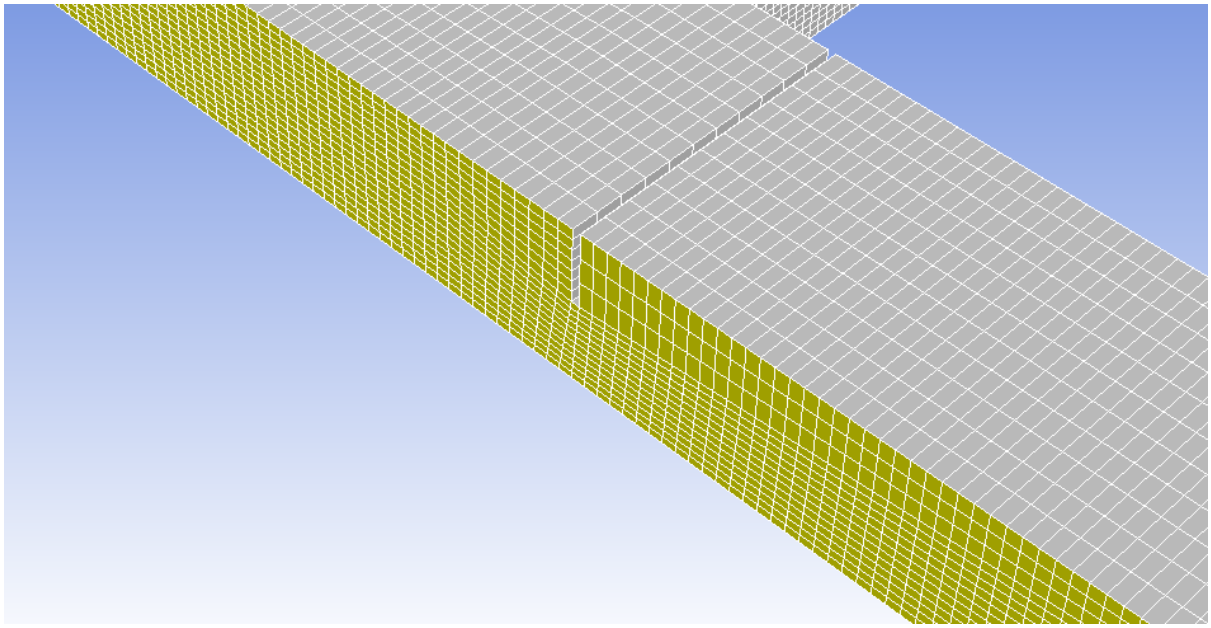


Figure 4-17: 60 mm mesh at the barrier.

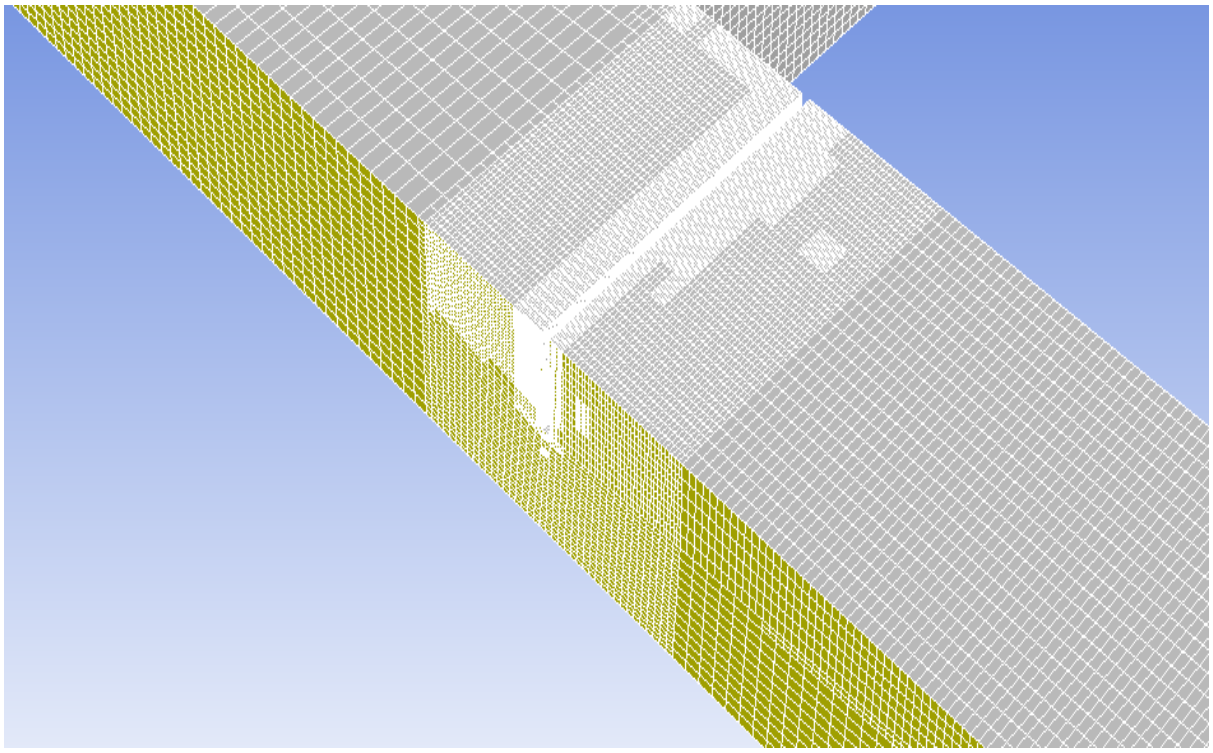


Figure 4-18: Refined mesh at the barrier.

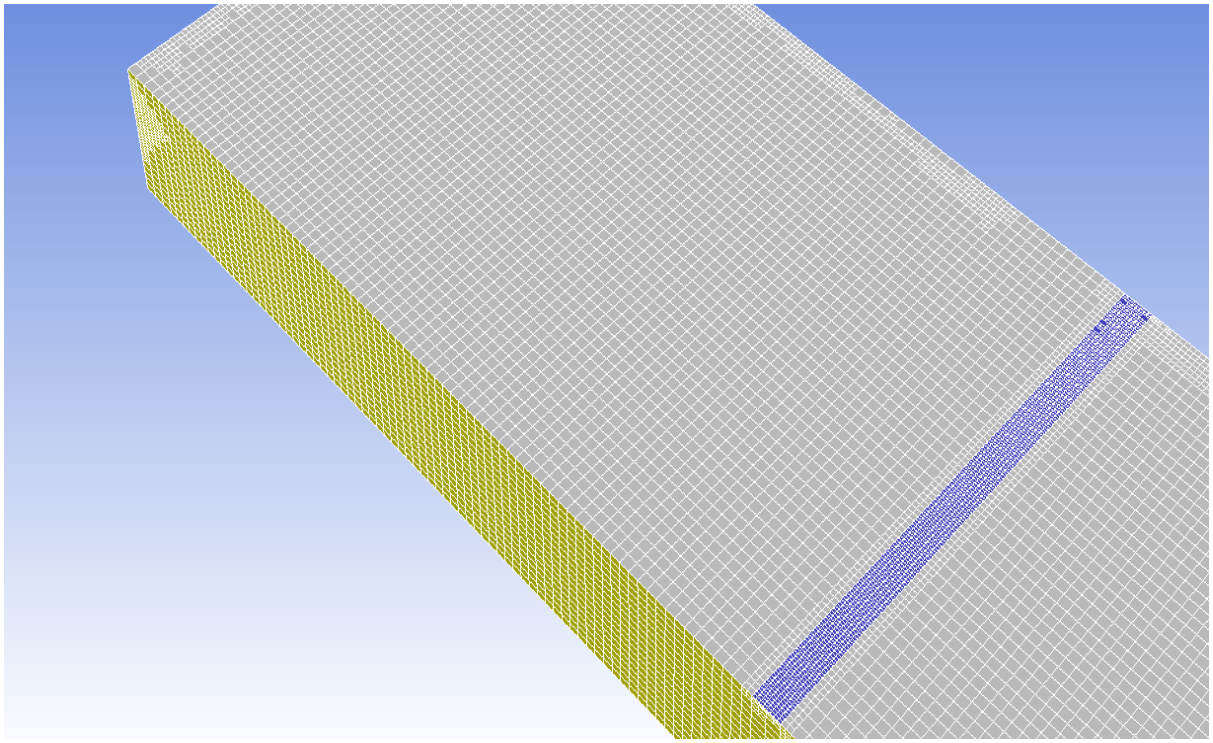


Figure 4-19: Refined mesh at the inlet and doghouse.

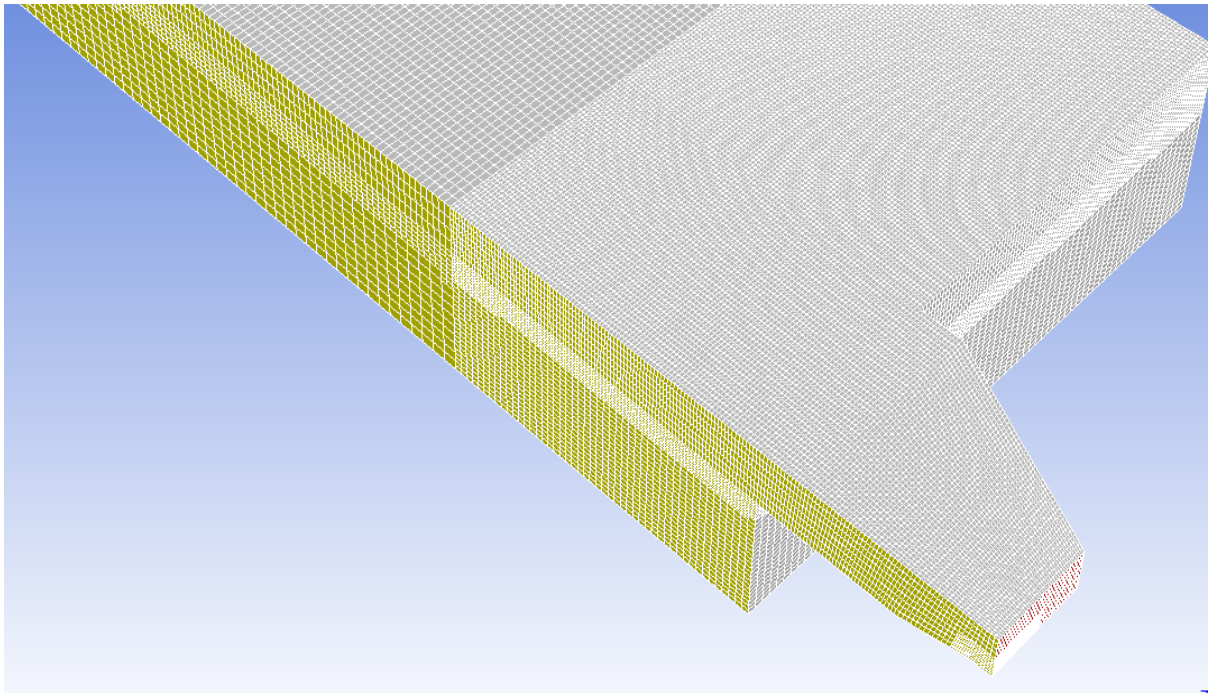


Figure 4-20: Refined mesh at the canal and working end.

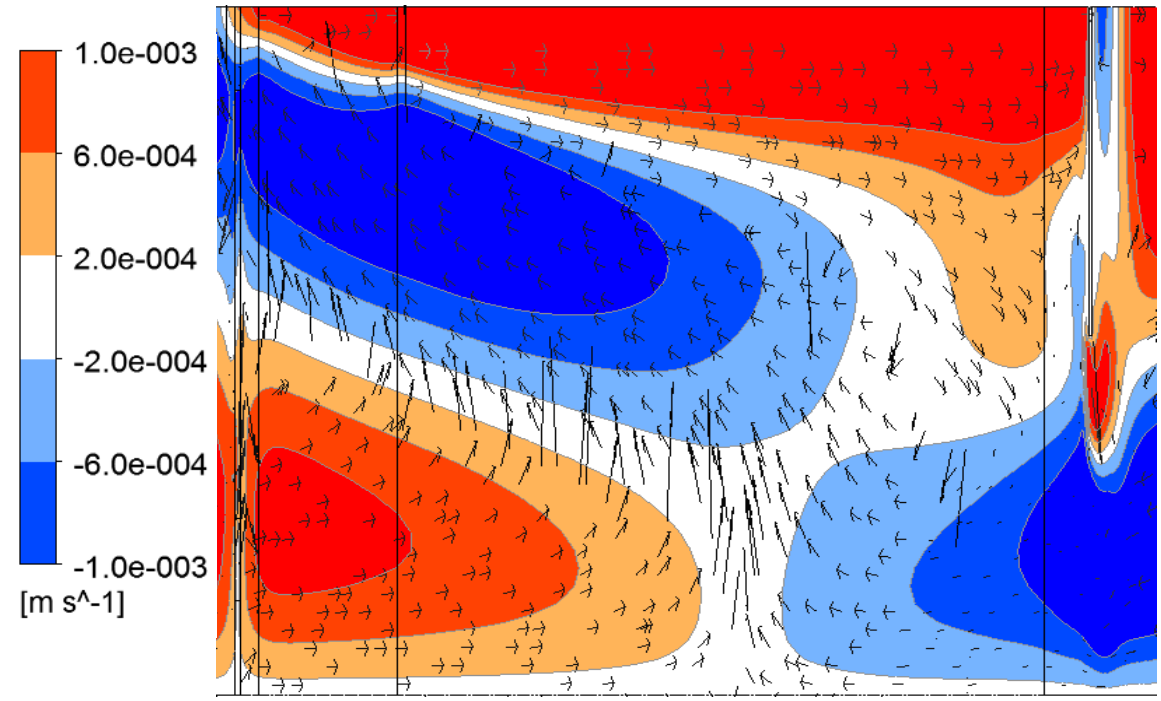


Figure 4-21: Schematic viewed from the side of the furnace showing the x-velocity component from the bubblers to the barrier for the 30 mm mesh.

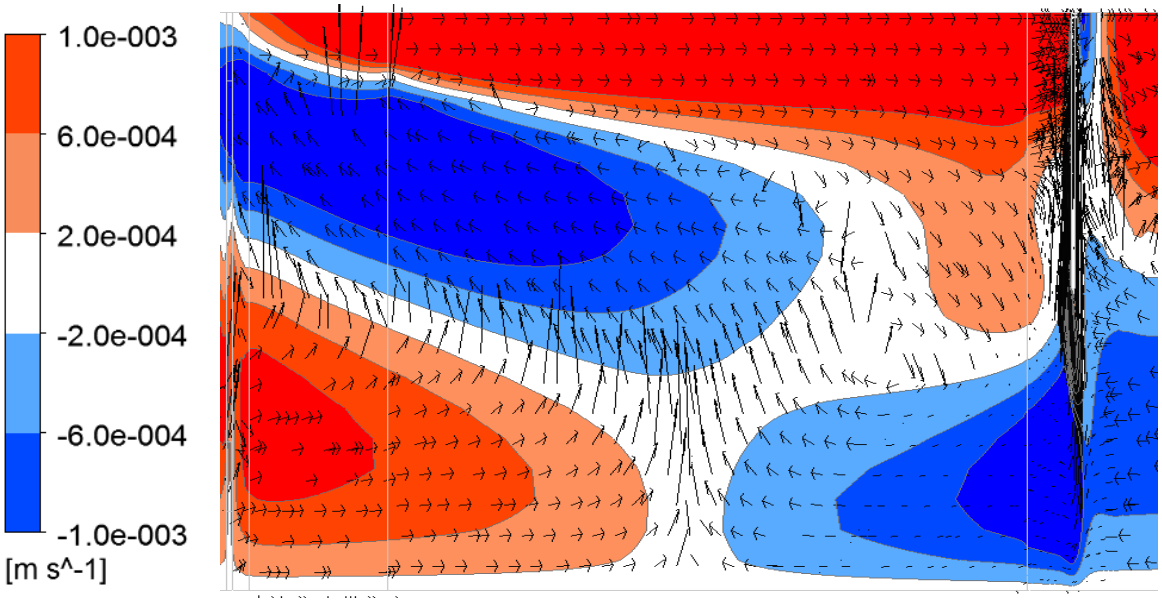


Figure 4-22: Schematic viewed from the side of the furnace showing the x-velocity component from the bubblers to the barrier for the refined mesh.

4.5 Steady state model results and discussions

The refined mesh model was used as it provided the most accurate simulation. The temperature comparison was shown in section 4.4.3. The temperature of the glass is very warm on the top surface and reduces towards the bottom with the working end bottom the coldest in the furnace as shown in Figure 4-25. This temperature distribution is the driving force for the flows inside the furnace as shown in Figure 4-7 to Figure 4-11. The flows in this furnace is similar to what theory suggested with a melt, refiner and working end cell. All three cells have inlets, outlets and recirculation. The flow for each cell is in agreement with the Pilkington (2008) theory as shown in Figure 4-23 with the melt cell slightly faster. The recirculation flow for the cells is added in Figure 4-24. This indicates that the melter could be modelled as three perfect mixers with inlet and outlets. This is not the case in the transient model as shown and discussed in section 4.7. Figure 4-26 indicates the flow of particles inside the furnace. The flow of particles also indicate that there is three cells in the furnace with the recirculation flow in the refiner.

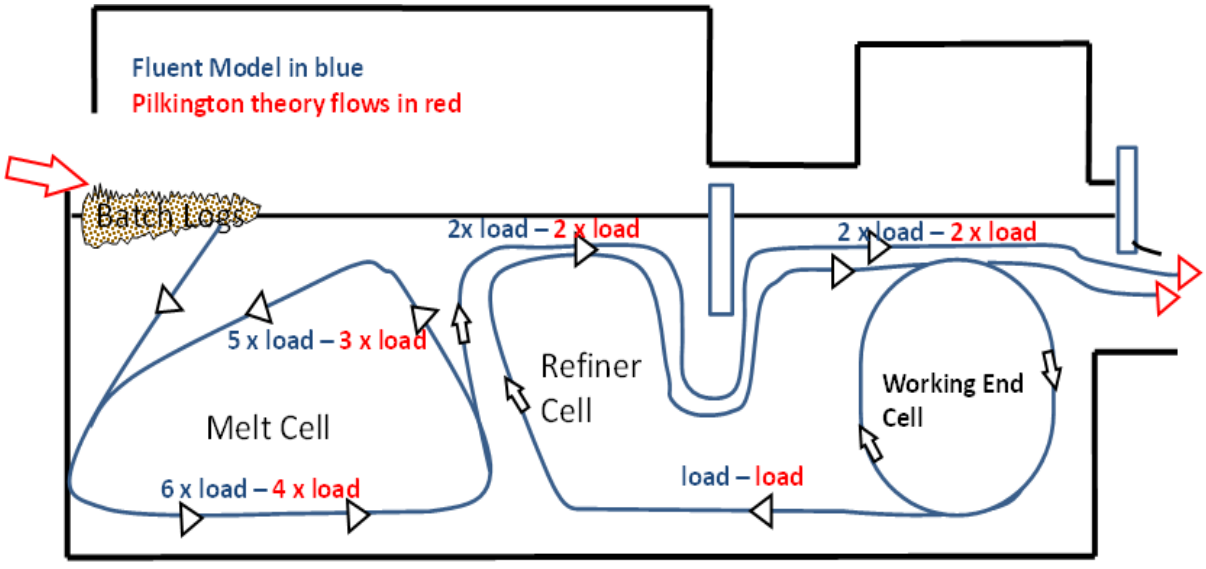


Figure 4-23: Flow magnitude of different cells. (adapted from Pilkington , 2008).

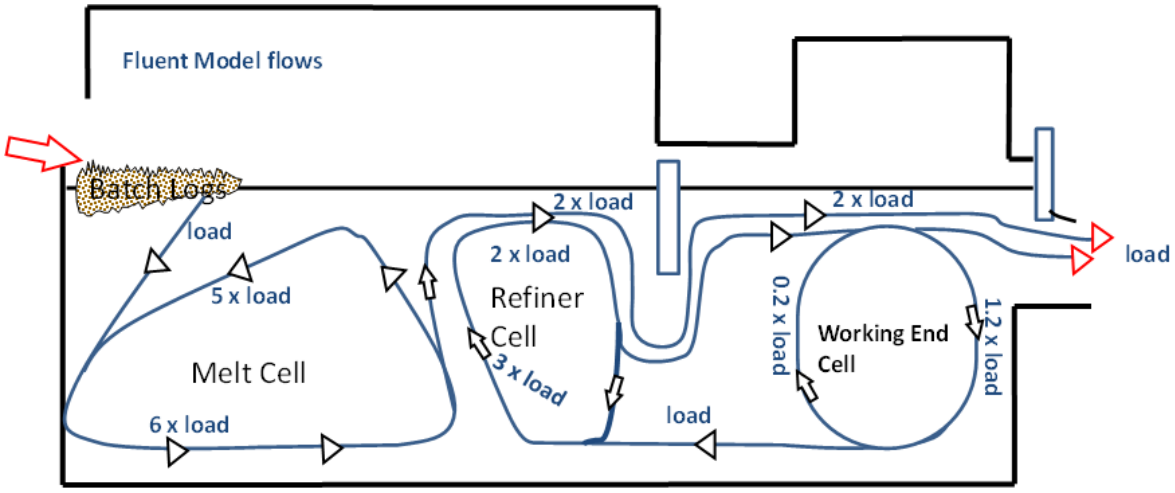


Figure 4-24: Flow magnitude of different cells and recirculation flows (this study).

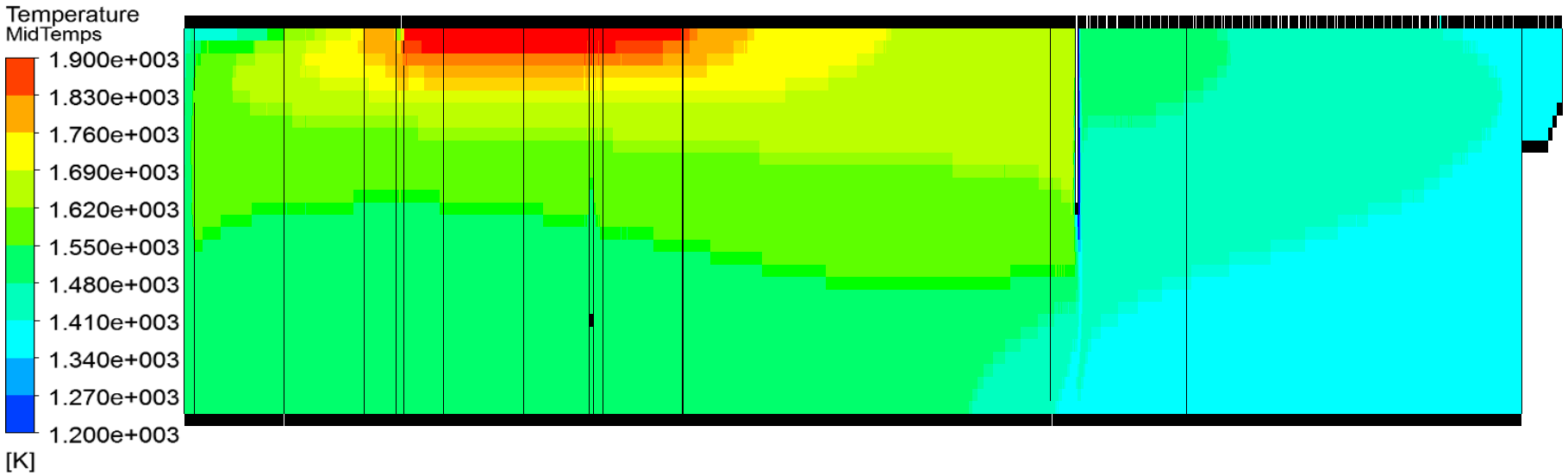


Figure 4-25: Temperature distribution on the symmetry axis of the furnace.

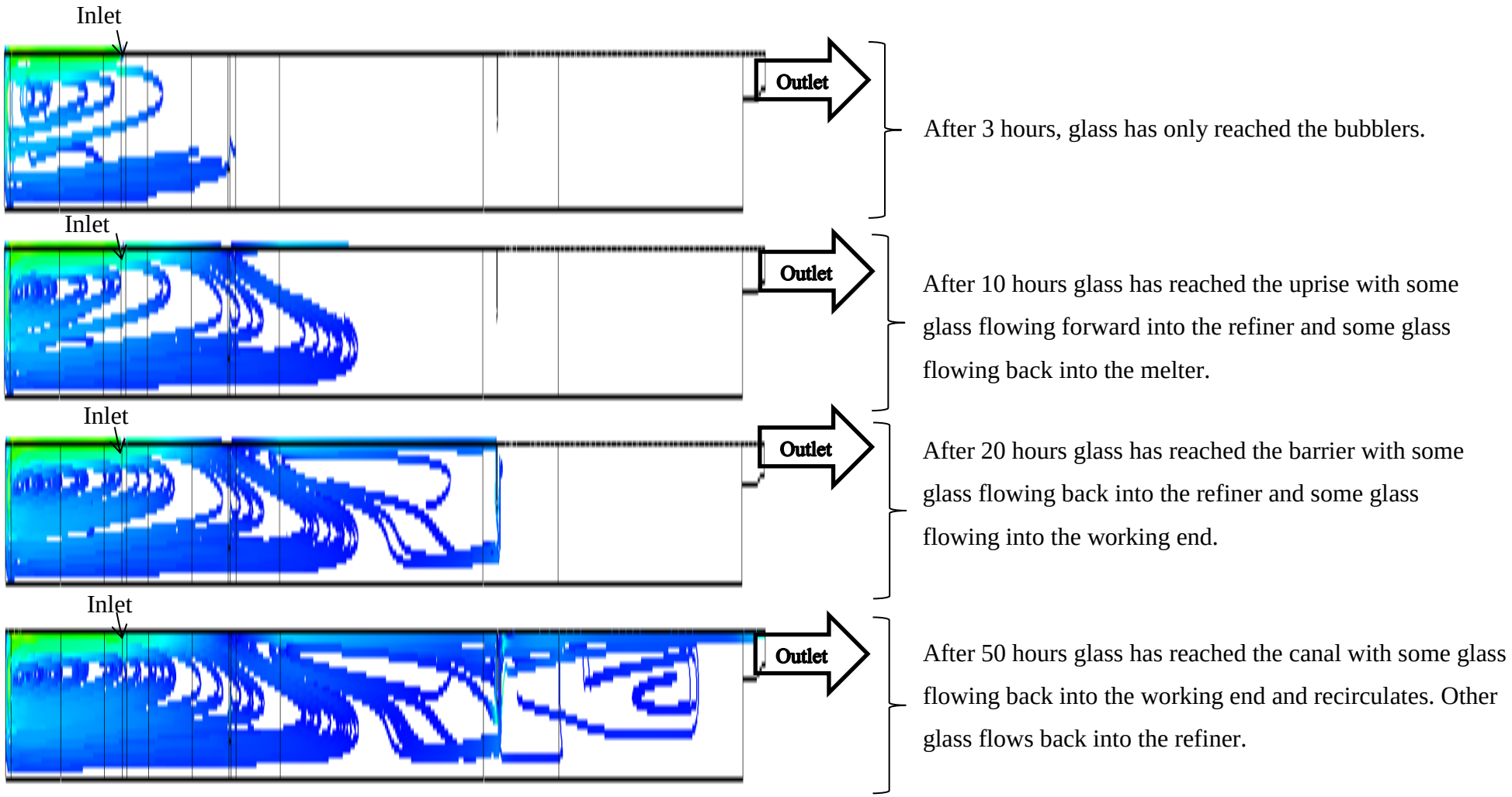


Figure 4-26: Glass streamlines with particles injected from section 0 to inlet.

4.6 Transient model set-up and optimization

The first step was to select the transient solver. In a colour change the following four steps are very important.

(i) The overdope or underdope rate; which determines the concentration of the inlet batch when changing colour.

(ii) The time when the overdope is stopped and the normal concentration is batched for.

(iii) The time when the barrier is removed.

(iv) The time when the barrier is inserted again.

These four steps were included in the transient model with the different glass properties for the different compositions playing a key role. The strategy used to model these four steps were as follows.

The species transport model was selected in the CFD software. The next step was to define the glass properties according to the three different glass chemistries, clear glass (0.1 % Fe_2O_3), tint glass (0.61 % Fe_2O_3) and the overdope glass, hereafter referred to as OD glass, which for this model is at 1.278 % Fe_2O_3. The clear glass properties were already defined in paragraph 4.3.2. The tint glass density is:

$$\rho = 2690.05753 - 0.1962T \tag{4.6}$$

With ρ, density in kg/m^3 ; and T, the temperature in K.

The temperature dependent equation for specific heat was taken as:

$$C_p = 1051.00082 + 0.32932T - 7.40231 \times 10^{-5}T^2 \tag{4.7}$$

With C_p, the heat capacity in J/(kg·K); and T, the temperature in K.

The temperature dependent equation for effective thermal conductivity was:

$$k = -0.06805 + 0.00302T - (2.05731 \times 10^{-6}T^2) + (3.26746 \times 10^{-9}T^3) \tag{4.8}$$

With k, the thermal conductivity in W/(m·K); and T, the temperature in K.

The temperature dependent equation for viscosity was:

$$\mu = 10^{-2.844+\frac{4650.0039}{T-507.5387}} \tag{4.9}$$

With μ, the viscosity in kg/(m·s); and T, the temperature in K.

The OD glass density was taken as:

$$\rho = 2709.6514 - 0.19816T \tag{4.10}$$

With ρ, density in kg/m^3 ; and T, the temperature in K.

The temperature dependent equation for specific heat was taken as:

$$C_p = 1052.03795 + 0.32952T - 7.4069 \times 10^{-5}T^2 \tag{4.11}$$

With C_p, the heat capacity in J/(kg·K); and T, the temperature in K.

The temperature dependent equation for effective thermal conductivity was:

$$\begin{aligned} k = 0.04203 + 0.00273T - (1.7798 \times 10^{-6}T^2) \\ + (2.79168 \times 10^{-9}T^3) \end{aligned} \tag{4.12}$$

With k, the thermal conductivity in W/(m·K); and T, the temperature in K.

The temperature dependent equation for viscosity was:

$$\mu = 10^{-2.844+\frac{4650.0039}{T-507.5387}} \tag{4.13}$$

With μ, the viscosity in kg/(m·s); and T, the temperature in K.

The viscosity for the three glass colours does not differ significantly especially at high temperatures with the viscosity of clear glass 1.32 Pas, for tint glass 1.34 Pas, and for OD glass 1.37 Pas. As with clear glass, a constant value was used for the range of 0-1073 K and 2000-2100 K as the properties are only defined between 1073 and 2000 K. The tint glass properties are in Table 4-9 and the OD glass properties in Table 4-10. It is especially the effective thermal conductivity that differs significantly from clear glass to tint glass.

Table 4-9: Tint glass properties.

Temperature Range	Density	Heat capacity	Thermal conductivity
K	kg/m3	J/(kg·K)	W/(m·K)
0-1073	2480	1319	4.84
2000-2100	2283	1416	24.67

Table 4-10: OD glass properties.

Temperature Range	Density	Heat capacity	Thermal conductivity
K	kg/m3	J/(kg·K)	W/(m·K)
0-1073	2466	1321	4.37
2000-2100	2299	1417	22.92

A mixture model was set up with the three different glass colours with the "volume weighted mixing law" chosen for the density, the "mixing law" for the heat capacity, "mass weighted mixing law" for thermal conductivity, viscosity defined by the UDF in Appendix A and the "unity lewis number" for the mass diffusivity. The mass diffusivity was taken as 10^{-12} m^2/s from Wijshoff et al. (2010). which is different to the mass diffusivity calculated from the "unit lewis number" defined as (ANSYS® Fluent release 18, 2017):

$$D = \frac{k}{\rho C_p} \tag{4.14}$$

With k, the thermal conductivity; ρ, the density; and C_p, the heat capacity (all in SI units). The "unity lewis number" calculated from Equation (4.2), (4.3) and (4.4) at 2000 K for clear

glass is 3.4×10^{-12} m^2/s. Both the mass diffusivities gave the same results, therefore, mass transfer is negligible.

With the glass properties defined, the inlet glass at time t=0 was selected as OD glass only. The solver was stopped after 37 hours and the inlet glass was chosen as tint glass only. A new mesh for no barrier was imported at 37 hours and then again a new mesh at 80 hours for 0.3 m deep barrier.

The solution method was chosen as first order implicit with non-iterative time advancement, warped face gradient correction and with higher order term relaxation deselected. The tint and OD discretization was chosen as second order upwind. All other methods were kept as specified by the steady state solver.

The under-relaxation factors for the tint and OD glass were taken as 1 with the momentum under-relaxation factor selected as 0.1, pressure as 0.3, density as 1, body forces as 0.7 and energy as 0.98. The time step size was taken as 600 s with 75 iterations per time step. The solution was saved every 6 time steps and was stopped at 34, 36 and 80 hours to alter the inlet mesh and boundary conditions.

4.7 Results and discussions of the transient model

The boundary conditions was changed throughout the transient solution to maintain the furnace actual temperatures. The temperatures stayed within the range of ± 50 °C to the actual furnace temperatures. The fluent transient model iron concentration corresponds closely with the actual iron as per Figure 4-27. The fluent model does however give higher iron concentrations at the period where the barrier was removed. What is important is to view the iron concentration in the melter with time. Figure 4-28 shows the iron concentration change with time inside the melter from start of the colour change to 1 hour before the barrier was removed. The iron inlet concentration changed to 0.61 % Fe_2O_3 from 1.278 % Fe_2O_3. The glass colour changes with time in plugs from the doghouse to the outlet. There are eight distinct areas with a specific iron concentration at 36 hours after the colour change started. These areas are referred to as plugs. From the CFD model the glass colour changes in the furnace were similar to plug flow and can be approximated by 8 perfect mixers in series for the 0.56 m barrier depth. These plugs collapse after the barrier was removed at 37 hours. At 41 hours, shown in Figure 4-29 the plugs in the refiner and working end have changed from 7

to 4 plugs and the refiner plug flows directly through the canal. This describes the sudden increase in the iron concentration as seen in Figure 4-27 after the barriers are removed. Also with no barrier the glass colour changes in the furnace similar to plug flow but with only 5 perfect mixers in series.

The CFD model gives insight into what model could be chosen to predict the colour change inside the furnace. The initial phase can be modelled as 8 perfect mixers in series if the barrier depth is 0.56 m. The seven plugs from the refiner to the canal have to be divided into four or three plugs after the barriers are removed with the concentration at that point in the furnace divided into the four plugs. The model changes from eight to five perfect mixers in series with no barrier. A trial is to be done with six, seven or eight perfect mixers in series for the 0.3 m barrier that was inserted, after 80 hours, as it is not visible from the model what combination of perfect mixers will be the most accurate for the 0.3 m barrier depth.

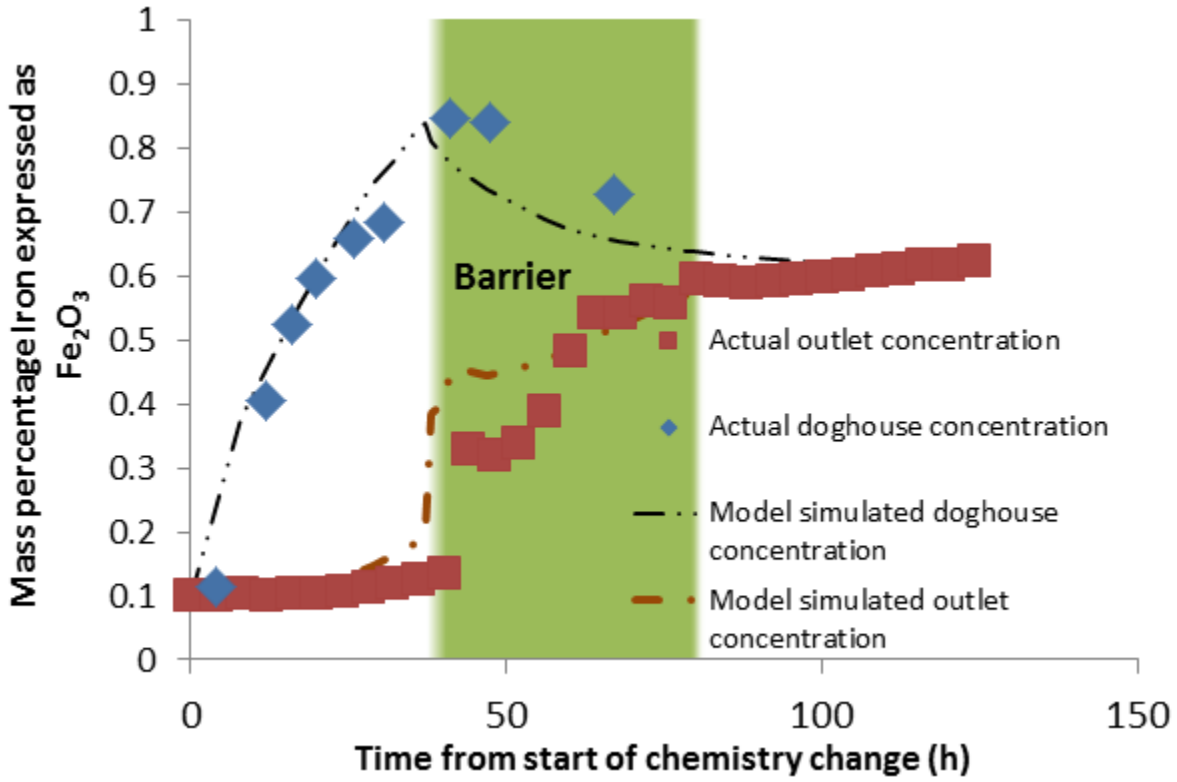


Figure 4-27: Iron during colour change

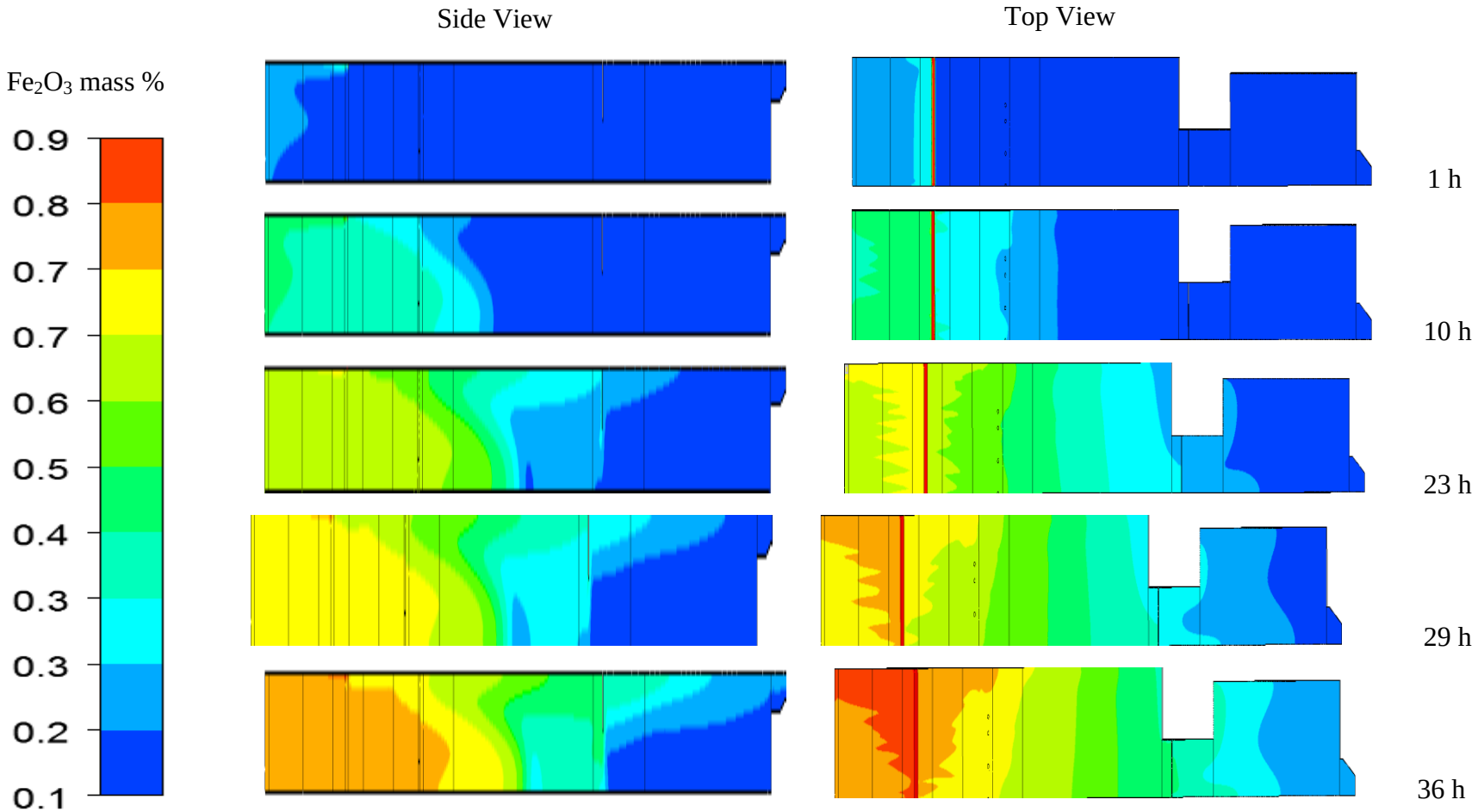


Figure 4-28: Iron concentration expressed as % Fe_2O_3 in the furnace during the colour change.

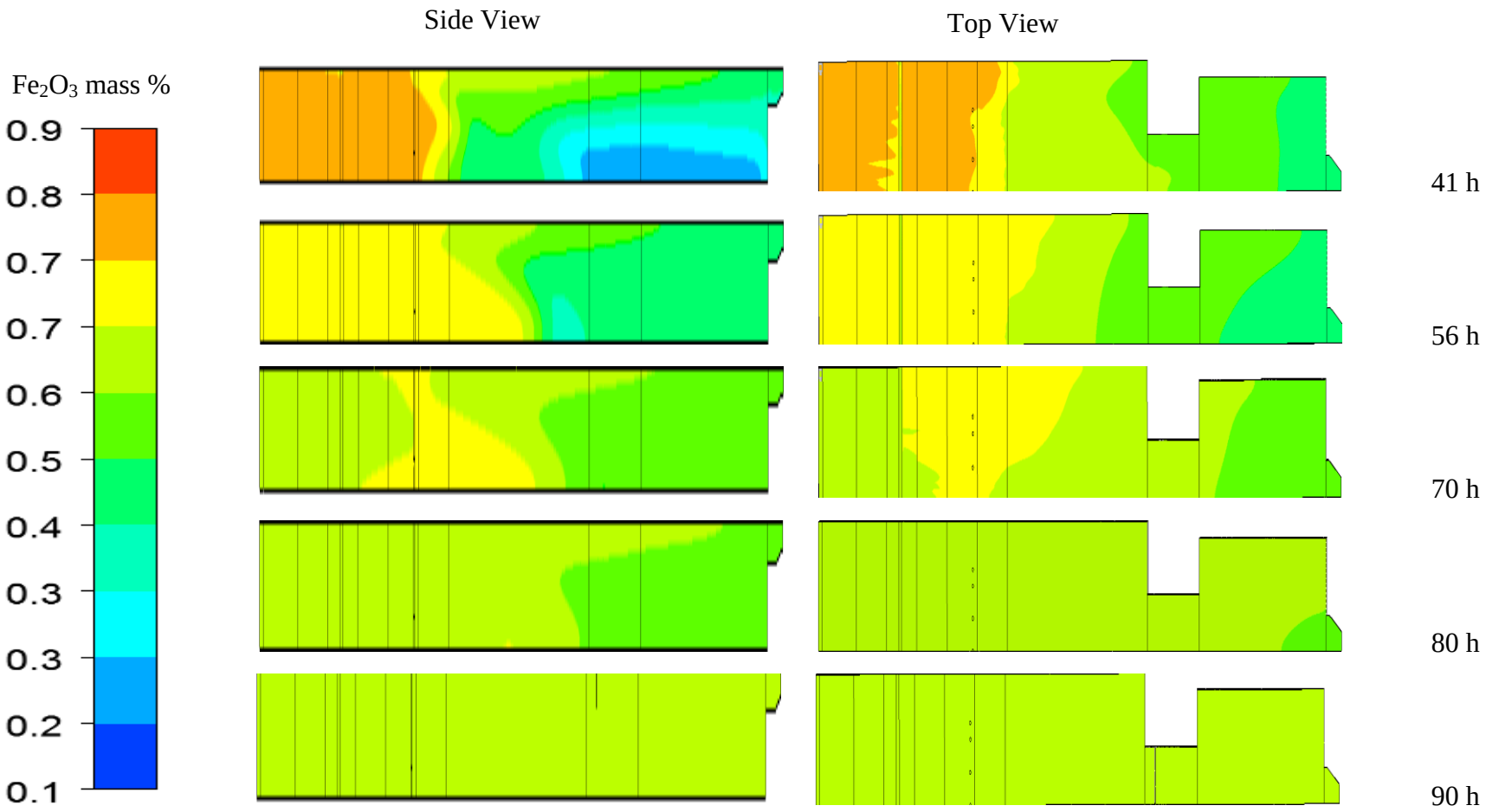


Figure 4-29: Iron concentration expressed as % Fe_2O_3 in the furnace during the colour change. The barrier was removed at 37 h and the inlet iron concentration changed to 0.61 % Fe_2O_3 from 1.287 % Fe_2O_3.The barrier was inserted at 0.3 m deep after 80 h.

5 Mathematical Mixing Model and Optimisation of the Colour Change Time

5.1 Mixing model equation

The mixing model was based on a one-parameter model of perfect mixers in series. An example calculation for two perfect mixers in series is shown below in Equation 5.1 for the first perfect mixer and Equation 5.2 for the second perfect mixer in series.

$$\frac{W_{tot}}{2} \times \frac{\mathrm{d}x_1}{\mathrm{d}t} = Q(x_{in} - x_1) \tag{5.1}$$

$$\frac{W_{tot}}{2} \times \frac{\mathrm{d}x_2}{\mathrm{d}t} = Q(x_1 - x_2) \tag{5.2}$$

With W_{tot}, the total furnace capacity in kg; x_1 and x_2, the Fe_2O_3 mass percentage in the mixer; x_{in} the inlet Fe_2O_3 mass percentage; t, the time in hours; and Q, the furnace throughput in kg/h. For the nth reactor in series Equation (5.2) becomes:

$$\frac{W_{tot}}{n} \times \frac{\mathrm{d}x_n}{\mathrm{d}t} = Q(x_{n-1} - x_n) \tag{5.3}$$

5.2 The root mean square error

The root mean square error or *RMS* was used to determine the error between the actual and model output Fe_2O_3 mass fraction. The *RMS* is defined as (Statweb, 2017):

$$RMS = \sqrt{\frac{\sum_{i=1}^{n}(x^i - \hat{x}^i)}{n}} \tag{5.4}$$

With x^i the model predicted Fe_2O_3 output mass percentage of sample i, and $\hat{x}^i$ the actual measured Fe_2O_3 output mass percentage with n the number of samples.

5.3 Initial mixing model design based on historical studies of the mixing inside a glass furnace

As mentioned in this study, historical studies done have shown that the response curve of the colorant outlet concentration in a glass furnace is the result of multi complete mixing cells that include perfect mixers in series or parallel with a plug flow cell or allowance for dead time.

There is however a shortcoming in these studies, as mentioned by Cooper (1959), because of the changes in the mixing of glass in a modern day float glass furnace; especially in cases where the secondary flows due to the thermal convection currents are changed when conditions in the melter is changed. Two of these conditions include the change in barrier height during a colour change and the change in glass chemistry.

The theory of complete mixers in series was tested by developing a mixing model with a number of perfect mixers in series; and then validating the results with experimental data obtained from the plant. There are a number of experimental data sets available for historical colour changes from clear to tint. Three data sets were used with each data set having the same overdope Fe_2O_3 concentration but different initial barrier heights. These three data sets are for three different colour changes that occurred in April 2015, April 2016 and March 2017, respectively. The important variables and time steps for these three colour changes is shown in Table 5-1.

Table 5-1: Colour change variables

Colour Change	Original Fe_2O_3 mass %	Overdope Fe_2O_3 mass %	Overdope time (h)	Time barrier removed (h)	Time barrier inserted again (h)
Apr-15	0.132	1.278	34	33	82
Apr-16	0.129	1.278	32	34	81
Mar-17	0.1	1.278	36	37	80

The mixing model was developed with the inlet Fe_2O_3 mass % in the furnace taken as the overdope Fe_2O_3 mass % shown in Table 5-1. The inlet Fe_2O_3 mass % was then changed to the required Fe_2O_3 mass % of 0.619 from when the overdope time was finished. The number of

perfect mixers in series for the mixing model was altered from two up to nine mixers in series. This was done to find what amount of perfect mixers in series is the most accurate; and if the results correspond with the observations from the CFD flow model. An example of a three perfect mixers in series model code is shown in Appendix E.1.

Only the 3, 6 and 8 perfect mixers in series mixing model is shown in Figures 5-1, Figure 5-2 and Figure 5-3 to make the comparison with the actual data, visually, easier. Figure 5-1, Figure 5-2 and Figure 5-3 indicate the comparison of a 3, 6 and 8 perfect mixers in series mixing model with the actual measured iron mass percentage for the April 2015, April 2016 and March 2017, respectively. Another validation used is the calculation of the RMS error. The smallest RMS error and, therefore, the most accurate mixing model as shown in Table 5-2 for all three colour changes is 3 perfect mixers in series. Visually the mixing model with 3 perfect mixers in series does not fit the actual data accurately throughout the time span as shown in Figure 5-1, Figure 5-2 and Figure 5-3.

There is a step change in the actual iron mass percentage after the barrier is removed shown in Figure 5-1, Figure 5-2 and Figure 5-3 by the green highlighted section. The perfect mixer in series model does not represent this step change. The barrier depth into the glass at the start of the colour change for 2015 was 0.45 m, 0.41 m for 2016 and 0.56 m for 2017. The RMS error for the period from the start of the overdope to the time that the barrier is removed is shown in Table 5-3. The most accurate perfect mixer in series model for the period before the barrier is removed for the 0.41 m barrier depth is five perfect mixers. Similarly the most accurate perfect mixers in series model for the 0.45 m barrier depth is six perfect mixers and for the 0.56 m barrier depth, eight perfect mixers. Three perfect mixers in series most accurately represents the period when the barrier is completely removed as shown in Figure 5-1, Figure 5-2 and Figure 5-3. This was also evident from the CFD flow model in section 4.7; where the colour change in the furnace with the 0.56 m barrier was used to validate the flow model. It was shown that the glass volume can be divided into eight boxes or mixers with its own independent iron mass percentage. Also, the period when the barrier is out can be divided into three or four boxes or mixers with independent iron mass percentages. The correlation between the number of perfect mixers in series and the final period when the barrier is inserted again is discussed in the following section.

Table 5-2: RMS errors for perfect mixers in series

Perfect mixers in series	RMS error		
	Apr-15	Apr-16	Mar-17
2	4.1×10^{-03}	4.0×10^{-03}	8.0×10^{-03}
3	9.9×10^{-04}	9.1×10^{-04}	3.3×10^{-03}
4	1.1×10^{-03}	9.2×10^{-04}	3.0×10^{-03}
5	2.4×10^{-03}	2.1×10^{-03}	4.4×10^{-03}
6	4.2×10^{-03}	3.9×10^{-03}	6.7×10^{-03}
7	6.3×10^{-03}	5.9×10^{-03}	9.3×10^{-03}
8	8.5×10^{-03}	8.0×10^{-03}	1.2×10^{-02}
9			1.5×10^{-02}

Table 5-3: RMS error for period before barrier is removed.

Perfect mixers in series	RMS error		
	Apr-15 Barrier 0.45 m	Apr-16 Barrier 0.41 m	Mar-17 Barrier 0.56 m
2	1.1×10^{-02}	8.5×10^{-03}	1.8×10^{-02}
3	3.0×10^{-03}	1.8×10^{-03}	6.2×10^{-03}
4	7.3×10^{-04}	3.9×10^{-04}	2.3×10^{-03}
5	1.3×10^{-04}	2.3×10^{-04}	8.4×10^{-04}
6	3.1×10^{-05}	3.7×10^{-04}	2.8×10^{-04}
7	8.0×10^{-05}	5.5×10^{-04}	7.8×10^{-05}
8	1.6×10^{-04}	7.1×10^{-04}	2.5×10^{-05}
9			3.2×10^{-05}

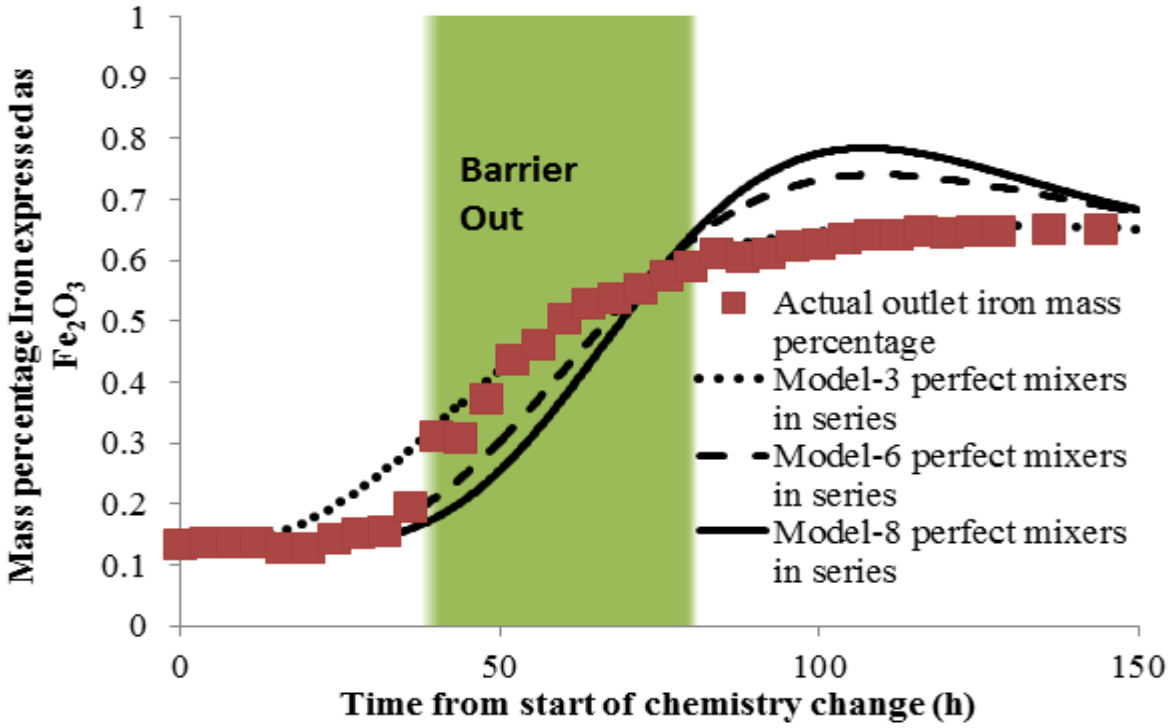


Figure 5-1: 2015 colour change outlet iron mass percentage comparison between mixing model and actual data.

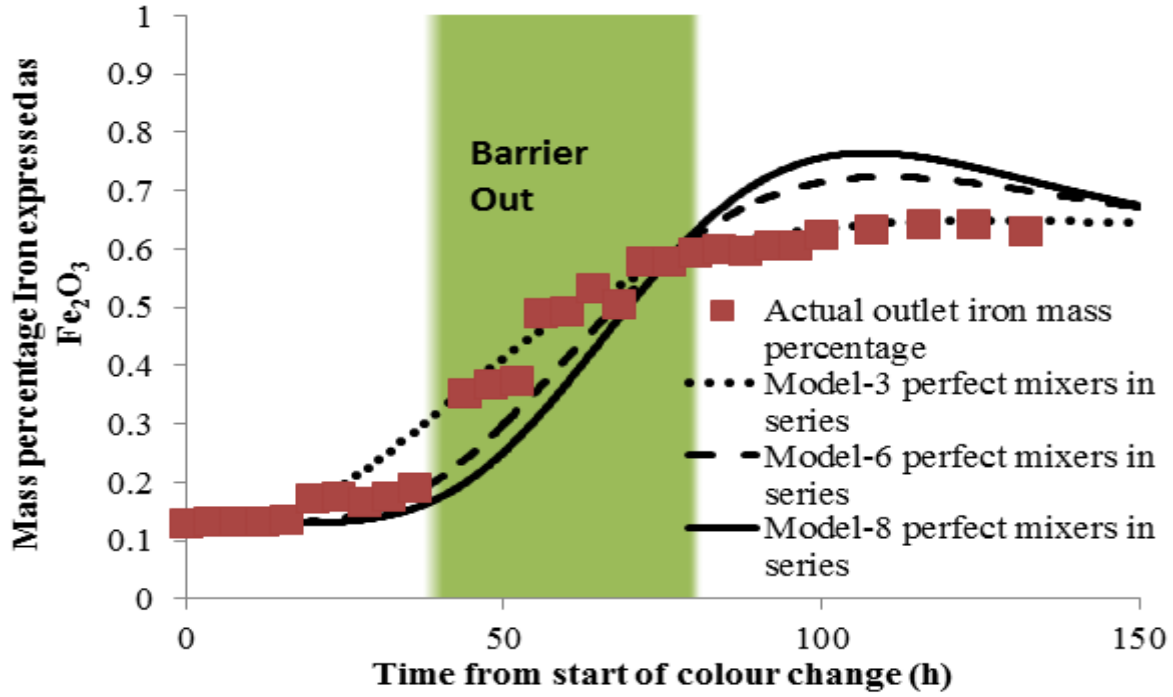


Figure 5-2: 2016 colour change outlet iron mass percentage comparison between mixing model and actual data.

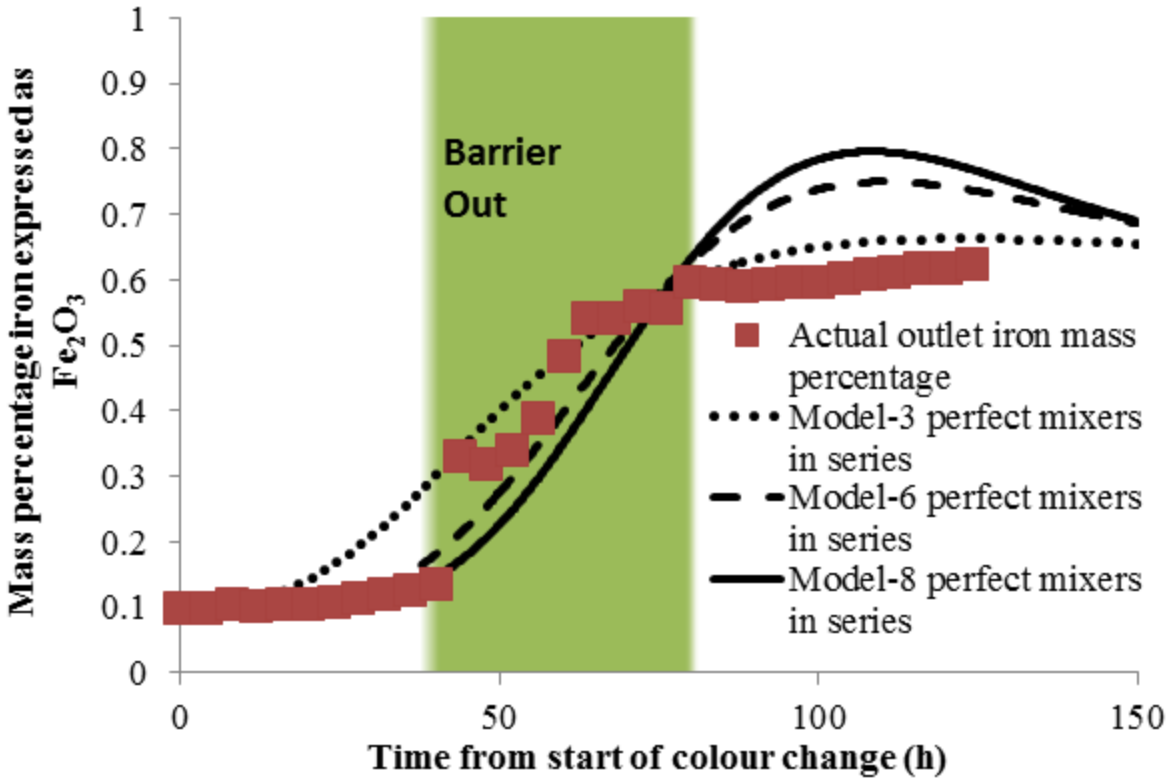


Figure 5-3: 2017 colour change outlet iron mass percentage comparison between mixing model and actual data.

The results from the CFD flow model and the initial mixing model indicate that the colour change can be separated into four parts. A one parameter mixing model with five to eight perfect mixers in series can describe the first stage of the colour change. The number of perfect mixers in series depends on the barrier depth with five mixers used for 0.41 m barrier depth, six mixers in series for 0.45 m barrier depth and eight mixers in series for 0.56 m barrier depth. The second stage of the colour change when the barrier is removed causes a change in the furnace mixing characteristics and a sudden increase of iron concentration at the outlet of more than 0.1 mass % Fe_2O_3 within 4 hours. The third stage follows this short period by an increase in the iron outlet concentration that can be modelled by three perfect mixers in series when the barrier is out and the inlet iron concentration is reduced to the required outlet iron concentration of 0.619. The fourth stage of the colour change is when the barrier is inserted again. This stage can be modelled by a four mixer in series model for the 0.3 m barrier depth.

5.4 Final mixing model design and optimization

To optimize the model a perfect mixers in series model with different amount of mixers in series is to be used for the different barrier positions. The mixing model has to be broken up into four stages because of the differenet stages of the colour change with regards to colorant (Fe_2O_3) inlet concentration and barrier removal and insertion. As stated in Section 5.1, the first perfect mixer was described by Equation (5.1):

$$\frac{W_{tot}}{2} \times \frac{\mathrm{d}x_1}{\mathrm{d}t} = Q(x_{in} - x_1) \tag{5.1}$$

With the nth reactor in series described by Equation (5.3):

$$\frac{W_{tot}}{n} \times \frac{\mathrm{d}x_n}{\mathrm{d}t} = Q(x_{n-1} - x_n) \tag{5.3}$$

The process followed to develop the model is as follows using the colour change variables as per Table 5-1 for the 2015 colour change as an example:

(i) The overdope Fe_2O_3 mass percentage of 1.278 % was used as the inlet concentration at time t = 0 hours, with the Fe_2O_3 mass percentage in the furnace at the clear glass Fe_2O_3 mass percentage of 0.132 %. The number of prefect mixers in series for the period 0 to 33 hours when the barrier was removed was optimised.

(ii) The second and third stage is where the inlet Fe_2O_3 mass percentage is changed after the 34-hour overdope at a Fe_2O_3 mass percentage of 1.278 % to the required mass percentage of 0.619 %, and a new number of perfect mixers in series is required due to the barrier being removed. The concentration per mixer also changes as the amount of mixers change from five, six or eight to three.

(iii) The fourth stage is for when the barrier is inserted again at time t = 82 hours, and the number of mixers in series have to change again based on the barrier depth.

The optimized model for the 2015 colour change was as follows: For the period 0 to 34 hours six mixers in series model was used for the 0.41 m barrier depth. Allowance is made for a 4 hour dead time when the barrier is removed; where after a three mixer in series model is used for when the barrier is out and then a four mixer in series model used again for when the barrier is placed in again at 0.3 m at time t = 82 hours.

The iron concentration per mixer changes after the barrier is removed and inserted. It is different for each barrier depth because of the different number of perfect mixers for that barrier depth. The number of perfect mixers change from six for the 0.45 m barrier depth to three for no barrier. The iron concentration for the new last perfect mixer in series, number three, changes to the average of mixer four and five. The new first mixer iron concentration to the average of mixer one, two and three; and the new second mixer iron concentration to the mixer six iron concentration. When the barrier is inserted again the iron concentration for mixer one stays the same, for mixer two stays number two and for three and four becomes mixer three iron concentration. The response curve for this model is shown in Figure 5-4 with a RMS error of 5.2×10^{-4} that is more accurate than the three perfect mixers in series model with RMS error of 9.9×10^{-4}. The model code is shown in Appendix E.2.

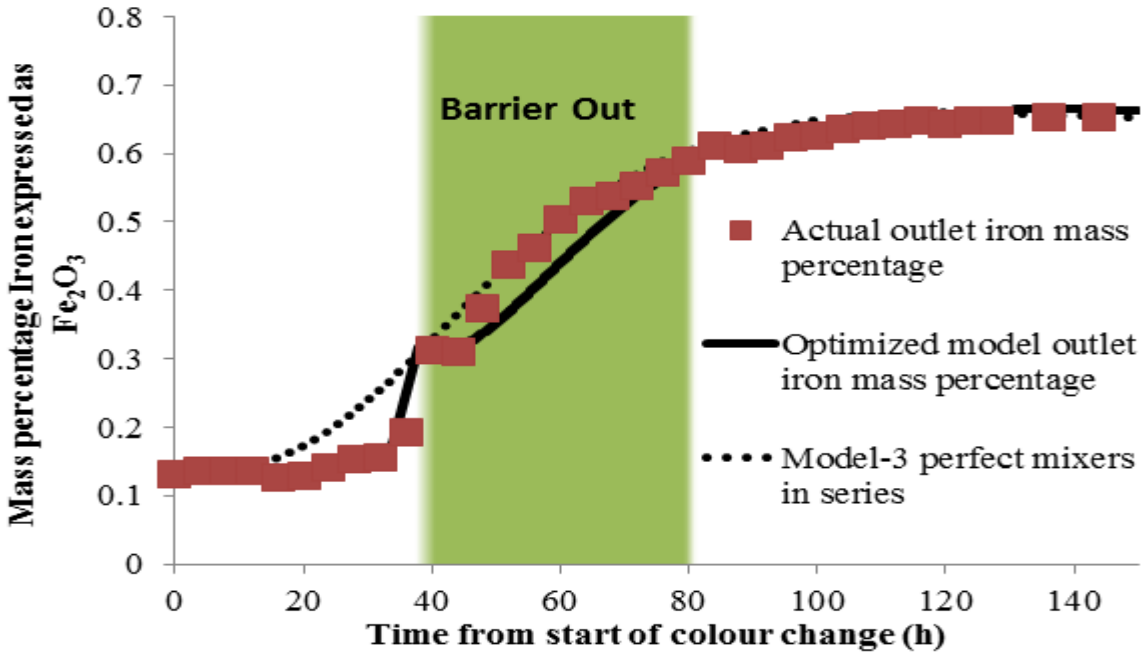


Figure 5-4: Optimized model prediction for the 2015 colour change outlet iron mass percentage and comparison with the actual data.

The optimized model for the 2016 colour change is five mixers in series for period 0 to 34 hours. Allowance was made for a 4-hour dead time when the barrier is removed; where after a three mixer in series model is used for when the barrier is out and then a four mixer in series model used again for when the barrier is placed in again at 0.3 m. The number of perfect mixers change from five for the 0.41 m barrier depth to three for no barrier. The iron concentration for the new last perfect mixer in series, number three, changes to the average of

mixer three and four. The iron concentration for the new first mixer to the average of mixer one and two and the iron concentration for the new second mixer to the mixer five iron concentration. When the barrier is inserted again the iron concentration for mixer one stays the same, for mixer two stays number two and for three and four becomes mixer three iron concentration. The response curve for this model is shown in Figure 5-5 with a RMS error 4.8×10^{-4} that is improved to the three perfect mixers in series model with RMS error of 9.1×10^{-4}. The model code is shown in Appendix E.3.

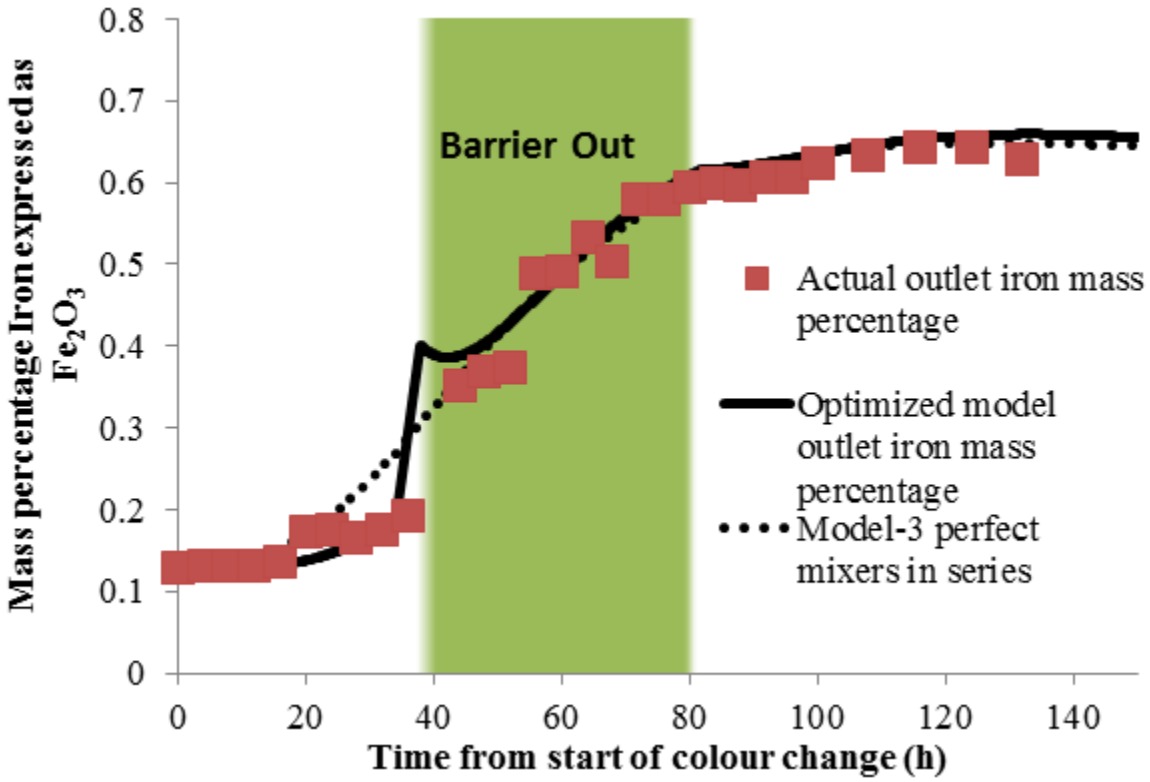


Figure 5-5: Optimized model prediction for the 2016 colour change outlet iron mass percentage and comparison with the actual data.

The optimized model for the 2017 colour change is eight mixers in series for period 0 to 38 hours. Allowance was made for a 4-hour dead time when the barrier is removed; where after a three mixer in series model is used for when the barrier is out and then a four mixer in series model used again for when the barrier is placed in again at 0.3 m. The number of perfect mixers in series change from eight for the 0.56 m barrier depth to three for no barrier. The iron concentration for the new last perfect mixer in series, number three, changes to the average of mixer five and six. The iron concentration for the new first mixer changes to the average of mixer one, two, three and four and the iron concentration for the new second

mixer to the average iron concentration of mixer seven and eight. When the barrier is inserted again the concentration for mixer one stays the same, for mixer two stays number two and for three and four becomes the mixer three iron concentration. The response curve for this model is shown in Figure 5-6 with a RMS error 8.8×10^{-4} that is improved to the three perfect mixers in series model with RMS error of 3.3×10^{-3}. The model code is shown in Appendix E.4.

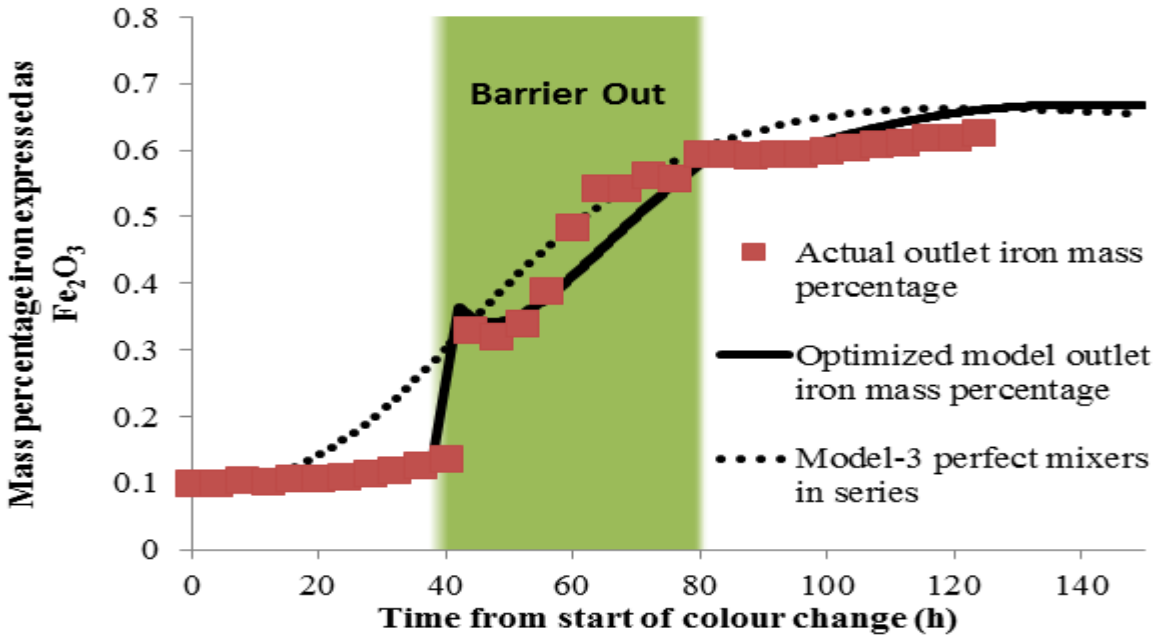


Figure 5-6: Optimized model prediction for the 2017 colour change outlet iron mass percentage and comparison with the actual data.

The doghouse sample results for the 2017 colour change was compared to the model and gives a large error as shown in Figure 5-7. The fluent model iron mass percentage is however more accurate. The reason the perfect mixers in series prediction for the doghouse is not accurate is because it considers the whole reactor or furnace as a combination of mixers with an average concentration per mixer, where the fluent model gives the iron concentration at that location. The purpose of the doghouse samples was to determine if the mixer concentration is representative of all the areas within that mixer and it is not. The reason being that the glass velocity is almost zero in some areas and will give a large difference in the mass transfer. The doghouse results is however not that important because the purpose is to achieve a model that can predict the outlet iron mass percentage.

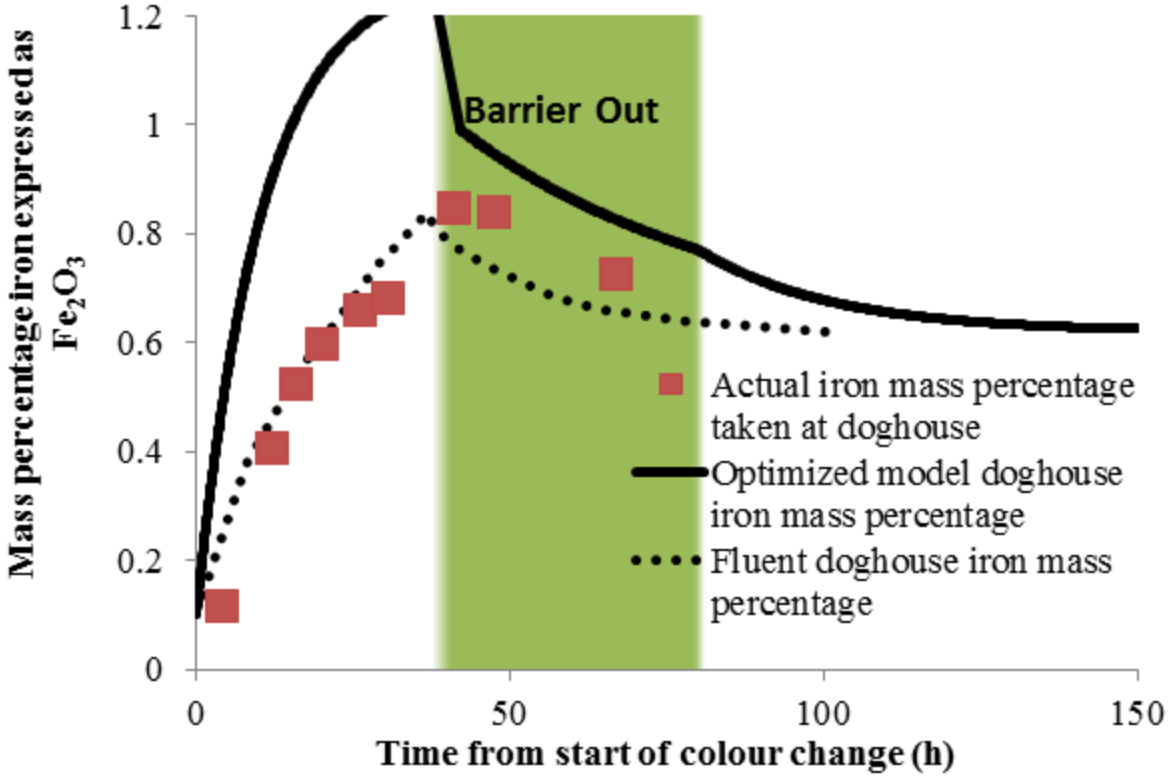


Figure 5-7: Optimized model prediction for the 2017 colour change doghouse iron mass percentage and comparison with the actual data.

5.5 Optimizing the colour change time

It was identified in this study that two important furnace variables affecting the colour change time is the barrier depth and the overdope rate. These two variables were adjusted within the reasonable limits of glass production to obtain the minimum colour change time, with respect to the glass iron concentration. Figure 5-8 shows the iron concentration change predicted from the model for four different times of removing the barrier. The base case of 0.45 m barrier depth was chosen, because the plant normally operates at this depth.

The sudden change in outlet iron concentration or step change after the barrier is removed, giving a higher iron concentration with increased time before removing the barrier. The iron concentration would be in specification within a shorter time; if the barrier could be removed at a time that would give an iron concentration of 0.6 % Fe_2O_3 after the step change when the barrier is removed. The optimal time, within allowed operating conditions, to remove the barrier is after 52 hours, with an overdope rate of 130 %, for a duration of 37 hours. The barrier has to be inserted then again after 70 hours. The concern with this approach is that the optical ream in the glass may be out of specification for longer due to the working end not

having enough time to homogenise the glass. The out of specification to in specification duration for the glass would be 10 hours less, with regards to the iron concentration.

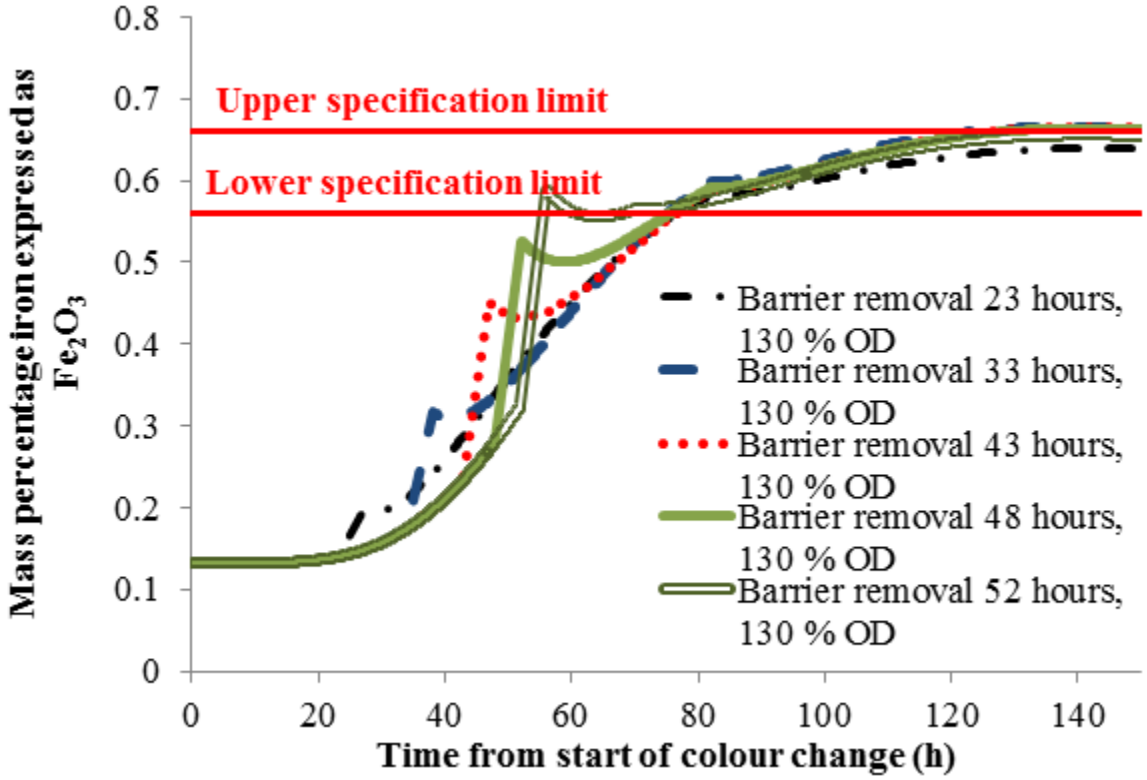


Figure 5-8: Model predicted outlet iron concentration change for different times when the barrier is removed.

Another option is to increase the overdope rate from 130 % to 180 % as shown in Figure 5-9. Removing the barrier at 48 hours with an overdope rate of 180 % reduces the time for when the outlet iron concentration will be in specification to 52 hours from the start of the colour change. This would possibly reduce the time of the colour change as the barrier can be inserted 10 hours earlier with the ream index in specification 10 hours earlier. There is a concern if there is enough time for the glass to homogenise in the working end with the barrier out for a shorter time. The barrier can be removed at 31 hours for the 180 % overdope, with the overdope duration 31 hours. This will give the working end enough time to homogenise and decrease the time for the iron concentration out of specification by 10 hours. The concern with an overdope of 180 % is that the furnace temperatures can be too cold as the glass in with the overdope will be 1.5 % Fe_2O_3. This will reduce the effective thermal conductivity of the glass in the furnace and may lead to temperatures in the furnace where the glass will stagnate and devitrify.

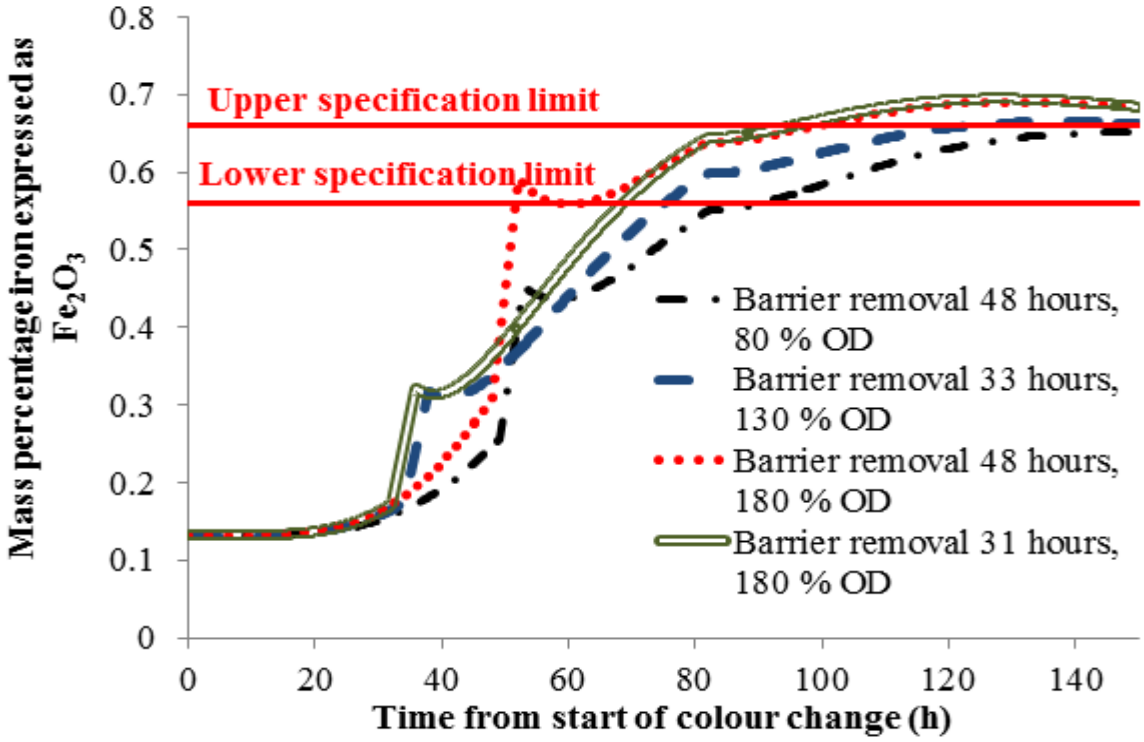


Figure 5-9: Model predicted outlet iron concentration change for different overdope (OD) rates.

6 Conclusions and Recommendations

The results from this study indicate that the colour change can be separated into four parts. A one parameter mixing model with five to eight perfect mixers in series can describe the first stage of the colour change, where the inlet iron concentration is set at a certain percentage more than the final required iron concentration. The number of perfect mixers in series depends on the barrier depth with five mixers in series used for 0.41 m barrier depth, six mixers in series for 0.45 m barrier depth and eight mixers in series for 0.56 m barrier depth. The second stage of the colour change when the barrier is removed causes a change in the furnace mixing characteristics and a sudden increase of iron concentration at the outlet of more than 0.1 mass % Fe_2O_3 within 4 hours. The third stage follows this short period by an increase in the iron outlet concentration that can be modelled by three perfect mixers in series when the barrier is out and the inlet iron concentration is reduced to the required outlet iron concentration. The fourth stage of the colour change is when the barrier is inserted again. This stage can be modelled by a four mixer in series model for the 0.3 m barrier depth.

The colour change time was reduced by 10 hours, with respect to the iron concentration, through adjusting key variables during the colour change. These were the overdope rate, overdope duration and the time when the barrier is removed. Multiple methods were tested with the mathematic mixing model of which two methods reduced the colour change time by 10 hours. One method was increasing the over dope rate to 180 % from the standard 130 % for a duration of 31 hours and also removing the barrier at 31 hours. Another method was to remove the barrier at 52 hours instead of 33 hours at an over dope rate of 130 % for 37 hours.

These methods will decrease the colour change time with respect to iron concentration, but may increase the time that the optical distortion is out of specification; as the glass may not homogenise within the required time in the furnace. It is also noteworthy to mention that this model was created for a specific furnace design and bubbling rate and will vary from furnace to furnace; but the perfect mixers in series model could be applied to other furnaces by using the response curve from that furnace.

It is recommended that a test be done with increasing the over dope rate to 180 % from the standard 130 % for a duration of 31 hours and also removing the barrier at 31 hours; to determine if it does decrease the time to when the glass is in specification for the iron

concentration. This test can be modelled in the CFD software to get a clearer understanding if it will be safe for the process.

The model only predicts the iron concentration and not the optical distortion. It does give uncertainty as to if the colour change will be optimized when optimized for iron as the optical distortion might take longer to be in spec due to the glass not allowed to homogenise in the furnace. A correlation between what the CFD model gives and the optical distortion can be done in future research.

The effect of the bubbler on the colour change is not clear in this study and does play an important role in the colour change as it does effect the flow cells. More research is to be done to create a more accurate CFD model for the bubblers.

The mixing model developed in this study can also be tested on other furnaces to create a normalized mixer in series model that can be used on any furnace design.

7 References

ANSYS® (2005). *Bubbling*. Document published to PFG.

ANSYS® Fluent (Version 18).[Help System] (2017). *Fluent.* Pittsburg: Ansys.

Bamford, C. R. (1977). *Colour Generation and Control in Glass*. Amsterdam: Elsevier Scientific Publishing Company.

Bergman, R. (1999). Mixing Model Simulation of an On-the-Fly Glass Conversion. *Ceramic Engineering and Science Proceedings, 20*(1), 171-180.

Cengel, Y. A. (2006). *Heat and Mass Transfer: A Practical Approach* (3rd edition). New York: McGraw-Hill.

Choudhary, M. K. (2002). Recent Advances in Mathematical Modeling of Flow and Heat Transfer Phenomena in Glass Furnaces. *Journal of the American Ceramic Society, 85*(5), 1030-1036.

Cooper, A. R. (1959). Mixing and Flow in Glass Tanks. *Journal of The American Ceramic Society, 42*(2), 93-101.

Fasilow, F. (2007). *Reduction of Color Change Time on Float Furnaces by the Help of 3D Numerical Simulations: Proceedings of the 9th International Seminar – Mathematical Modeling of Furnace Design and Operation – 1st Glass Forming Simulation Workshop* (pp. 60-70). Vsetin: Glass Service, INC.

Feng, Z., Li, D., Qin, G., & Liu, S. (2008). Study of the Float Glass Melting Process: Combining Fluid Dynamics Simulation and Glass Homogeneity Inspection. *Journal of the American Ceramic Society, 91*(10), 3229-3234.

Fogler, H.C. (2006) *Elements of Chemical Reaction Engineering* (4th ed.). Upper Saddle River, NJ: Pearson Education, Inc.

Octave. (2012). GNU Octave 3.2.4. Retrieved from https://gnu-octave-repository.soft112.com/.

Pilkington. (2008).*Melting Training*. Melting Services Pilkington.

Rhodes, M. (2008). *Introduction to Particle Technology* (2nd ed.). West Sussex: John Wiley & Sons Ltd.

Schäfer, M. (2006) *Computational Engineering-Introduction to Numerical Methods*. Berlin, Germany: Springer.

Statweb. (2017). *RMS Error*. Retrieved from http://statweb.stanford.edu/~susan/courses/s60/split/node60.html

Welty, J.R., Wicks, C.E., Wilson, R.E., & Rorrer, G.L. (2008). *Fundamentals of Momentum, Heat, and Mass Transfer* (5th ed.). Hoboken, NJ: John Wiley & Sons, Inc.

Wijshoff, L., Schep, J., Kahl, S-R., Faber, A., Roolvink, W., Goossens, J., Boogaardt, J., Potter, T., Hendriks, M., van Herten, R., Wijbenga, G.,van Limpt, H., & Brouwer, S., (2010). *NCNG Course on Glass Manufacture* (3rd ed.).

Xu, S., Liu, S., Xing, Z., & Li, H. (2016). 3D Fluid Flow Regularity in a Float Glass Furnace. Part 2. Circulation Disorder Phenomenon due to Changing the Iron Content. *Glass Technology: European Journal of Glass Science and Technology Part A, 57*(2), 70-77.

Appendices

Appendix A: UDF for viscosity

```
DEFINE_PROPERTY(user_vis,cell,thread)
{
 real T,expo,vis;

 T = C_T(cell, thread);
{
 if      (T <= 1250)    vis = 3150;
 else if (T >= 2150.0) vis = 1.0;
 else
    {
     expo = -2.845   + 4644.0189 / (T - 507.333567);
     vis  =  pow (10.0, expo);
    }
}
 return vis;
}
```

Appendix B: UDF for bubblers (ANSYS®, 2005).

```
#include "udf.h"
#include "sg.h"
#include "prop.h"

real bubbler_vol = 0;
DEFINE_SOURCE(bubbler_source, cell, thread, rj, eqn)
{
#define pi 3.14159
#define gravity 9.81
#define bub_rad 0.2
 real bub_vel,f_d,bub_freq = 0.016,bub_ht = 0.869, source;
 real bub_num;
 cell_t cc;
 rj[eqn]=0;
 if (bubbler_vol == 0)
   {
    begin_c_loop(cc,thread)
     bubbler_vol = bubbler_vol + C_VOLUME(cc,thread);
    end_c_loop(cc,thread)
   }
 bub_vel = 2.0*gravity*pow(bub_rad,2.)*C_R(cell,thread)/(9.0*C_MU_L(cell,thread));
 f_d     = 4.*pi*C_MU_L(cell,thread)*bub_rad*bub_vel;
 bub_num = bub_freq*bub_ht/bub_vel;
 source  = bub_num*f_d/bubbler_vol;

 return source;
}
```

Appendix C: Top surface heat flux calculations

The usefull yield or percentage of combustion energy into glass is in the range of 0.5 to 0.8 for a float glass furnace using natural gas. The range is large due to the complexity of the combustion space where there is radiation from the flame on that port or other ports and from the structure to the glass and vice-versa.

The glass in a float furnace also has sections that is covered on top with batch and foam. The area covered with the batch blanket will extract heat from the glass as the batch is colder than the glass and needs to melted. Soda lime silica glass raw materials include limestone, dolomite and soda ash. The carbonation of these three raw materials is an endothermic reaction and the batch needs to be heated to the glass temperature. This batch blanket is generally from the doghouse up to port 2.5 and has a shape shown in Figure C-1.

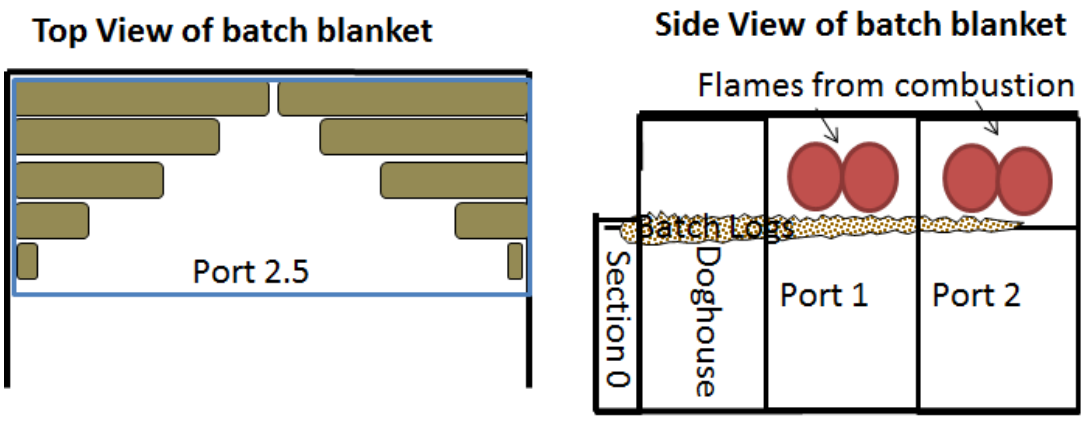


Figure C-1: Batch blanket

The energy balance equation for the areas covered with batch is given in Equation (C.1) and shown in Figure C-2.

$$Q_C + Q_A + Q_{rad} + Q_B = Q_L + Q_G + Q_F \quad \text{(C.1)}$$

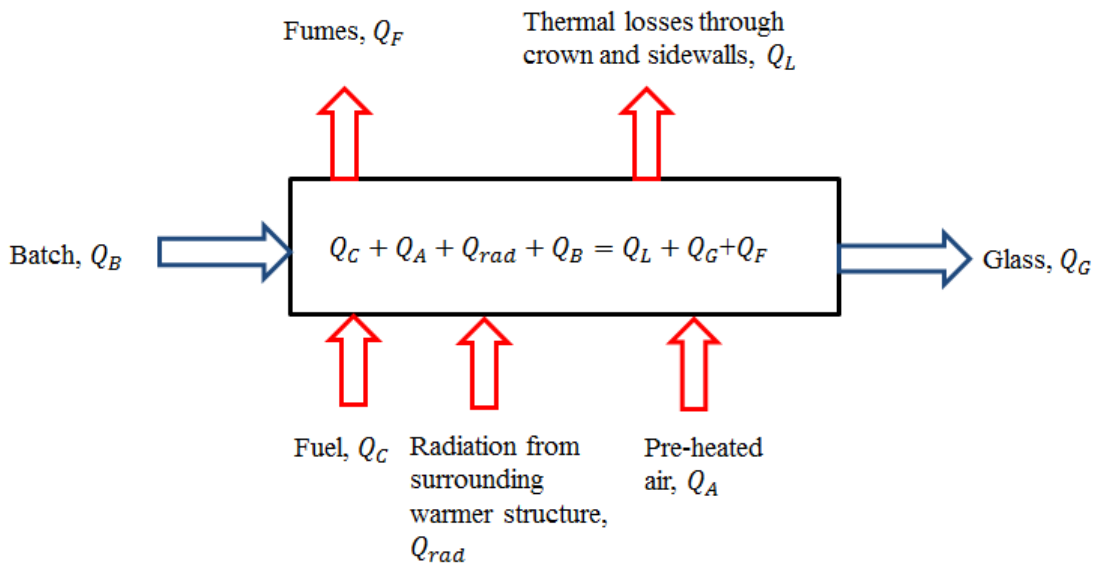


Figure C-2: Combustion space energy diagram

The batch comes into the furnace at 40 to 50 °C. There is negligible structural heat loss in section 0 and there is also no combustion. In section 0 Equation (C.1) can be reduced to:

$$Q_{rad} + Q_B = Q_G \tag{C.2}$$

In section 0 the batch is heated by the glass and the radiation from the superstructure. The radiative heat transfer coefficeint from the superstructure to the batch can be calculated from Equation (C.3) (Verheijen, 2003):

$$h_{rs} = \frac{\sigma\left(T_{sup}^2 + T_b^2\right)\left(T_{sup} + T_b\right)}{\frac{1}{\varepsilon_{sup}} + \frac{1}{\varepsilon_b} - 1} \tag{C.3}$$

With σ the Stefan-Boltzmann constant, T_{sup} and T_b the superstructure and the batch temperature in K respectively and ε_{sup} and ε_b the superstructure and batch emissivity respectively. Assumking that no calcination occurs in section 0 the batch will be heated to 973 K which is the onset temperature for calcination (Verheijen, 2003). The measured superstructure and top surface batch temperature is 1387 K and 1300 K. The batch emmisivity given by Verheijen (2003) is 0.7 and the superstructure emissivity 0.3. This gives:

$$h_{rs} = \frac{5.67 \times 10^{-8}(1387^2 + 1300^2)(1387 + 1300)}{\frac{1}{0.3} + \frac{1}{0.7} - 1}$$

$$h_{rs} = 146 \text{ W/(m}^2\text{K)}$$

With the doghouse area being 3.904 m2 and the superstructure and batch temperature as given above the radiation heat into the batch is:

$$Q_{rad} = \frac{146 \times 3.904 \times (1387 - 1300)}{1000} = 50 \text{ kW}$$

The heat required to increase the batch temperature to an average temperature of 973 K from 313 K is calculated from the average heat capacity of 1100 J/(kgK) given by ANSYS® (2005). At a load of 2300 tons per week this gives

$$Q_B = -2\,760 \text{ kW}$$

The batch energy is negative because it comes in at a lower temperature than required. Section 0 comprises a very small percentage of the batch blanket and therefore the batch heat has to be multiplied by this factor of 0.1.

The energy from the glass top surface in section 0 can then be calculated as:

$$Q_G = 50 - 2\,760 \times 0.1 = -226 \text{ kW}$$

The batch is then heated further and melted by energy from the glass and radiation from the superstructure for the doghouse. There is structural heat loss in the doghouse but no combustion. Equation (C.1) can be reduced to:

$$Q_{rad} + Q_B = Q_L + Q_G \qquad \text{(C.4)}$$

The energy required to melt the batch can be calculated from Equation (C.5) (Verheijen, 2003):

$$\Delta H_r = H_{r,i} \times m_i^0 \quad \text{(C.5)}$$

With the reaction heat $H_{r,i}$ and mass flow rate in the batch of calcium, magnesium and soda ash given in Table C-1 (Knacke, Kubaschewski & Hesselmann, 1991). The total energy required for the reactions is 6 760 kW.

Table C-1: Heat of reaction data for SP4 batch

Reaction	$H_{r,i}$	m_i^0	ΔH_r
	kJ/kg	**kg/s**	**kW**
Thermal decomposition of calcium carbonate	13 474	0.25	3 419
Thermal decomposition of magnesium carbonate	13 953	0.14	1 890
Reactive decomposition of soda ash	11 885	0.02	181
Total			5 490

The energy to heat the batch to 973 K is $2\,760 \times 0.95$ = 2 622 kW. The energy require to heat the batch excluding cullet, limestone, dolomite and soda ash to 1400 K is 1 409 kW. The total energy to melt the batch is:

$$Q_B = -(5\,490 + 2\,622 + 1\,409) = 9\,521 \text{ kW}$$

This total energy is divided into a percentage for the doghouse, port 1and port 2 upstream. Assuming the batch starts at the centre line and dissipates in a triangular shape up to port 2.5 as shown in Figure C-3. The doghouse contains 67 % of the batch with port 1, 29% and port 2 upstream 4%.

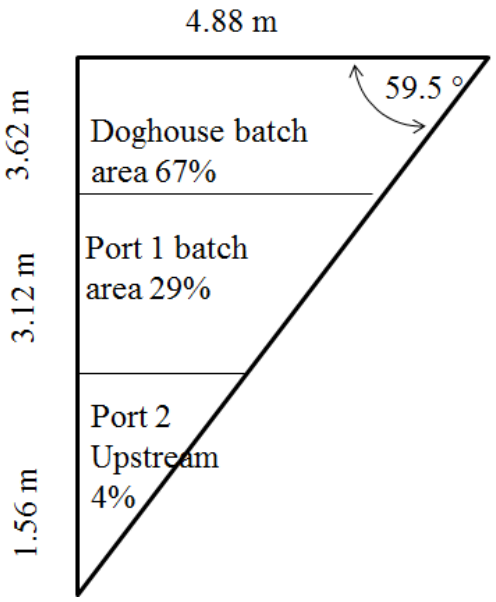


Figure C-3: Batch coverage

The radiation heat into the batch at the doghouse is

$$Q_{rad} = \frac{146 \times 34.355 \times (1449 - 1387)}{1000} = 311 \text{ kW}$$

The heat from the glass for the doghouse is:

$$311 - 9\,521 \times 0.67 = 96 + Q_G$$

$$Q_G = -6\,164 \text{ kW}$$

The heat balance from port 1 to port 5 has combustion energy. The amount of combustion energy absorbed by the glass is 0.5 to 0.8 of the total combustion energy per port also called the useful yield. The foam layer generally prominent in port 2 downstream and port 3 reflects radiation back to the crown and the useful yield will be lower in port 2 and 3 when compared to other ports. Port 4 will be used as an example to calculate the uefull yield. There is no batch blanket at port 4 giving $Q_B = 0$. Equation (C.1) can be written for Port 4 as:

$$Q_C + Q_A + Q_{rad} = Q_L + Q_G + Q_F \qquad \text{(C.6)}$$

The combustion energy Q_C is determined from the net calorific value of natural gas measured from an Emerson (2014) Rosemount 370XA gas chromatograph on site. The CV at 15.6 °C is 37 187 kJ/Nm^3 with 607 Nm^3/h of gas fired on port 4. The combustion energy $Q_C = 6\,270$ kW. The Energy with the air in on port 4 with a total of 5933 Nm3/h air in at 1313 °C gives $Q_A = 3\,083$ kW. The heat lost from the surrounding structure trough the crown and sidewalls is calculated to be $Q_L = 98$ kW. The fumes from port 4 from with a mole percentage of 8.8 % CO_2, 1.7 % O_2, 72.1 % N_2 and 17.5 % H_2O and a temperature of 1573 °C gives $Q_F = 4\,557$ kW. The radiation element is assumed to be zero this gives

$$6\,270 + 3\,083 + 0 = 98 + Q_G + 4\,557$$

$$Q_G = 4\,698 \text{ kW}$$

Divide the energy into the glass with the combustion energy in to get the useful yield of 4698/6270 = 0.75.

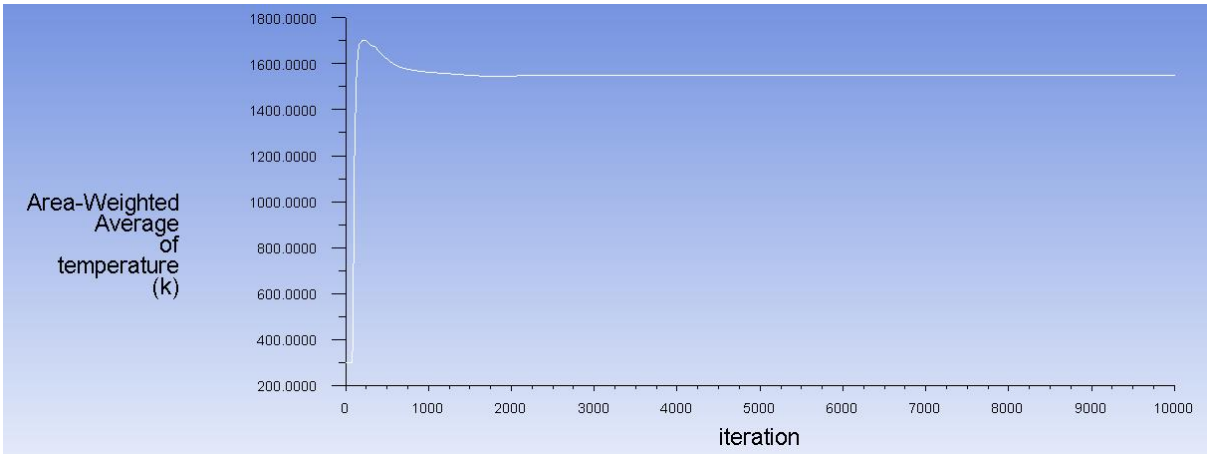
The estimated energy for Port 1 to the working end is shown in Table C-2. It is assumed that some of the radiation from port 5 gives energy to the refiner more than what is lost from the superstructure. The waist is based on superstructure heat loss and the working end calculated similar to port 4.

Table C-2: Top surface heat loss values

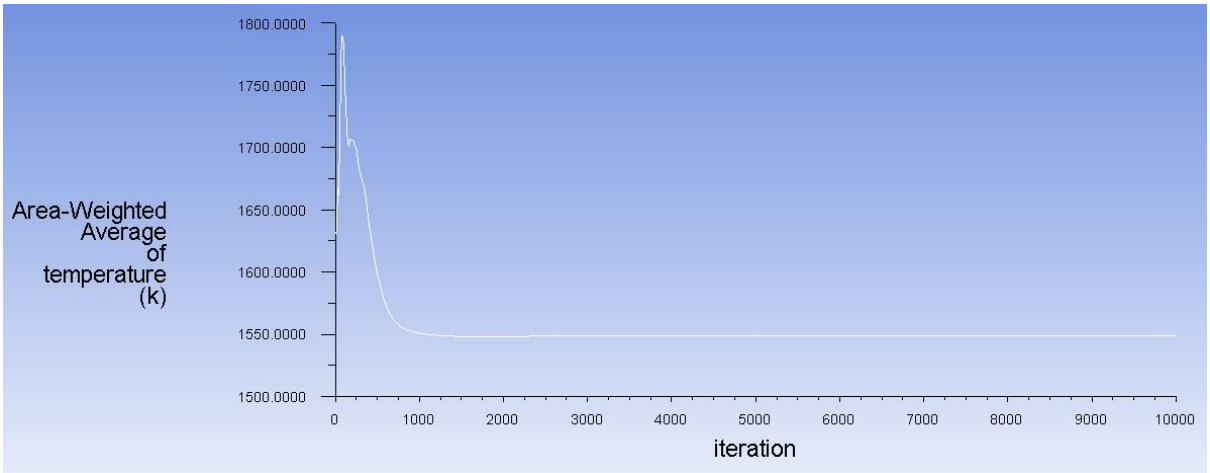
Section	**Usefull yield factor**	**Fuel**	**Energy to melt batch**	**Total Energy into glass**
		Nm3/h	**kW**	**kW**
Port 1	0.20	569	2 761	-1 586
Port 2 DS	0.20	596	381	850
Port 2 US	0.20	596		1 231
Port 3	0.70	607		4 389
Port 4	0.75	607		4 703
Port 5	0.75	446		3 455
Refiner				155
Waist				-114
WE				-323

Appendix D: Convergence of glass temperatures

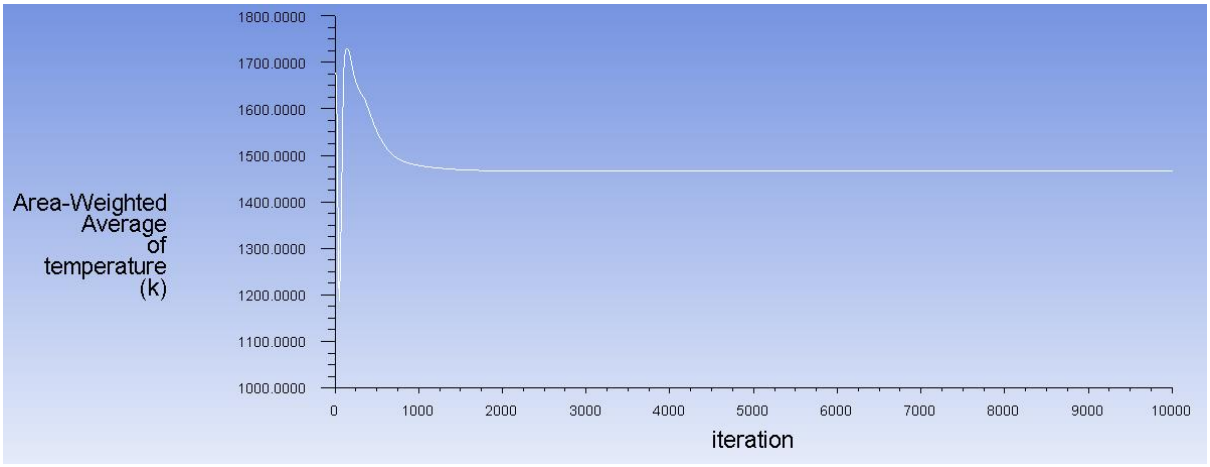
D.1 Filling pocket temperature



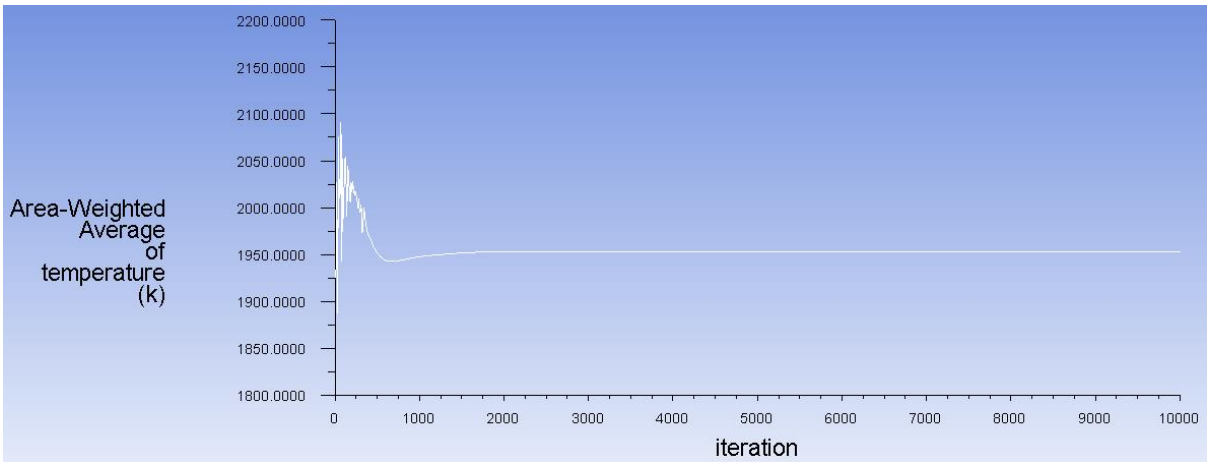
D.2 Bottom hotspot temperature (Bottom 6)



D.3 Outlet temperature



D.4 Crown 4 temperature



Appendix E: Octave (2012) model codes

E.1 2017 colour change mixer in series code

```
%Colour change 2017 model calculations
Load = 2500;%tpw
Qmass = 1257*1000; %kg in furnace
Qtot = Load/7/24*1000 %kg/h
xin = 1.278; %iron mass percentage in with overdope
xor = 0.1; %Original iron mass percentage in melter
n = 3;

%Three perfect mixer in series model
f1 = @(c,t) (xin-c(1))*Qtot/(Qmass/n); %Mixer one
f2 = @(c,t) (c(1)-c(2))*Qtot/(Qmass/n); %Mixer two
f3 = @(c,t) (c(2)-c(3))*Qtot/(Qmass/n); %Mixer three

%Overdope from 0 to 36 hours
time = linspace(0,36,1000);
Initialvalue = [xor;xor;xor];
dcdt = @(c,t) [f1(c,t);f2(c,t);f3(c,t)];
pdcdt = lsode(dcdt,Initialvalue,time);

%Normal batch of 0.62 % iron from 36 to 150 hours
t = length(pdcdt)
```

```
Cel1conc = pdcdt(t,1)
Cel2conc = pdcdt(t,2)
Cel3conc = pdcdt(t,3)

Initialvalue2 = [Cel1conc;Cel2conc;Cel3conc];
xin = 0.62; %Iron In
n=3;
f1 = @(c,t) (xin-c(1))*Qtot/(Qmass/n); %Mixer one
f2 = @(c,t) (c(1)-c(2))*Qtot/(Qmass/n); %Mixer two
f3 = @(c,t) (c(2)-c(3))*Qtot/(Qmass/n); %Mixer three
dcdt = @(c,t) [f1(c,t);f2(c,t);f3(c,t)];
time2 = linspace(36,150,1000);
rdcdt = lsode(dcdt,Initialvalue2,time2);

%Results
results = [pdcdt(:,3);rdcdt(:,3)];
totaltime = [time time2];

for i = 1:length(totaltime)
timerow(i,1) = totaltime(i);
end

dlmwrite('ConcM4.txt',results,'\t');
dlmwrite('timeM2.txt',timerow,'\t');

plot(totaltime,results,'-r')
```

E.2. 2015 colour change optimized model code

```
%2015 colour change
Load = 2500;%tpw
Qmass = 1257*1000; %kg in tank
Qtot = Load/7/24*1000 %kg/h
xin = 1.278; %Iron In
xor = 0.132; %Iron in melter
```

```
n = 6;
%Melter to WE tanks
f1 = @(c,t) (xin-c(1))*Qtot/(Qmass/n);
f2 = @(c,t) (c(1)-c(2))*Qtot/(Qmass/n);
f3 = @(c,t) (c(2)-c(3))*Qtot/(Qmass/n);
f4 = @(c,t) (c(3)-c(4))*Qtot/(Qmass/n);
f5 = @(c,t) (c(4)-c(5))*Qtot/(Qmass/n);
f6 = @(c,t) (c(5)-c(6))*Qtot/(Qmass/n);

%First part with OD in and pipes in
time = linspace(0,34,1000);
initvalue = [xor;xor;xor;xor;xor;xor];
dcdt = @(c,t) [f1(c,t);f2(c,t);f3(c,t);f4(c,t);f5(c,t);f6(c,t)];
pdcdt = lsode(dcdt,initvalue,time);

%Second part with pipe out
t = length(pdcdt)
Cel1conc = (pdcdt(t,1)*Qmass/n+pdcdt(t,2)*Qmass/n+pdcdt(t,3)*Qmass/n)/(Qmass/n*3)
Cel2conc = (pdcdt(t,6)*Qmass/n)/(Qmass/n*1)
Cel3conc = (pdcdt(t,4)*Qmass/n+pdcdt(t,5)*Qmass/n)/(Qmass/n*2)
initvalue2 = [Cel1conc;Cel2conc;Cel3conc];
xin = 0.619; %Iron In
n=3;
f1 = @(c,t) (xin-c(1))*Qtot/(Qmass*3/6);
f2 = @(c,t) (c(1)-c(2))*Qtot/(Qmass*1/6);
f3 = @(c,t) (c(2)-c(3))*Qtot/(Qmass*2/6);
dcdt = @(c,t) [f1(c,t);f2(c,t);f3(c,t)];
time2 = linspace(38,82,1000);
rdcdt = lsode(dcdt,initvalue2,time2);

%Third part with pipe in
initvalue3                                                                    =
[rdcdt(length(rdcdt),1);rdcdt(length(rdcdt),2);rdcdt(length(rdcdt),3);rdcdt(length(rdcdt),3)];
xin = 0.619; %Iron In
```

```
n=4
f1 = @(c,t) (xin-c(1))*Qtot/(Qmass/n);
f2 = @(c,t) (c(1)-c(2))*Qtot/(Qmass/n);
f3 = @(c,t) (c(2)-c(3))*Qtot/(Qmass/n);
f4 = @(c,t) (c(3)-c(4))*Qtot/(Qmass/n);
dcdt = @(c,t) [f1(c,t);f2(c,t);f3(c,t);f4(c,t)];
time3 = linspace(82,150,1000);
sdcdt = lsode(dcdt,initvalue3,time3);

%Results
results = [pdcdt(:,6);rdcdt(:,3);sdcdt(:,4)];
M2 = [pdcdt(:,1);rdcdt(:,1)];
totaltime = [time time2 time3];

for i = 1:length(totaltime)
timerow(i,1) = totaltime(i);
end

dlmwrite('ConcM2.txt',M2,'\t');
dlmwrite('ConcM4.txt',results,'\t');
dlmwrite('timeM2.txt',timerow,'\t');
plot(totaltime,results,'-r')
```

E.3. 2016 colour change optimized model code

```
%2016 colour change
Load = 2500;%tpw
Qmass = 1257*1000; %kg in tank
Qtot = Load/7/24*1000 %kg/h
xin = 1.278; %Iron In
xor = 0.129; %Iron in melter
n = 5;
%Melter to WE tanks
f1 = @(c,t) (xin-c(1))*Qtot/(Qmass/n);
f2 = @(c,t) (c(1)-c(2))*Qtot/(Qmass/n);
```

```
f3 = @(c,t) (c(2)-c(3))*Qtot/(Qmass/n);
f4 = @(c,t) (c(3)-c(4))*Qtot/(Qmass/n);
f5 = @(c,t) (c(4)-c(5))*Qtot/(Qmass/n);


%First part with OD in and pipes in
time = linspace(0,34,1000);
initvalue = [xor;xor;xor;xor;xor];
dcdt = @(c,t) [f1(c,t);f2(c,t);f3(c,t);f4(c,t);f5(c,t)];
pdcdt = lsode(dcdt,initvalue,time);

%Second part with pipe out
t = length(pdcdt)
Cel1conc = (pdcdt(t,1)*Qmass/n+pdcdt(t,2)*Qmass/n)/(Qmass/n*2)
Cel2conc = (pdcdt(t,5)*Qmass/n)/(Qmass/n*1)
Cel3conc = (pdcdt(t,3)*Qmass/n+pdcdt(t,4)*Qmass/n)/(Qmass/n*2)
initvalue2 = [Cel1conc;Cel2conc;Cel3conc];
xin = 0.619; %Iron In
n=3;
f1 = @(c,t) (xin-c(1))*Qtot/(Qmass*2/6);
f2 = @(c,t) (c(1)-c(2))*Qtot/(Qmass*1/6);
f3 = @(c,t) (c(2)-c(3))*Qtot/(Qmass*2/6);
dcdt = @(c,t) [f1(c,t);f2(c,t);f3(c,t)];
time2 = linspace(38,82,1000);
rdcdt = lsode(dcdt,initvalue2,time2);

%Third part with pipe in

initvalue3                                                                    =
[rdcdt(length(rdcdt),1);rdcdt(length(rdcdt),2);rdcdt(length(rdcdt),3);rdcdt(length(rdcdt),3)];
xin = 0.619; %Iron In
n=4
f1 = @(c,t) (xin-c(1))*Qtot/(Qmass/n);
f2 = @(c,t) (c(1)-c(2))*Qtot/(Qmass/n);
```

```
f3 = @(c,t) (c(2)-c(3))*Qtot/(Qmass/n);
f4 = @(c,t) (c(3)-c(4))*Qtot/(Qmass/n);
dcdt = @(c,t) [f1(c,t);f2(c,t);f3(c,t);f4(c,t)];
time3 = linspace(82,150,1000);
sdcdt = lsode(dcdt,initvalue3,time3);

%Results
results = [pdcdt(:,5);rdcdt(:,3);sdcdt(:,4)];
M2 = [pdcdt(:,1);rdcdt(:,1)];
totaltime = [time time2 time3];

for i = 1:length(totaltime)
timerow(i,1) = totaltime(i);
end

dlmwrite('ConcM2.txt',M2,'\t');
dlmwrite('ConcM4.txt',results,'\t');
dlmwrite('timeM2.txt',timerow,'\t');
plot(totaltime,results,'-r')
```

E.4. 2017 colour change optimized model code

```
%2017 colour change
Load = 2500;%tpw
Qmass = 1257*1000; %kg in tank
Qtot = Load/7/24*1000 %kg/h
xin = 1.278; %Iron In
xor = 0.1; %Iron in melter
n = 8;
%Melter to WE tanks
f1 = @(c,t) (xin-c(1))*Qtot/(Qmass/n);
f2 = @(c,t) (c(1)-c(2))*Qtot/(Qmass/n);
f3 = @(c,t) (c(2)-c(3))*Qtot/(Qmass/n);
f4 = @(c,t) (c(3)-c(4))*Qtot/(Qmass/n);
f5 = @(c,t) (c(4)-c(5))*Qtot/(Qmass/n);
```

```
f6 = @(c,t) (c(5)-c(6))*Qtot/(Qmass/n);
f7 = @(c,t) (c(6)-c(7))*Qtot/(Qmass/n);
f8 = @(c,t) (c(7)-c(8))*Qtot/(Qmass/n);

%First part with OD in and pipes in
time = linspace(0,38,1000);
initvalue = [xor;xor;xor;xor;xor;xor;xor;xor];
dcdt = @(c,t) [f1(c,t);f2(c,t);f3(c,t);f4(c,t);f5(c,t);f6(c,t);f7(c,t);f8(c,t)];
pdcdt = lsode(dcdt,initvalue,time);

%Second part with pipe out
t = length(pdcdt)
Cel1conc =
(pdcdt(t,1)*Qmass/n+pdcdt(t,2)*Qmass/n+pdcdt(t,3)*Qmass/n+pdcdt(t,4)*Qmass/n)/(Qmass
/n*4)
Cel2conc = (pdcdt(t,7)*Qmass/n+pdcdt(t,8)*Qmass/n)/(Qmass/n*2)
Cel3conc = (pdcdt(t,5)*Qmass/n+pdcdt(t,6)*Qmass/n)/(Qmass/n*2)
initvalue2 = [Cel1conc;Cel2conc;Cel3conc];
xin = 0.619; %Iron In
n=3;
f1 = @(c,t) (xin-c(1))*Qtot/(Qmass*4/8);
f2 = @(c,t) (c(1)-c(2))*Qtot/(Qmass*2/8);
f3 = @(c,t) (c(2)-c(3))*Qtot/(Qmass*2/8);
dcdt = @(c,t) [f1(c,t);f2(c,t);f3(c,t)];
time2 = linspace(42,80,1000);
rdcdt = lsode(dcdt,initvalue2,time2);

%Third part with pipe in
initvalue3 =
[rdcdt(length(rdcdt),1);rdcdt(length(rdcdt),2);rdcdt(length(rdcdt),3);rdcdt(length(rdcdt),3)];
xin = 0.619; %Iron In
n=4;
f1 = @(c,t) (xin-c(1))*Qtot/(Qmass/n);
f2 = @(c,t) (c(1)-c(2))*Qtot/(Qmass/n);
```

```
f3 = @(c,t) (c(2)-c(3))*Qtot/(Qmass/n);
f4 = @(c,t) (c(3)-c(4))*Qtot/(Qmass/n);
dcdt = @(c,t) [f1(c,t);f2(c,t);f3(c,t);f4(c,t)];
time3 = linspace(80,150,1000);
sdcdt = lsode(dcdt,initvalue3,time3);

%Results
results = [pdcdt(:,8);rdcdt(:,3);sdcdt(:,4)];
M2 = [pdcdt(:,1);rdcdt(:,1);sdcdt(:,1)];
totaltime = [time time2 time3];

for i = 1:length(totaltime)
timerow(i,1) = totaltime(i);
end

dlmwrite('ConcM2.txt',M2,'\t');
dlmwrite('ConcM4.txt',results,'\t');
dlmwrite('timeM2.txt',timerow,'\t');
plot(totaltime,results,'-r')
```

Appendix F: Appendix references

ANSYS® (2005). *Bubbling*. Document published to PFG.

Emerson. (2014). *BTU Analysis Using a Gas Chromatograph.* Retrieved from https://www.emerson.com/documents/automation/application-note-btu-analysis-using-a-gas-chromatograph-en-72722.pdf

Knacke, O., Kubaschewski, O., & Hesselmann, K. (1991). *Thermochemical Properties of Inorganic Substances* (2nd ed.). Heidelberg: Springer-Verlag Berlin.

Octave. (2012). GNU Octave 3.2.4. Retrieved from https://gnu-octave-repository.soft112.com/.

Verheijen O.S. (2003). *Thermal and chemical behaviour of glass forming batches* (Doctoral dissertation). Technische Universiteit Eindhoven. Eindhoven: Netherlands. Retrieved from https://pure.tue.nl/ws/files/2075516/200311763.pdf

Appendix G: Paper submitted for publication

Elsevier Editorial System(tm) for Chemical Engineering Research and Design
Manuscript Draft

Manuscript Number:

Title: Modelling and experimental investigation of mixing and flow inside a float glass furnace towards reduction in colour change time

Article Type: Full Length Article

Keywords: Modelling; Optimization; Glass colour change; Flow; Mixing

Corresponding Author: Dr. Michael Olawale Daramola, Ph.D

Corresponding Author's Institution: University of the Witwatersrand

First Author: Johan Lotter

Order of Authors: Johan Lotter; Michael Olawale Daramola, Ph.D

Abstract: The objective of this investigation was to develop a mathematical mixing model that could describe accurately the residence time inside a float glass furnace with the purpose of using that model to optimise the duration of the colour change. A 3-dimensional glass flow model was developed using the ANSYS® Fluent environment and validated using actual plant data. The developed glass flow model was used to develop a one/two parameter mixing mathematical model for the furnace and validate it using actual plant data. Different scenarios involving barrier removal time, barrier depth and over-dope concentrations were tested using the developed mixing model to reduce the colour change time. The results of the investigation show that the number of perfect mixers in series that could result in optimized colour change time depends on the barrier depth. Understanding this flow and mixing pattern and mechanism in the reactor could be instrumental to obtaining optimal conditions to reduce crushing time during the colour change. Furthermore, since the optimal conditions will vary from furnace to furnace, the proposed perfect mixers-in-series model could be applied to other furnaces in predicting the colorant concentration with the key parameter being the number of perfect mixers in series to use.